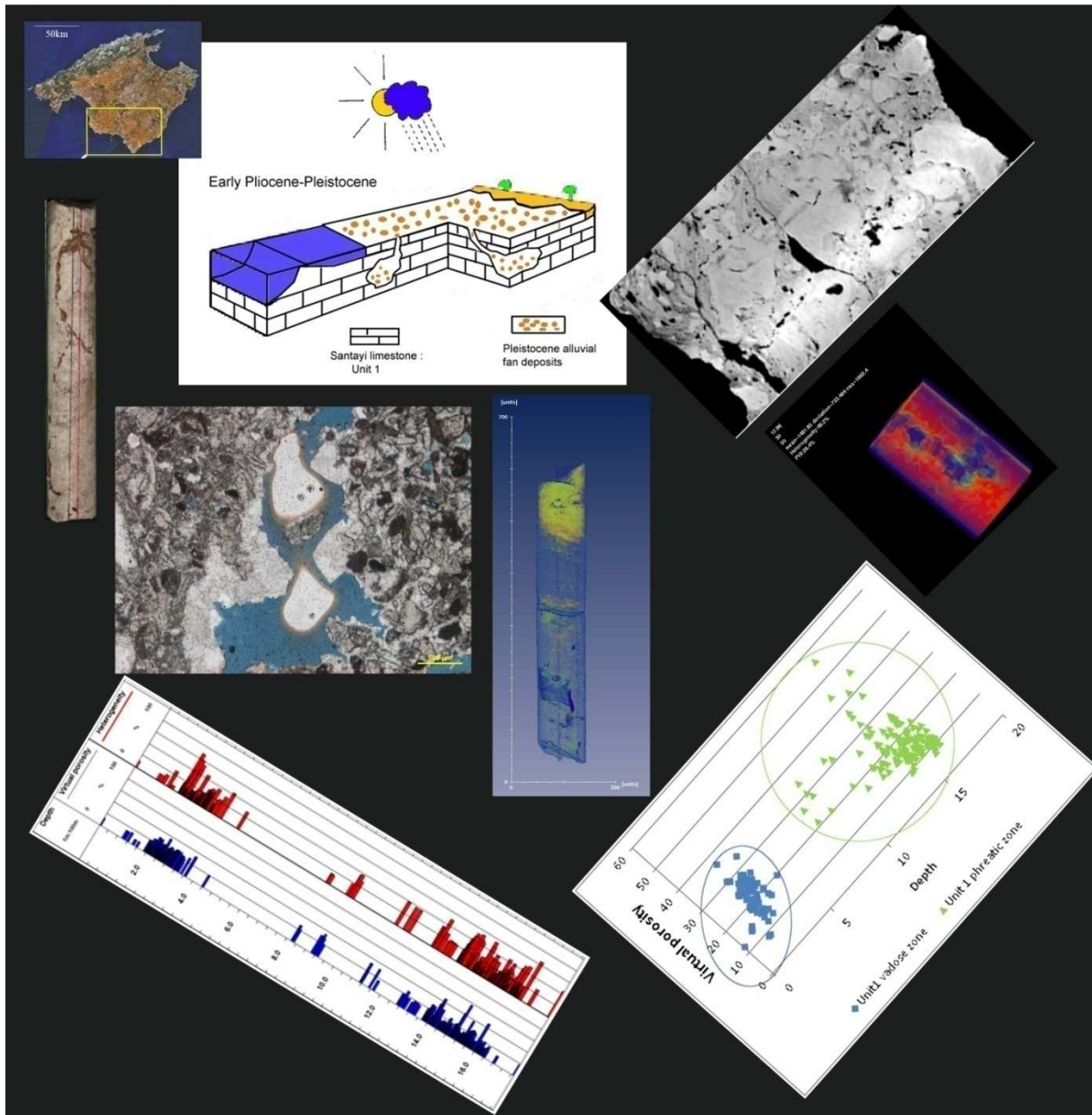


Report of Master 2008-2009

Prepared by Papa Ousmane Mangane

Sedimentological, Diagenetic, and Petrophysical study from cores of the Upper Miocene carbonate complex, Mallorca (Spain).



Supervisor: Jean Louis Cappelli (DGEP/TG/ISS/CARB TOTAL S.A.)

TABLE OF CONTENTS

ABSTRACT	2
I) INTRODUCTION	3
II) GEOLOGICAL SETTING	5
1. Geology of Mallorca	6
2. Chrono-stratigraphy of Mallorca	7
2.1- Upper Miocene deposits	
2.2- Post-Miocene rock	
III) Sedimentology	10
1. Well S26	10
a) Lithofacies description.....	11
b) Log data analysis.....	18
2. Well S27	19
a) Lithofacies description	20
b) Log data analysis.....	26
IV) Diagenesis features	28
1. Vadose fabrics.....	28
a) Cementation in undersaturated zone	28
b) Dissolution features.....	31
2. Phreatic fabrics.....	32
a) Cementation in saturated zone	32
b) Fabrics in vadose-phreatic mixing zone.....	33
c) Dissolution features.....	33
3. Cathodoluminescence Microscopy	34
4. Dolomitization of the breccias of unit3	35
V) Origin of Font Sant anomaly (unit2/unit3)	36
1. Origin of filled-paleokarst	36
a) Meteoric karst	36
b) Geo/hydrothermal karst.....	38
c) Nature of unit2 cement (coarse crystal of calcite)	40
VI) Karst reservoir characterization	41
1. Petro-physical survey from X-ray image of cores	41
a) Computed Tomography Scanning (CT Scan) presentation.....	41
2. X-Ray Image interpretation.....	42
3. Petro-physical treatment	45
a) Virtual plugging and virtual porosity.....	45
b) Results: Case of well S26.....	48
c) Interpretation.....	48
4. Visualisation of porous network	50
VII) Discussion and conclusion	53

Abstract:

Located in the eastern part of Mallorca, Santayi complex corresponds to an analogous aquifer to karst-fractured carbonate reservoir. Latest Messinian in age, Santayi limestone are actually affected by many dissolution structures, as paleokarst, vugs and dissolution channels. Fractures slightly tilted (5°) also affect this aquifer.

All the dissolution structures recorded in Santayi Platform are mainly epigenic (sub-surface karst), so are created during subaerial exposure phase of the platform. The exposure of the rock is principally controlled by high-frequency sea-level fluctuations recorded in Mallorca. The main fall of sea level recorded after deposit of these limestone is Early Pliocene in age.

Become emergent, Santayi Platform is subdivided in two distinct diagenesis environments: Vadose environment (subaerial exposed area) and phreatic environment (Mallorca aquifer). Major of dissolution structures are created in vadose zone due to the meteoric karst action.

In addition to meteoric karst action, later burial diagenesis processes, as geo/hydrothermal diagenesis or chemical reactions due to mixing of chemically-distinct water (near the water table and in marine-meteoric mixing zone), control subsequently the karst development. Fluid circulations through fractures affecting these limestone also generate dissolution structures onto the rock by percolation.

Dissolution porosity (caverns, vugs, moldic porosity and dissolution channels) due to the karst action, is the predominant porosity type in Santayi reservoir. This leached porosity is coupled with inter-granular (primary porosity) and fracture porosity.

Both, intergranular and dissolution porosity are currently slightly reduced or totally occluded by late calcite cementation mainly controlled by meteoric diagenesis (vadose and phreatic diagenesis).

In vadose zone many re-precipitation of stable carbonate, due to the karst action, occur. As consequence, primary porosity commonly is filled during the meteoric diagenesis, and secondary porosity is created. Secondary leached pores can sometimes be partly filled by these re-precipitations, and often by insoluble materials which infiltrated into them during the karst action.

Large paleokarst affecting the Santayi Limestone are sometimes filled by Pleistocene alluvial fan deposits overlaying the rocks: In the western part of this shelf, precisely in Font Sant area, a large paleokarst (17 meters thick), filled by breccias is recorded in the limestone.

Porosity of the rock is therefore substantially variable in vadose environment. The values range is from 8.8% to peaks at 36.5%.

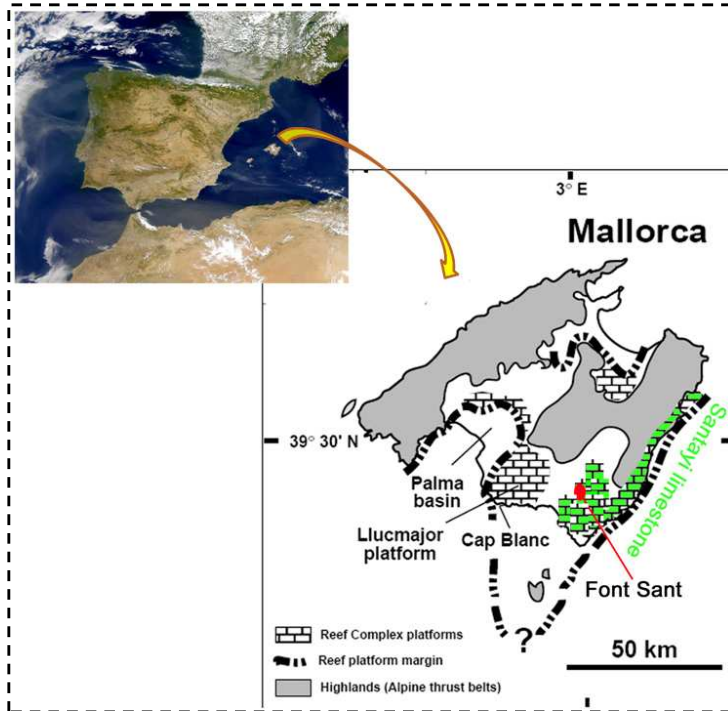
Phreatic environment is characterized by an extensive cementation reflecting the complete saturation of pore by water. Thus, primary porosity is totally filled by calcite cement. Globally, range of porosity in phreatic zone is ten percent lower than the porosity in vadose zone.

According to the present configuration of the Santayi reservoir, its quality is therefore mainly controlled by meteoric diagenesis. Contrary to the porosity, permeability is strongly affected by this meteoric alteration through cementation of interconnected primary pores, due to re-precipitations processes. However fractures induced by uplift of the aquifer can highly ameliorate this petrophysical parameter.

Introduction:

Karst-fractured carbonate reservoirs show substantial lateral and vertical heterogeneities in amount and distribution of its petrophysical properties. Karsts affecting these carbonate result mainly from meteoric karst development occurred during subaerial exposure phase of rock. Later burial diagenesis processes can also control karst development whenever limestone are buried or submerged in phreatic environment. Fracture and faulting inducing by uplift episode of these complexes, as further control of karst development due to fluid circulation through these tectonics structures.

As analogous reservoir, Santayi platform located in Eastern part of Mallorca (Fig1) is the model used to analyze and characterize variability of petrophysical parameters in karst-fractured



reservoir. Precisely, this memory undertakes study of karst aquifer that is localized in Western part of Santayi platform: Font Sant aquifer (“Fontaine sacrée” in French). Font Sant area is characterized by the presence of geo/hydrothermal baths using as therapies.

Fig 1: Map showing location of Santayi platform on the western part of Mallorca island, in the western Mediterranean sea. Note the location of Font Sant area in the Eastern part of Santayi platform (red circle). Santayi limestone are also located to the western side of Palma basin, onlapping the reef core of Llucmajor Platform.

Preliminary studies realized (coring and geophysical campaign) in this region show existence of a particular zone in depth, that is characterized by:

- Geophysics: a high radioactivity.
- Geology: Carbonate rock composed of coarse crystals of calcite, and quartz crystal.

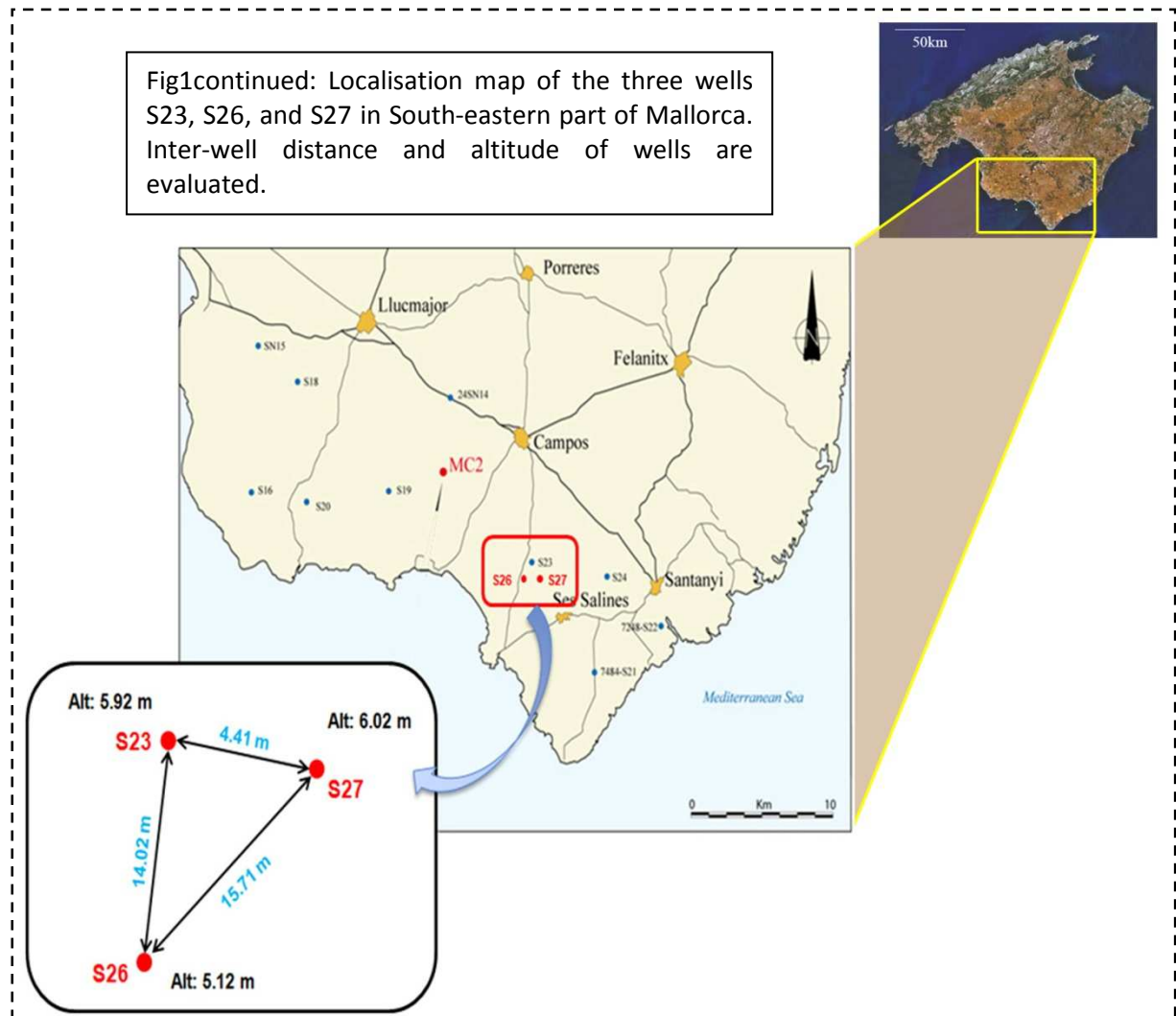
This anomaly identified in Font Sant is interpreted as filled-paleokarst created by dissolution process, due to geo/hydrothermal fluids circulation through an eventual fault that affects the limestone (Font Sant fault). Although hydrothermal activity is proved in regional-scale, the existence of possible hydrothermal fluids flow in our study area is just a hypothesis, according to the anomaly detected in this local zone.

Thus this paper, from core and thin sections, intends to provide criteria showing existence of possible Fault associated to geo/hydrothermal fluid circulation in this area.

A substantial part of the investigation is centred on geological aspects, in order to characterize the karst-fractured reservoir in term of lithofacies, karst features, deformation (fracture) and porosity. This paper consists also in realize diagenesis analyses from thin sections, that permit to define the nature (meteoric or burial) of distinct karst development affecting Santayi limestone. These analyses are also used to characterize the impacts of diagenesis processes associated to karst action, on petrophysical parameters of the reservoir. Geochemical studies and cathodoluminescence microscopy are in addition realized completing diagenesis analyses done from thin sections.

In order to well estimate the quality of Font Sant reservoir, petrophysical analysis from X-Ray core image is done. In addition to evaluate virtually the porosity of rock, this virtual technique is also used to visualize in 3D the porous network, especially meso and macro porous network (pores created by karst action), in order to define the pore connectivity of this karst-reservoir.

For realized this investigation, three wells have been drilled (Fig1) in the karst-fractured aquifer: S23, S26, S27. Contrary to S26 and S27 the drilling of S23 is destructive; therefore there is no core for this well. Nevertheless log data are available in every well (Gamma ray, ph, conductivity...).



II) Geological setting

Belong to the large archipelago of the Balears; Mallorca is the biggest island of the insular complex

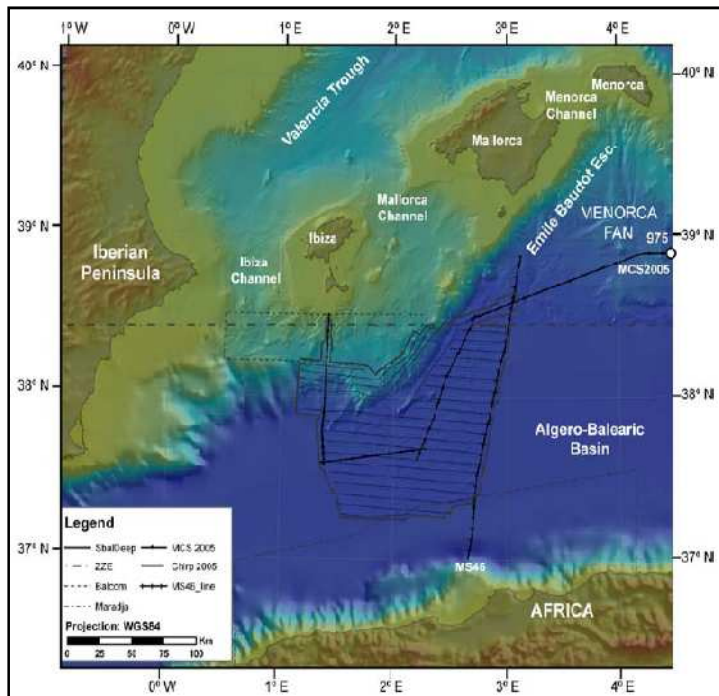


Fig2: Location map of the Balearic promontory from Costa et al., 2008.

Mallorca is the biggest island of the insular complex of Balears. The Balearic Islands (Mallorca, Menorca, Ibiza, Formentera and Cabrera) are the emerged part of a ridge: “the Balearic Promontory”, which extends into the western Mediterranean Sea. The Balearic promontory is 348 Km in length, 150 Km wide and from 1000 m to 2000 m in high (Fig2).

It is located between the Balearic-Provencal basin to the north and the Balearic-Algerian basin to the south. Its southwest end is attached to the Iberian Peninsula margin but further northeast it is separated by the Valencia Trough collecting the terrigenous inputs from the Ebro margin (Canal et al., 2004).

The Southeastern end of the

archipelago is limited by a NE-SW scarp, the Emile Badot Scarp (EBS), which has been interpreted as

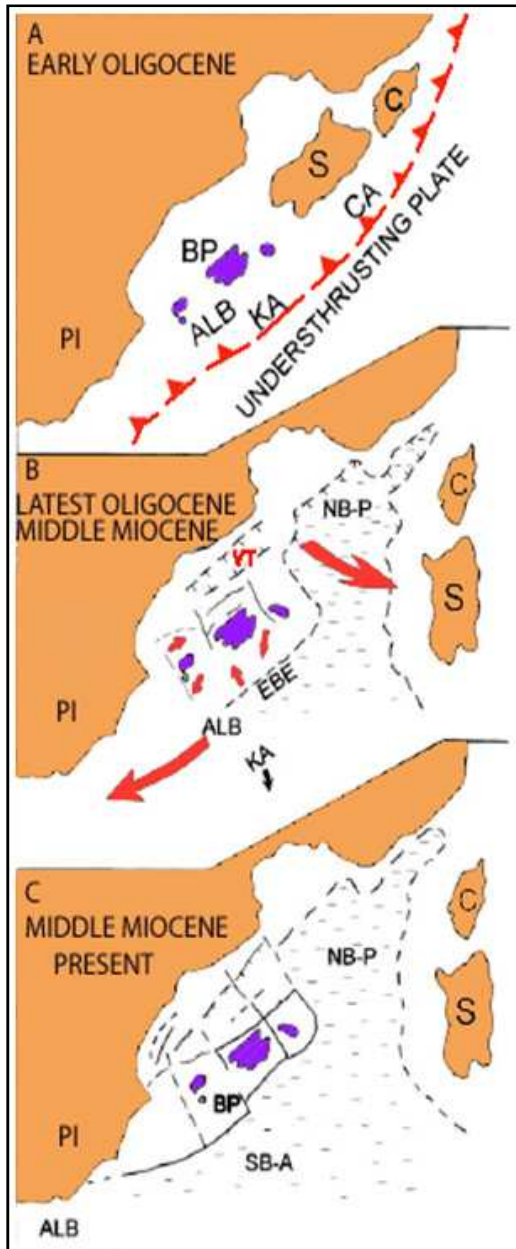
of possible transform fault, early Neogene in age, formed as the Corso-Sardo block rotated counter-clock away from the Gulf of Lyon by Acosta et al.2001.

Kinematics/Geodynamic:

The present configuration resulted from a combination of the pre-Oligocene subduction of Africa beneath Eurasia, the Oligocene rifting/drifting and the oceanic accretion during the Miocene (Rehault et al., 1985).

This configuration features of the Balearic Promontory is due to the clockwise rotation of Mallorca and Evisa blocks, resulting from the West-ward migration of the Alboran Microplate (Acosta et al. 2001).

This West-ward migration is directly related to the convergence between African and Eurasian plates in the region of Gibraltar that subsequently led to the alpine orogenesis and after in the late Oligocene –early Miocene to the opening of the Gulf of Lyon.



As the Alboran microplate moved westerward along the EBE, the blocks making up the Balearic Promontory were made to rotate clockwise (Parés, Freeman, & Roca, 1992) and the South Balearic-Algerian basin behind the micro-plate opened by rifting and subsequent sea floor spreading.

As the islands moved away from the Spanish margin during the clockwise rotation in the late Oligocene-middle Miocene along the transform faults, the Valencia Trough (VT) opened behind them (Fig).

Synchronous with the opening of the through, clockwise rotation in the late Oligocene-middle Miocene of the Mallorca and Ibiza blocks led to compression (Fault and fold) along the northwest and southeast sides of both islands and between Mallorca and Menorca. This deformation supposedly was the consequence of the concurrent westerly displacement of the Alboran microplate in south of the islands (Vegas, 1992).

The compressive phase was followed by an extensional phase that was initiated with the opening of the South Balearic–Algerian Basin (ALB) behind the Alboran micro-plate (Vegas, 1992) corresponding to a back-arc basin. This extensional phase led to the collapse of the Balearic Promontory to form the Central rift (CR) in Mallorca and the over 1000m deep Central depression (CD) between Mallorca and Ibiza.

Fig 3: Schematic diagrams showing the tectonic evolution of the western Mediterranean from early Oligocene to present. From Acosta et al.2001. ALB=Alboran microplate; BP=Balearic Promontory; CA=Calabria microplate; S=Sardinia; C=Corsia; KA=Kabylies; NB-P=North Balearic Provençal Basin; SB-A=South Balearic-Algeria Basin; VT=Valencia Trough.

This Mediterranean geodynamics history, affecting the different islands of the Balearic Promontory, allows to understand the current morphological configuration of Mallorca Island. According to Robledo (2005), Mallorca presents six geomorphological units: 1) The Serra de Tramuntana, 2) the Serres de Llevant, 3) The Serres central, 4) The Neogene basins, 5) The Lluçmajor platform and 6) The Santanyi platform.

1) Geology of Mallorca

Island of Mallorca is characterized by grabens and horsts topographical configuration (Fig4) that resulted from combination of Late Miocene to Early Pleistocene compressive and extensional phase (Pomar, 2006). The both phase are related to the clockwise rotation of Alboran microplate.

The Northwestward, the Southeastward and central part of the island were established mountain ranges oriented NE-SW (Serra Tramuntana, Serra Llevant and Serres Centrals). The highlands, from Mesozoic to Lower-middle Miocene in age, correspond to horst-blocks of the alpine fold belt.

Surroundings this ranges are located Plio-Pleistocene conglomeratic basins (Palma, Inca, Sa Pobla and Campos). These grabens consist in subsiding areas with heights inferior at 100 meters.

Upper Miocene carbonate deposits onlap the folded Mesozoic to Middle Miocene rocks, building sub-horizontal shelves (Marina Lluçmajor and Marina Santanyi) around the ranges and filling the subsident basins (Palma, Inca, Sa Pobla and Campos). Subsidence occurred in relation to normal faults principally during the Pliocene and early Pleistocene (Pomar 1991). The Lluçmajor platform is spreading up to 20 Km; its height is increasing from SE to NW up to 90 m in Cabo Blanco. The Santanyi platform, localized in Southwestward of the island, is 60 km in Length and on the average 30 km in high. This limestone deposits are overlade by Pleistocene eolianites.

The graben (Palma, Inca, Sa Pobla and Campos) filled by massif limestone and conglomeratic deposit are the result of the action of NE-SW post alpine normal listric faults with shifting of kilometers, of Miocene age. These normal faults shaping these rift are formed during the late Oligocene-middle Miocene extensional phase that led to the collapse of Balearic promontory.

The ranges (Serres Tramuntana, Llevant and Centrals), corresponding to horts result of Oligocene-middle Miocene compressive phase (Gelabert, 1998) associated to the clockwise rotation of Mallorca. These highland regions are folded (Post-Alpine anticlinal) and thrust (Fig5).

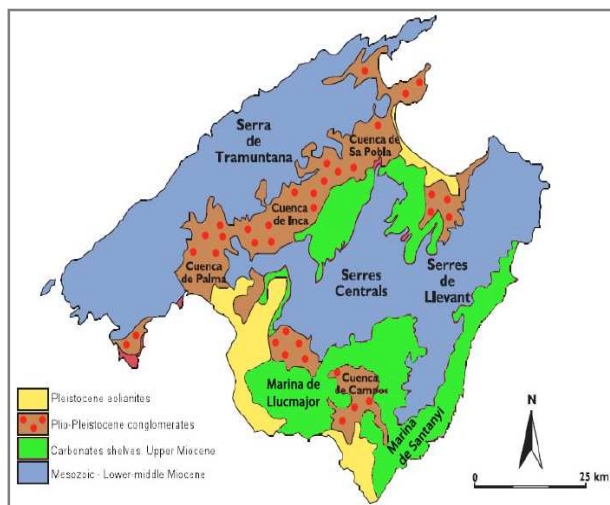


Fig 4: Geomorphological units of the island of Mallorca. From Robledo, 2005.

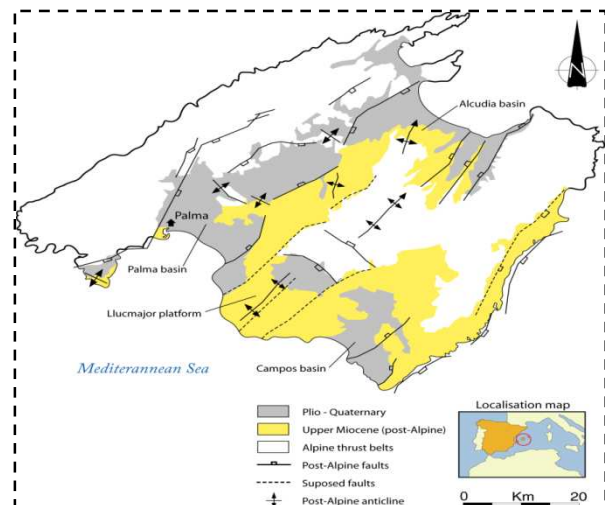


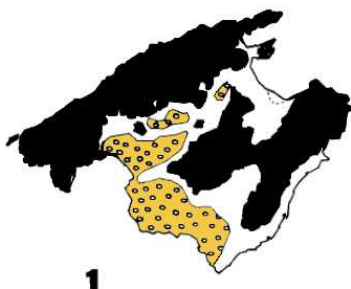
Fig 5: Structural map of the island of Mallorca.

2) Chrono-stratigraphy of Mallorca

2.1- Upper Miocene

The upper Miocene is extensively exposed on the Mallorca Island (fig4/5). This Late Serravallian-Messinian sequence is characterized by five major sedimentary units (Pomar, 1983).

Heterostegina Calcisiltites



The lower sequence (200 m in thick), Late Serravallian or early Tortonian Heterostegina Calcisiltites, is known from borehole data and small outcrops. It is composed of pebbly sandstone at its base, and a bioturbated bioclastic calcisiltites deposit with Heterostegina, red alga, bryozoa, miliolids, mollusks and echinoids (Pomar 2006). These bioclasts correspond to different shorface, foreshore and open-shelf non-reefal environment.

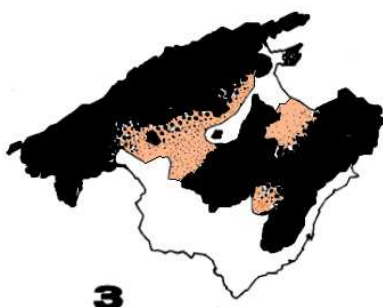
Reef complex



This Upper Tortonian-Lower Messinian unit is approximately 150 m thick and prograde over the basal Heterostegina Calcisiltites or over the folded basement (the case of non-deposit or total erosion of Heterostegina Calcisiltites).

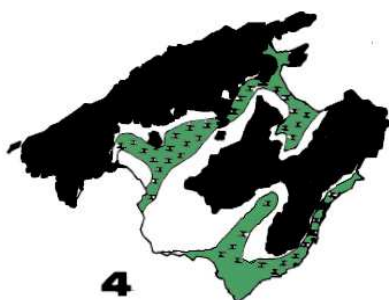
It is characterized by bioturbated calcisiltites and calcarenites (open-platform facies), large-scale clinofoms (reef-slope facies), extensive coral framestone (reef-wall facies) and horizontal grainstone to mudstone lagoonal deposits (Pomar, 1991).

Bonanova Marls



Messian sequence deposits, Bonanova Marls are composed of marl at the base, evolving upwards to conglomerats and red clays corresponding to alluvial fan deposits (Pomar, 1991). This 35 m thick sequence, found only surrounding the highlands (Serres Tramuntana, Llevant and Central), onlap unconformably the margins reef complex. It is overlain by the Santayi limestone or the Pleistocene eolianites (Pomar 2006).

Santayi limestones



Located to the Mallorca eastward behind Serre Llevant and to the western side of the Palma basin, this unit is interpreted as facies equivalent to the terminal Carbonate Complex corresponding to the latest Messinian in age (Pomar 2006).

They are formed by miliolid packstones and grainstones, stromatolitic bindstones and mudstones, and cross-bedded oolitic grainstone with stromatolites (Pomar 1991). These deposits overlie lagoonal deposits of the reef complex (Fig6).

Gypsum and Grey Marls

This unit corresponds to gypsiferous and grey marls with stromatolites and fish debris overlie the slope and basinal deposits of the reef complex (Pomar, 1991. Pomar, 2006). Its thickness seldom surpasses 10 meters (Pomar 2006). This sequence is interpreted as the equivalent of evaporitic deposits characterizing the Messinian age in the Mediterranean.

Stratigraphical correlation of the Messinian deposits

According to the lack of chronostratigraphical data and correlation problems because of the outcrop conditions and distribution, the stratigraphical relationship of these units remains doubtful:

The Gypsum and grey Marls represent a regressive succession of restricted shallow marine deposits which conformably overly the slope and basinal realms of the reef Complex.

The Bonanova Marls also represent a regressive succession on the top of the shallow reefal platform and may be correlated with the regression recorded by the Gypsum and Grey Marls.

The Santayi Limestone, however, represents a transgressive unit, overlying an erosional surface on top of the shallow realms (reef core and lagoon) of the reef complex. The erosional truncation at the top of this last unit might be correlated with the earlier mentioned regression (Gypsum and Grey marl). Nevertheless, the Santayi Limestone represents shallow open marine deposition on top of the shallow reefal platform.

2.2- Post Miocene rocks

Son Mir calcisiltites and Jordi Calcarenites

These units consist of a regressive succession with a maximum thickness of 370 m in the Palma Basin, overlaying a major erosion surface on top of previously described units toward the margins. Environments of deposition range from shallow marine (Son Mir calcisiltites) at the base, to eolian (San Jordi calcarenites) at the top (Fig6). Both units represent the latest infilling of the remaining basins rimmed by the Miocene reefs. The calcisiltites contain Ammusium and planktonic foraminifera. The foraminiferal assemblage dates this unit as early Pliocene.

Palma siltstones

Pleistocene deposits include up to 200-m-thick conglomerates (alluvial fan) and red silts in the grabens of Mallorca. These deposits un-conformably overlie the Sant Jordi Calcarenites, the reef complex and the Santanyi Limestones.

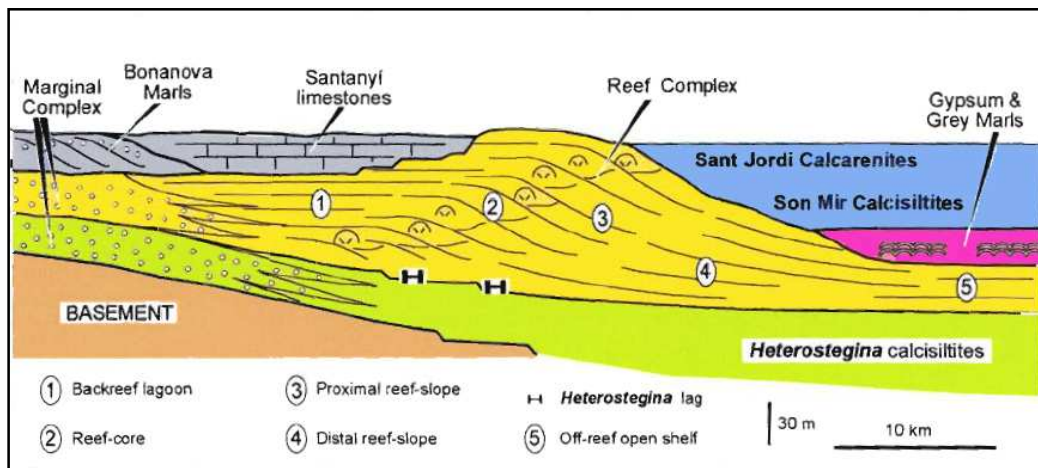


Fig 6: Stratigraphical cross-section of the late Neogene and Pleistocene depositional units in Mallorca; Modified from Pomar, 2006.

Related to the lowstands of sea level, the Messinian and early Pliocene regressive succession previously described, involved subaerial exposure episodes of the Late Serravallian-Upper Tortonian-Latest Messinian Limestone. Thus, Messinian age in Mallorca was characterized by the development of epigenic karst due to the directly infiltration of the acid meteoric water into the subaerial exposed rocks.

SERIES	STAGES	CICLES (3RD ORDER)	PLANKTONIC FORAMS BIOCHRONOZONES	Stratigraphic units MALLORCA	
HOLOCENE					
PLEISTOCENE		3.10	N23	Palma Silts	
		3.9	N22		
PLIOCENE		3.8	N21		
		3.7			
	3.5	3.6	N20		
		3.5	N19		
		3.4	N18	Sant Jordi Calcarenites Son Mir Calcisiltites	
UPPER MIOCENE	MESSINIAN	5.2		Santanyi Limestones Bonañova Marls	
		6.3	3.3	N17	Gypsum & Grey Marls
	TORTONIAN		3.2		Reef Complex Unit
				N16	
			3.1		Heterostegina Calcisiltites Unit
			N15		

Fig6continued: Chrono-startigraphic units of Mallorca; Modified from Pomar, 2006.

III) Sedimentology

In order to establish in Font Sant vertical changes in sedimentary facies, the cores S26 and S27 are wholly described. First a macro-description of core is realized in term of facies, karstic features and porosity. Subsequently this description is followed by a study of microscopic component (micro-facies, minerals, fossils, porosity) from thin sections permitting to refine first description done on cores. The thin sections, half-colored with alizarin to distinguish calcite from dolomite crystals, are sample in the bottom of plugs taken on the cores. Facies description proposed in this report corresponds to the synthesis of both descriptions (Macro/Micro), and the first well to be considered is well S-26.

1. Well S26

34.30 meters in length, this well consists of three main lithological units:

- Unit 1 (00.0 to 16.50 m): Skeletal grainstone and packstone.
- Unit 2 (16.50 to 21.00 m): Crystalline rock.
- Unit 3 (21.00 to 34.30 m): Polygenic breccias, probably corresponding to a karst cavity filled by the breccias.

On all along the well, grain size is medium to coarse, except the base of unit 1 that is composed of fine-grained chalky grainstone, and the fine-grained breccias of unit 3.

The main biological components of these facies are benthic foraminifers, bivalves, echinoids and red algae. Presence of detritic elements, principally grains of quartz, is frequently observed in these units.

Unit 2 and 3 show a high karst action probably due to the acid-meteoric-waters infiltration onto the rocks. Some fractures slightly tilted (5°) are mainly distinguished in the base of unit 1.

Porosity of unit 2 and 3 is generally fair to mean and consist to dissolution porosity (vugs, cavern and moldic porosity).

Nevertheless, unit 1 show a good primary inter-granular porosity which is slightly reduced by one late cementation process. These inter-particular voids are coupled with a good leached secondary porosity (vugs, caverns, channels).

a) Lithofacies description (S26)

Unit 1 : (Fig 7/8)

0.00 to 0.86 m: Skeletal medium-grained grainstones/packstones. Foraminifers (miliolids, penoroplis, and rovalia) are throughout abundant. Bivalves (mollusks, gastropods, and lamellibranches), red algae and quartz (%) are common.

According to their red tint, this rock is highly oxidized so probably altered by the oxygenated meteoric water (Fig7). Percentage of karst on this core section is estimated to 75%. Dissolution structures related to karst development are millimetric to centimetric scale.

Porosity is mean to high and mainly corresponds to a good primary inter-granular porosity. On some layers the initial porosity is totally occluded or slightly reduced by calcite cement. According to karst alteration of rock, this primary porosity is coupled with secondary dissolution porosity (cavern, vugs and channels).

0.86 to 0.95 m: Fine grain-size brown shale. Micro-facies of this shale has not been described because there are no thin sections on this core section.

0.95 to 1.7 m: Medium-grained grainstones/packstones rich in foraminifers (miliolids, penoroplis, rovalia) with bivalves (mollusks, gastropods), red algae, echinoids, and quartz.

The rock presents a red tint, so is highly oxidized too. Percentage of karst affecting this rock is estimated to 29, 3%. Structures (vugs and channels) associated to karst process are millimetric to centimetric scale.

Porosity is mean to good. The rock shows commonly a good initial porosity (inter-particular). Currently this primary porosity is slightly reduced or totally occluded by a late cementation process. Secondary voids (vugs, channel, and caverns) created by karst action come ameliorate the porosity.

1.7 to 1.82 m: Core zone corresponding to a void which is probably induced by karst action.

1.82 to 4.2 m: Medium-grained grainstones/packstones composed of abundant foraminifers (miliolids, penoroplis, and rovalia). Bivalves (mollusks, gastropods, and lamellibranches), echinoids are commons. Grains of quartz in some layers are common and in others are rare or absent.

The rock is oxidized too (rock colored in red). This core section is less karstified, so is better recovery. Percentage of karsts is estimated to 8.4 %.

Porosity is fair to mean. The inter-granular porosity is highly affected by calcite cementation. Actually initial porosity is slightly reduced and currently totally occluded by this cementation. Secondary leached porosity (vugs, channel, and cavern) arising from the low karst action is coupled with this primary inter-particular porosity.

4.2 to 9.00 m: Coarse-grained grainstone/packstone, which show a white tint. The rock is composed of plentiful foraminifers (miliolids, penoroplis, rovalia, uniserial/biserial forms). Echinoids, gastropods and red algae are common.

According to its white color, the rock is not oxidized. Nevertheless the core section presents a high rate of karstification which is estimated to 71%. Voids due to the karst action consist in structures of milli-metric to pluri-centimetric scale.

Total porosity is fair to mean. The primary inter-granular porosity is currently slightly reduced or totally occluded by calcite cement. Predominant porosity of this rock corresponds to a secondary dissolution porosity (moldic, vugs, channel) arising from leaching of bioclast's shells, or cement, and or packstone's matrix (karst action).

9.00 to 9.60 m: Coarse-grained grey grainstone with abundant foraminifers (miliolids, penoroplis, uniserial/biserial forms). Echinoids, bivalves (mollusks, gastropods) and red algae are common. The bioclasts, especially the bivalves, show a large size (Fig8).

According to the large size of the biological components, the rock presents a good depositional porosity: inter-granular porosity. This initial porosity is coupled in addition with secondary leached porosity: dissolution moldic porosity, vugs and channels.

9.60 to 16.5 m: Fine grain-size chalky grainstone/packstone composed of abundant foraminifers (miliolids, peneroplis, uniserial/biserial forms, rotalia). Echinoids are in mean common to abundant. Bivalves are common contrary to red algae which are rare. Some layers of the rocks contain large and small bioclasts (500 to 1000 µm in size).

Dissolution structures of milli-metric to centi-metric scale, due to karst action, highly affect the rock. These structures are commonly partly filled by red clay and calcite cement. In addition high density of fractures, which are slightly tilted, is recorded on the rock (Fig7).

These chalky grainstone correspond to a very cemented-facies. Thus, they denote a very poor primary inter-granular porosity. Predominant porosity corresponds to secondary dissolution porosity (caverns, vugs, dissolution moldic porosity, and channels) due to the karst action.

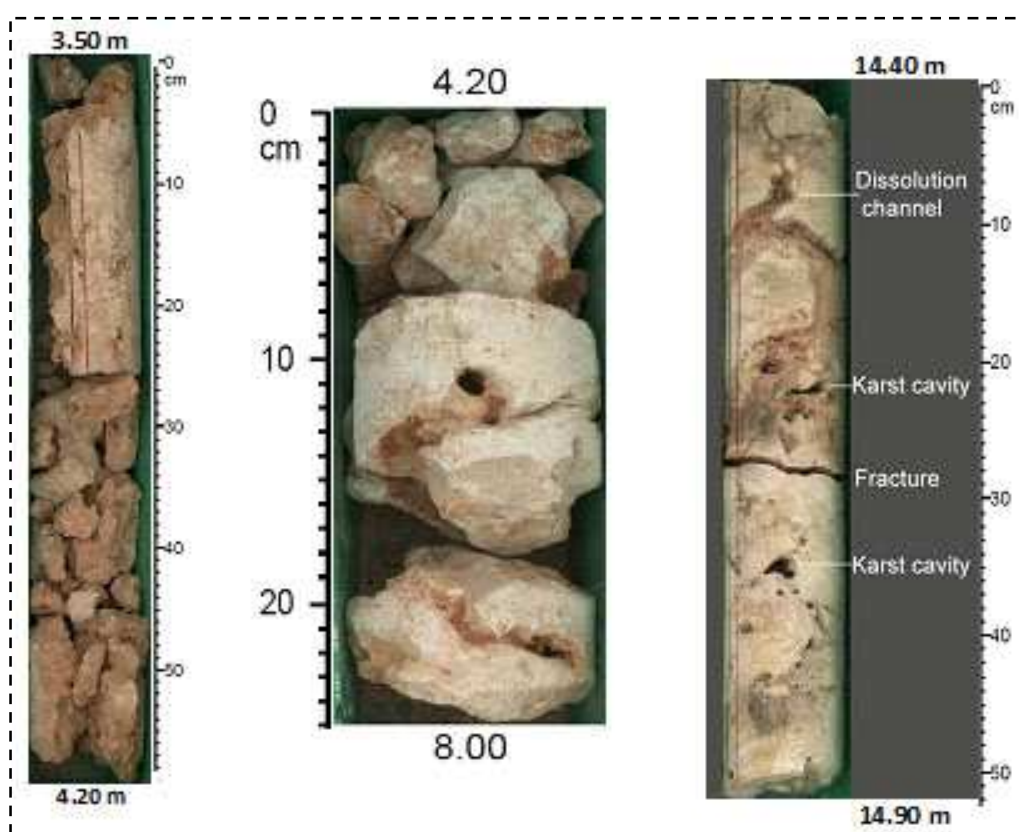


Fig7: Photo of core mainly showing the alteration (karstification and oxidation) of the rock due to the karst action. **Left:** Core section highly karstified and oxidized (red tint). This core section supposed length in 70 cm is 59 cm length. This shifting in length reflects the presence of karsts, millimetric to centimetric scale, onto the rock. **Centre:** White tint grainstone affecting karsts millimetric to centimetric scale. Supposed length in 3.80 m, this section is 25 cm length. So 93.42% of this core section is represented by voids created by karst process. Porosity of this section is so very good and corresponds to dissolution porosity. **Right:** Chalky grainstone affected by dissolution channels, which are totally filled by oxidized-insoluble-materials. Note the presence of karst cavity (millimetric to centimetric scale), and slightly tilted fracture.

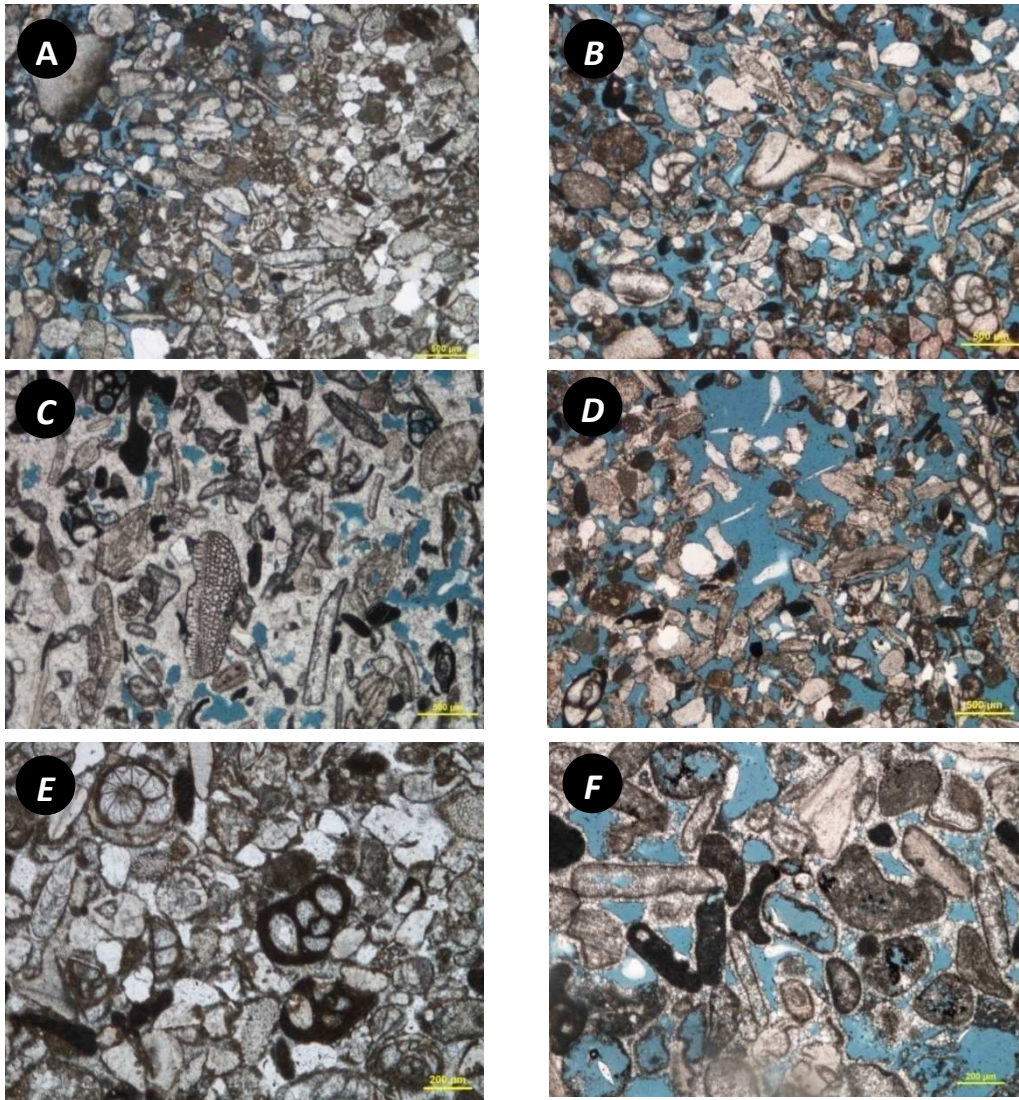


Fig 8: Thin sections illustrating the microfacies features of unit 1. **A:** Section showing the partial cementation of the oxidized rocks. Note the good inter-granular porosity of these facies. **B:** This primary inter-granular porosity is illustrated on this section. **C:** This layer of the oxidized rocks shows a total occlusion of its initial porosity. **D:** Inter-granular porosity coupled with a secondary leached porosity (Vugs and dissolution channels). **E:** The couple intergranular porosity/secondary dissolution porosity (dissolution channels and moldic) is illustrated on this thin section, taken in the white tint grainstones (5.63 m). The primary porosity is highly reduced by a calcite cementation. **F:** Chalky grainstones characterized by large fossils which are generally leached thus creating large pores. This secondary dissolution porosity is coupled with intergranular porosity slightly reduced by calcite cementation.

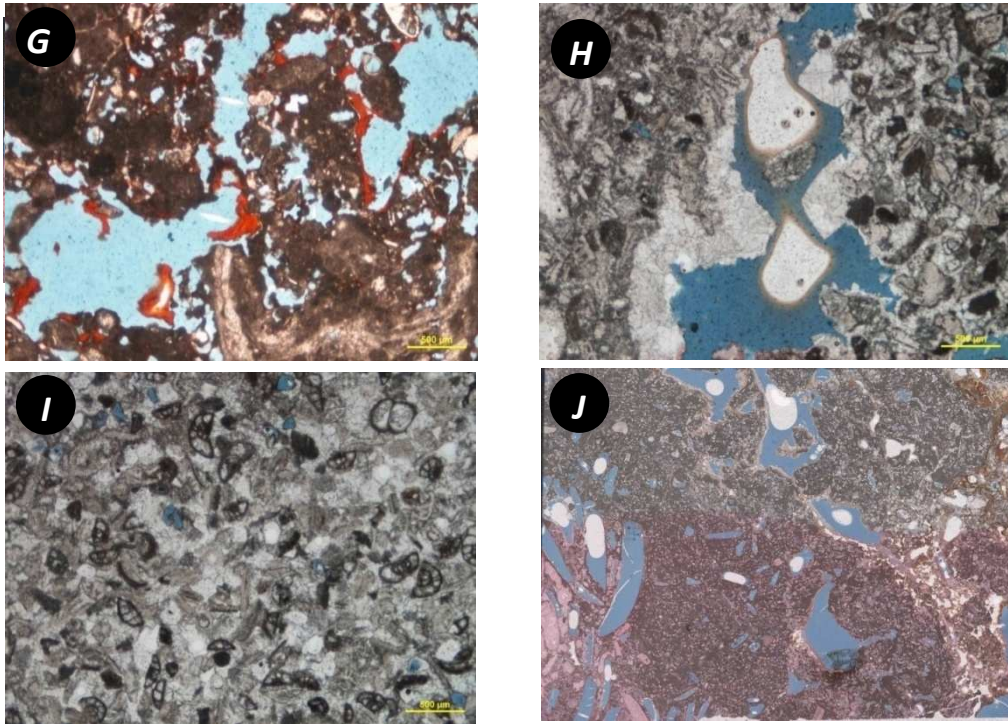


Fig 8 continued: Thin sections illustrating the microfacies features of unit 1 **G**: Packstone at 9.71 m mainly showing good dissolution porosity (moldic, dissolution channels and caverns). These dissolution pores are partly filled by red clay probably corresponding to the insoluble materials which are infiltrated in these voids during the karst action. **H**: The chalky grainstones present a high cementation (total occlusion of the primary porosity). These predominant porosity in these rocks corresponds to dissolution secondary porosity (Caverns, vugs and channels). The dissolution structures are commonly partly filled by calcite cement. **I**: This thin section shows the high cementation of these chalky grainstones rich in foraminifers. **J**: Scan of thin section illustrating the large dissolution pores present in some layer of packstone. These pores are created by leaching of large bivalve shells (Moldic porosity). Note the presence of other dissolution structures (vugs and channels).

Unit 2: (Fig9/10)

16.50 to 21.00 m: Carbonate rock constituted of coarse crystals of calcite, and microcrystal of quartz. Many deformation structures as stylolites and fissures are recorded on this rock (Fig10). The porosity is fair and is mainly represented by dissolution porosity (vugs and caverns). The dissolution structures are partly filled by organic matter and red clay. The rock has in addition a fair inter-crystalline porosity corresponding to the voids which are not yet filled by these coarse crystals of calcite (Fig10).

Unit 3: (Fig9/11)

21.00 m to 34.30 m: Polygenic breccias/Micro-breccias composed of carbonate pebble and grains of quartz. The rocks also contain lithoclasts, which are constituted of grains of quartz and carbonate pebbles (Fig9/11).

Some layers of this rock are highly dolomitized. Dolomites crystals principally show euhedral fabrics, and are characterized by theirs clear rims (Fig11). These particles are of micrometric to centi-metric size. The breccias are lithified by a white calcite matrix, confirmed by HCl test.

Porosity is poor, there is intraclast porosity arising from particle dissolution. Vugs and caverns, generated by leaching of the matrix, are represented too (Fig11). Nevertheless dolomitized layers show a very good porosity corresponding to inter-dolomite crystal porosity, and to a leached porosity arising from the dissolution of dolomite crystal's cores. From X-Ray images of these breccias, we will notice in addition that rock denote a good micro-porosity certainly corresponding to matrix porosity.

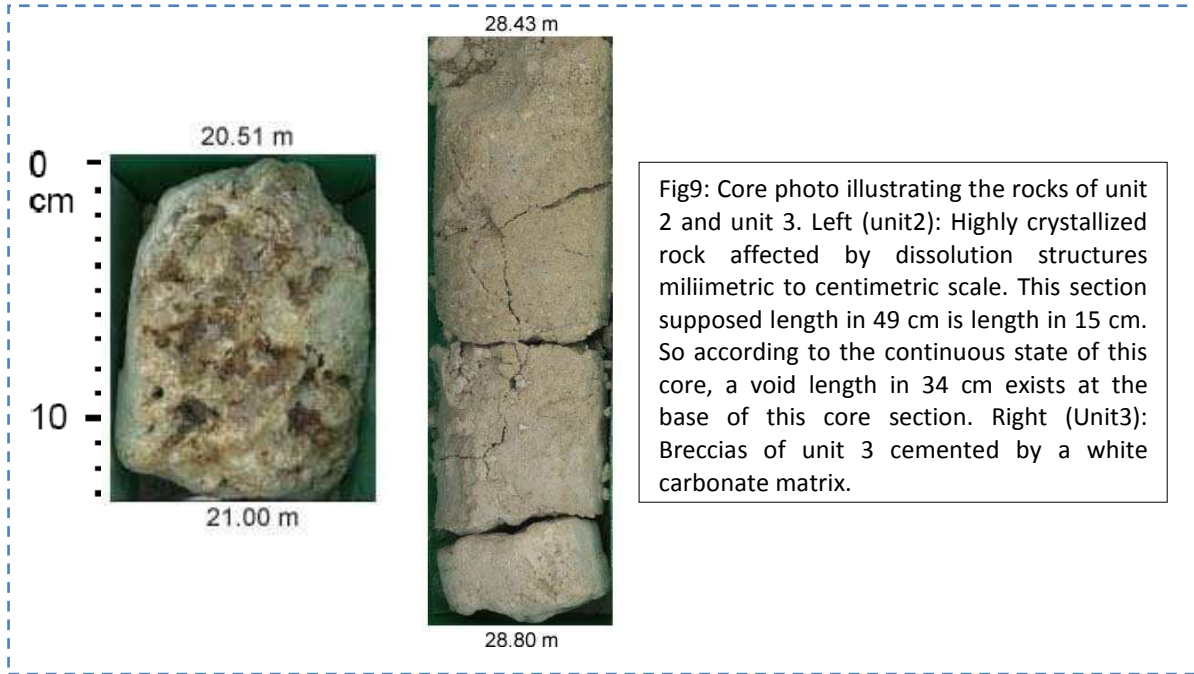


Fig9: Core photo illustrating the rocks of unit 2 and unit 3. Left (unit2): Highly crystallized rock affected by dissolution structures millimetric to centimetric scale. This section supposed length in 49 cm is length in 15 cm. So according to the continuous state of this core, a void length in 34 cm exists at the base of this core section. Right (Unit3): Breccias of unit 3 cemented by a white carbonate matrix.

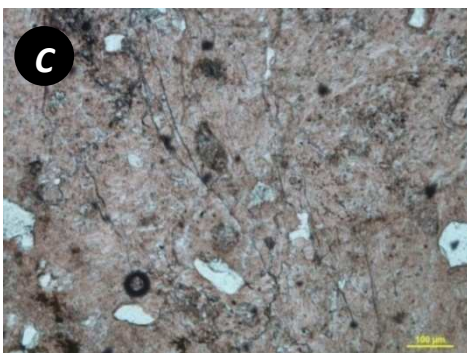
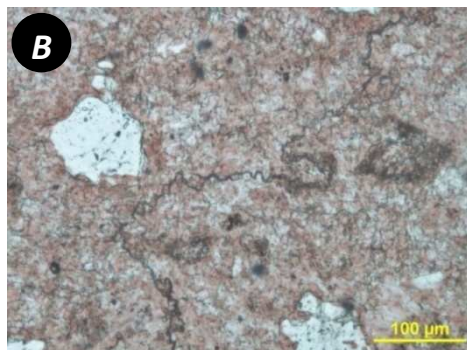


Fig10: Thin sections illustrating the texture of unit2 rocks.
A: These crystallized rocks are composed of coarse crystal of calcites and quartz crystal.
B/C: Deformation structures like stylolites and fissures affect these rocks.

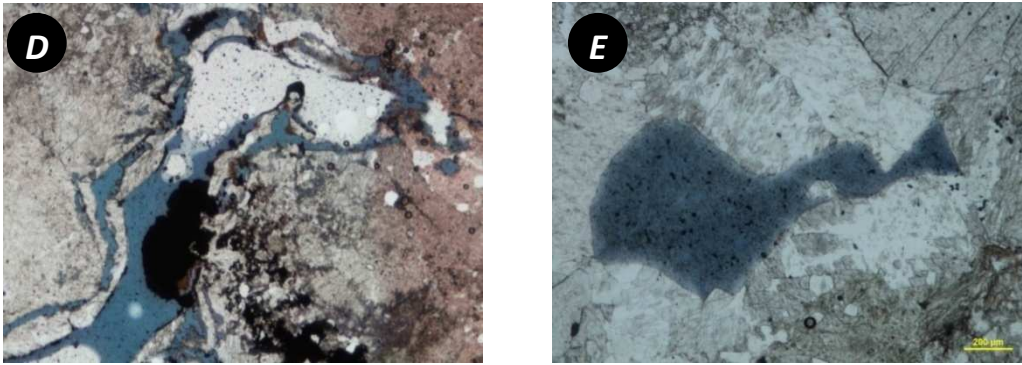


Fig 10 continued: Thin sections illustrating the texture of unit2 rocks. **D:** According to the high crystallisation of these facies the porosity is mainly represented by crystal dissolution porosity (caverns and vugs) which is partly filled by red clay and organic matter. **E:** Inter-crystal porosity is coupled with the leached porosity and is progressively occluded by growth of calcite crystals.

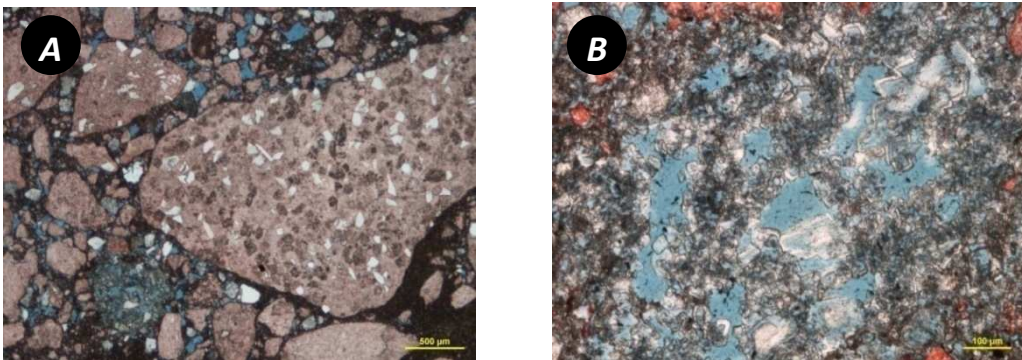


Fig 11: Thin sections illustrating the texture of the unit3's rocks. **A:** Composed of carbonate pebbles, crystals of quartz and lithoclasts, this breccias show a fair to mean inter-granular porosity. **B:** Dolomitized layers of these breccias present a good porosity. Inter-crystal dolomite porosity is coupled with a very good late porosity created by the selective leaching of the core of dolomite crystals.

Mangane Papa Ousmane M2 RG 2008-2009

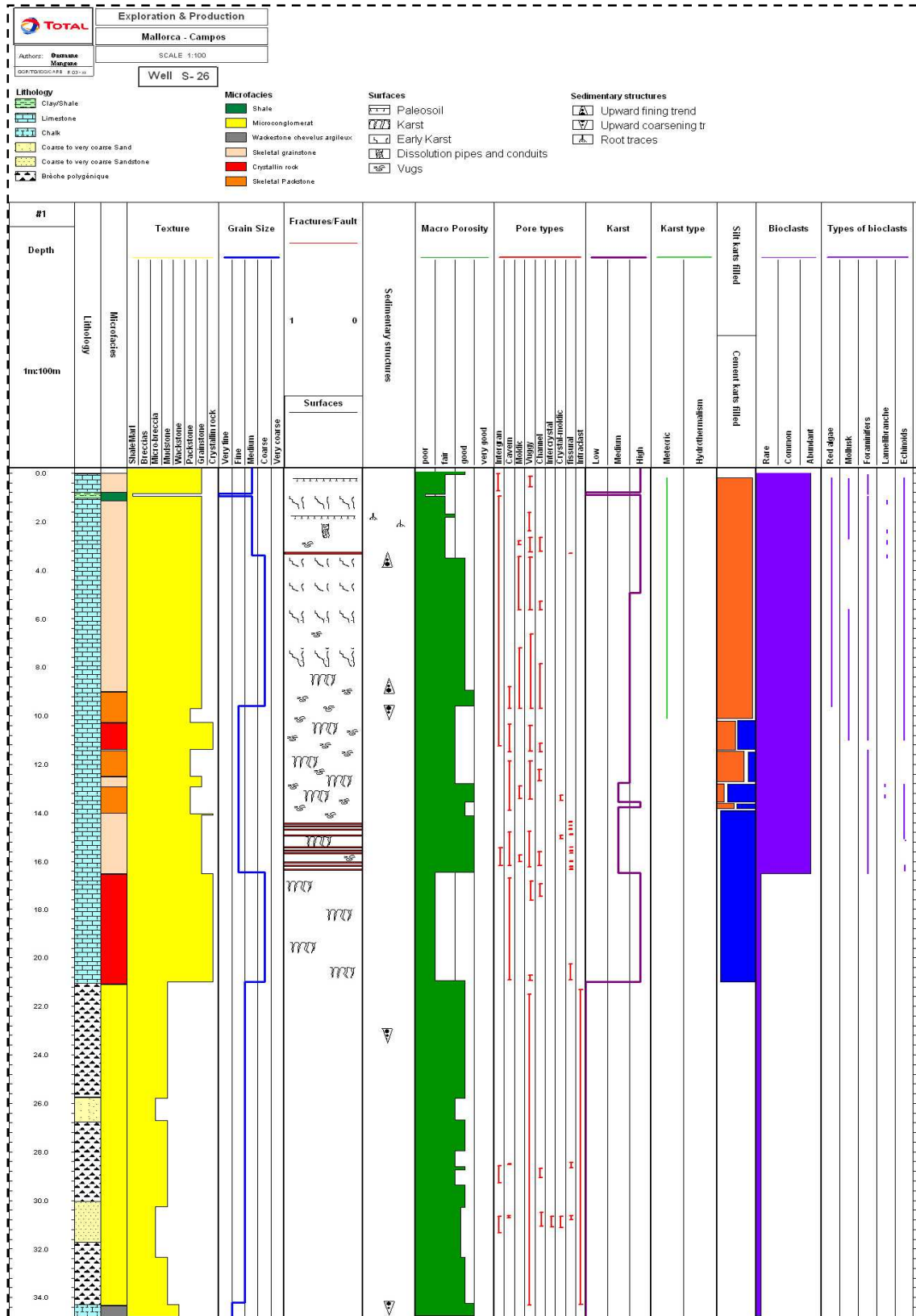


Fig12 : Descriptive log of Well S-26 using the software Wellcad

b) Log data analysis: (Well S6)

From logging campaign, in collaboration with Geosciences Team of Montpellier 2 university, borehole data are acquired on all the wells S23, S26, S27:

Gamma ray log, Potassium/Thorium/Uranium log, Conductivity and Ph log, Electrical log (ILD) and magnetic log (ILM).

The analysis of these log permits to characterize in term of geophysics' the different lithological units and especially to distinguish the actual horizontal limits of the Font Sant aquifer (Vadose zone/Phreatic zone/Mixing zone).

Unit 1 (00.0 to 16.50 m): This sequence corresponds to a low resistive zone. This characteristic proves and confirms that rocks of unit 1 are poorly compact, so highly affected by karts (Fig13).

pH and conductivity data are only evaluated in an aquatic context. So the superficial part of unit 1 (0.00 to 5.40 m), where these data are not available, corresponds to the emerged zone of this basin. This subearial-exposed zone can be interpreted as the vadose zone. Actually, according to the percentage karst log and the core description, this part consists to oxidized and highly karstified rocks due to the infiltration of acid meteoric water onto the subearial rocks.

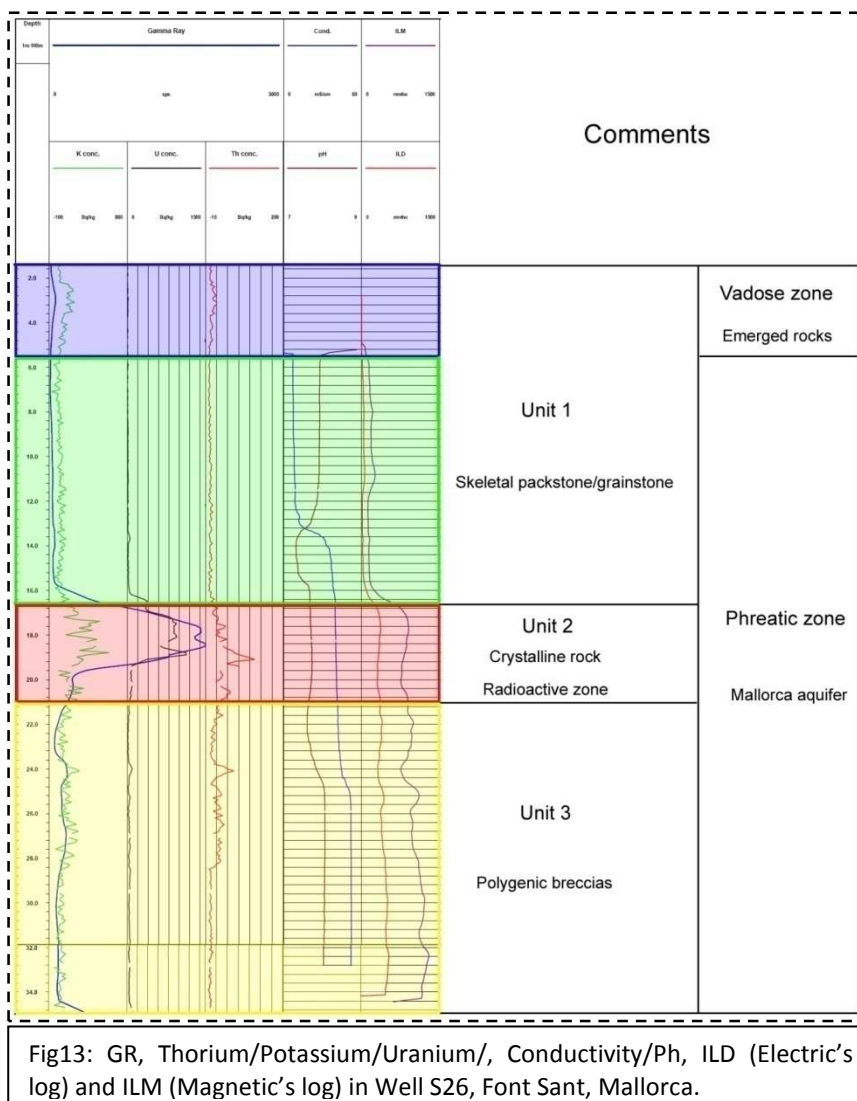
From 5.40 m pH and Conductivity data are available, so this depth can be interpreted as the actual level of water table which is the transition of vadose and phreatic zone. From 5.40 to 12.27 m conductivity log is stable with a low value (7.55 mS/cm) providing the presence of fresh water lens in this zone. In addition the pH log, constant too, show an acid features (pH = 7.9) of this fresh water. So this zone corresponds actually to the phreatic zone consisting to a fresh and acid water lens created by the infiltration of acid meteoric water from surface toward the water table.

From 12.27 to 16.50 m the conductivity is slightly increasing and in the other hand the pH is slightly decreasing (Fig13). The slightly variations of these parameters result probably from mixing between a fresh-acid water and a salt-basic water. Related to the over-drafting due to agricultural use, Mallorca aquifer is in fact currently affected by marine water intrusions which create a phreatic water/salt marine water mixing.

Unit 2 (16.5 to 21.00 m): Contrary to unit 1, rocks of unit 2 are characterized by a high Electric's resistivity. This geophysics' result provides and confirms the compact feature of these facies corresponding to crystalline rocks with a poor porosity.

Gamma ray, Uranium, Potassium and Thorium logs show a substantial peak corresponding to the radioactive anomaly distinguished in Font Sant. This high radioactivity will be subsequently interpreted from diagenesis studies.

Unit 3 (21.00 to 34.30 m): Similar to unit 2, this third lithological zone show a high Electric's resistivity providing and confirming the compact features of the facies of this unit. In fact these lithofacies corresponds to cemented breccias, so rocks very compact with a poor porosity.



2. Well S27

In this core, length in 28.15 meters, the same three units as those observed in well S26 have been identified:

- Unit 1 (0.00 to 14.10 m): Bedded bioclastic grainstone and packstone.
- Unit 2 (14.10 to 19.83 m): Crystalline rock
- Unit 3 (19.83 to 28.15 m): Polygenic breccias

Similar to core S26, the grain-size all along the core is generally medium to coarse, except the base of unit 1 and unit 3's breccias corresponding to fine-grained rocks. The main bioclastic components of these facies are benthic foraminifers, bivalves, echinoids and red algae. Similar to well S26, detritic elements specially the grains of quartz are common to abundant.

The two first units are highly karstified and altered probably related to infiltration onto the land of acid-meteoric waters. The fractures slightly tilted (5°) are identified.

Unit 2 and unit 3 show a fair to mean porosity. The predominant porosity in these units corresponds to secondary dissolution porosity (vugs, cavern and moldic porosity). Unit 1 shows a good inter-granular primary porosity. Currently the initial porosity is slightly reduced or totally occluded by a late cementation process. In addition, the initial porosity of unit 1 is coupled with a good leached secondary porosity (vugs, caverns, channels).

a) Lithofacies description (Well S27)

Unit 1: (Fig14/15/16/17/18)

0.00 to 2.80 m: Medium-grained grainstone/packstone with abundant foraminifers (miliolids, peneroplis, nummilites, planktonic foraminiferal ooze, universal/beserial forms). Echinoids, red algae and bivalvs (gastropods) are common. Grains of quartz are too frequent in this facies. Some root traces are observed at 1.00 meters.

According to their red color the rocks are oxidized, and are highly altered (Fig14). The percentage of karst on this core section is mean. The dissolution structures are of millimetric to centi-metric scale. Currently the rocks show a high cementation. Porosity is so fair to mean. The predominant porosity of the rocks is secondary dissolution porosity (vugs, channel, caverns and dissolution moldic porosity) arising from karst action (Fig16). The leached porosity is coupled with a poor to fair initial inter-granular porosity. Actually this primary porosity is generally slightly reduced or totally occluded by late calcite cement. Nevertheless on some layers the rocks denote a good primary inter-granular porosity.

2.80 to 6.55 m: Coarse white tint grainstone/packstone (Fig14/17). These facies are rich in foraminifers: miliolids, peneroplis, nummilites, planktonic foraminiferal ooze, universal/beserial forms. Echinoids, gastropods, red algae and grains of quartz are commons.

These deposits correspond to fine-laminated facies. The beds are slightly tilted (up to 5°) or horizontal.

According to their white color, the rocks are not oxidized. This core section is highly affected by dissolution structures (vugs, caverns and dissolution channel) which are milli-metric to pluri-centimetric scale. Late calcite cement partly fills these voids.

Porosity is good and mainly represented by dissolution porosity (vugs, channel, and dissolution moldic porosity). The secondary leached porosity is coupled with a fair initial inter-granular porosity.

6.55 to 6.87 m: Skeletal wakstone (Fig14/18) with abundant echinoids and foraminifers (miliolids, peneroplis, nummilites and biserial forms). Gastropods, red algae and grains of quartz are common.

Porosity is fair. Dissolution porosity is the predominant porosity: Moldic porosity (partial dissolution of bioclast), and vugs and dissolution channels (dissolution of the matrix). This leached porosity is coupled with fissure porosity.

6.87 to 8.01 m: Coarse-grained grey grainstone (Fig14/19) composed of small shells bioclasts. The rock is rich in foraminifers (numilites, penoroplis and miliolids). Some echinoids are observed.

Sedimentary features are present as fine parallel litages slightly tilted (up to 5°) or horizontal.

The dissolution of the large shells generates a good moldic porosity. This leached porosity is coupled with a good inter-granular porosity. Both are slightly reduced by late calcite cement.

8.01 to 14 m: Fine-grained-size grainstone with abundant foraminifers: Peneroplis, miliolids, nummilites, planktonic foraminiferal ooze and uniserial forms. The rock shows a chalky aspect (Fig15/20). Echinoderm and red algae are commons. Grains of quartz are rare.

The rock is very compact and cemented. Many dissolution structures (vugs and channels) due to karst action affect the rock. These structures are millimetric to centimetric scale. In addition the compact grainstone is also affected by many deformation structures as slightly-tilted (up to 5°) fractures.

Porosity of the rock is very variable. Shells are often dissolved that imply good moldic porosity. Other dissolution porosities as vugs and caverns are created by late leaching of the cements, probably due to the karst action. Nevertheless these voids are slightly reduced by a partly filling of red clay or by further calcite cementation. Fair primary inter-particle porosity is coupled with this secondary dissolution porosity.

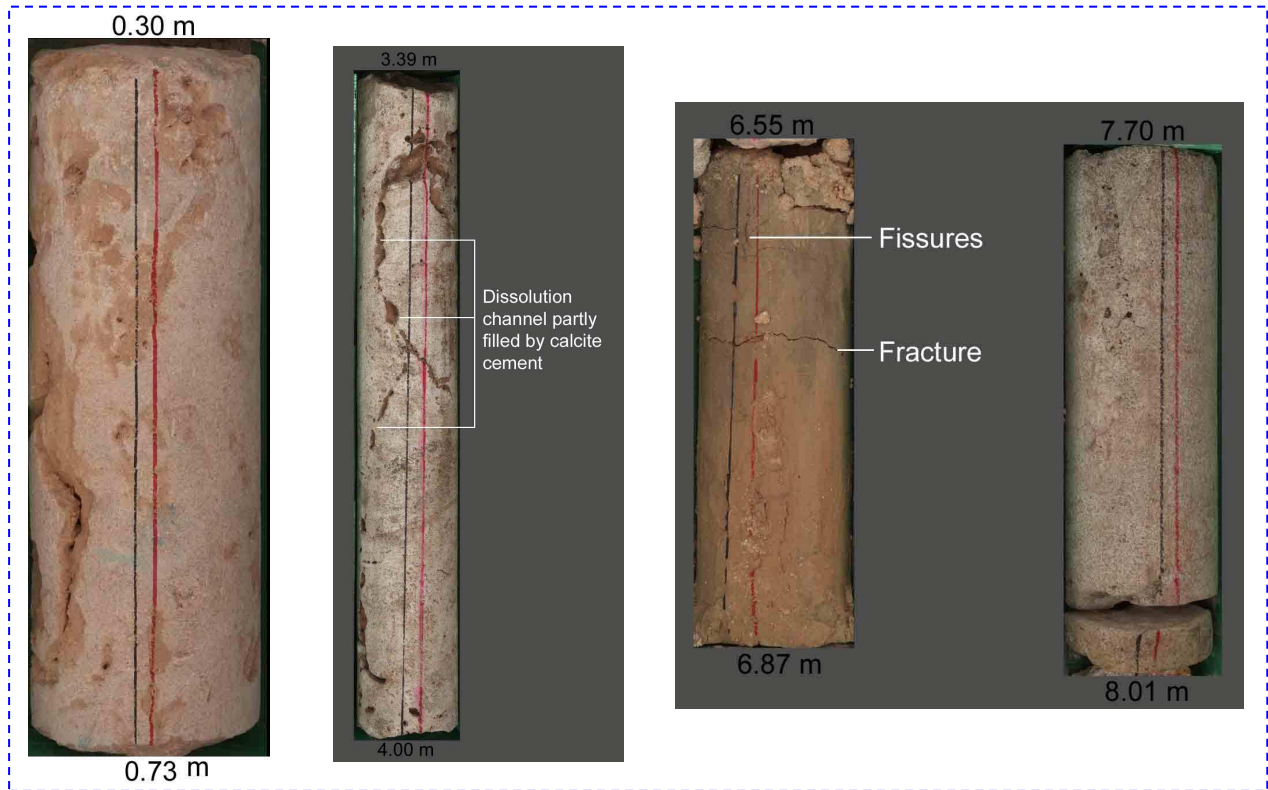


Fig14: Photo of different core sections of unit1. Left: According to its red tint, this core section corresponds to highly oxidized rocks. Oxygenise fluids alterate these facies creating dissolution structures (dissolution channels, vugs, caverns) onto the rocks. The dissolution channels show a sub-vertical geometry. Centre: No-oxidized laminated grainstone affected by vertical dissolution channels partly filled by calcite cement. The rocks show other dissolution structures like vugs. Right: The core setions of the brown shales and the grey grainstones of unit 1 are illustrated on this picture . The brown shales corresponding to sekeletal wakstones facies are affected by deformation structures (fissures and fractures). The last picture presents the coarse-grained grey grainstone.

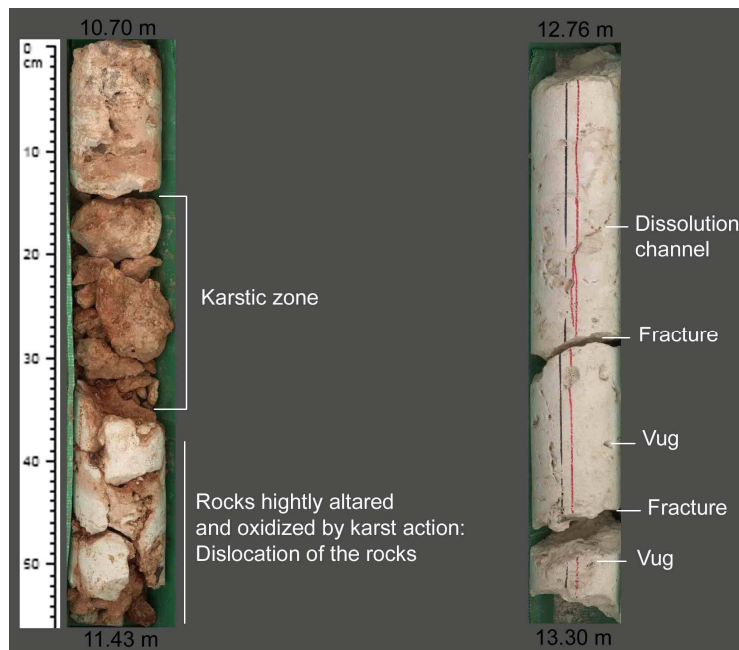


Fig15: Photo of core illustrating the chalky grainstone of unit 1. Left: Core section highly karstified and oxidized according to the red tint of rocks. The core section supposed length in 73 cm is 56 cm length, so 23% of this section is represented by voids created by karst action. The infiltration of fluids associated to the karst action, involve a dislocation of the rocks. Right: This chalky grainstone are affected by fractures slightly tilted and dissolution structures (dissolution channels and vugs)

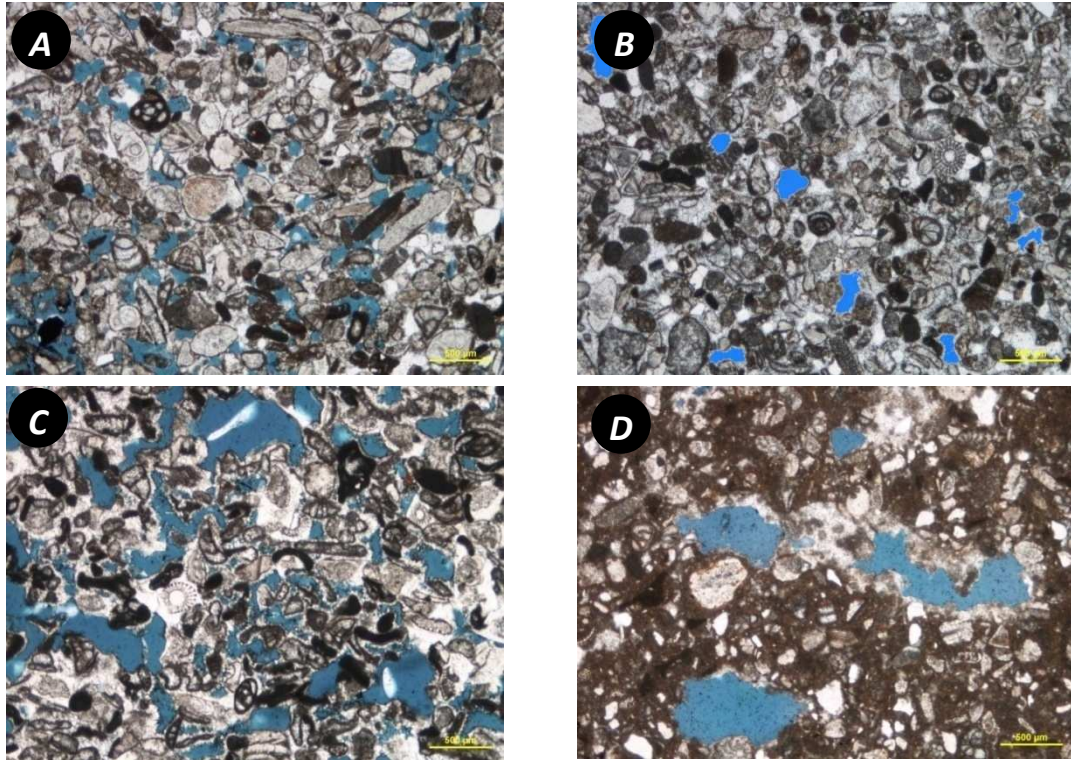


Fig16: Thin sections illustrating the facies of the oxidized-rocks of unit1. A: Lot of layers of the grainstone of these rocks denote a good primary inter-granular porosity which slightly reduced by calcite cement. B: Currently this initial porosity is totally occluded by calcite cement. C: Nevertheless secondary dissolution porosity is coupled with the primary porosity ameliorating the capacity of stocky of this part of Font Sant reservoir. The cementation of initial porosity is probably due to the re-precipitation in situ of dissolution saturated-fluid. D: The skeletal packstone of this oxidized section denote principally a leached porosity (vugs and channel) arising to the dissolution of the matrix.

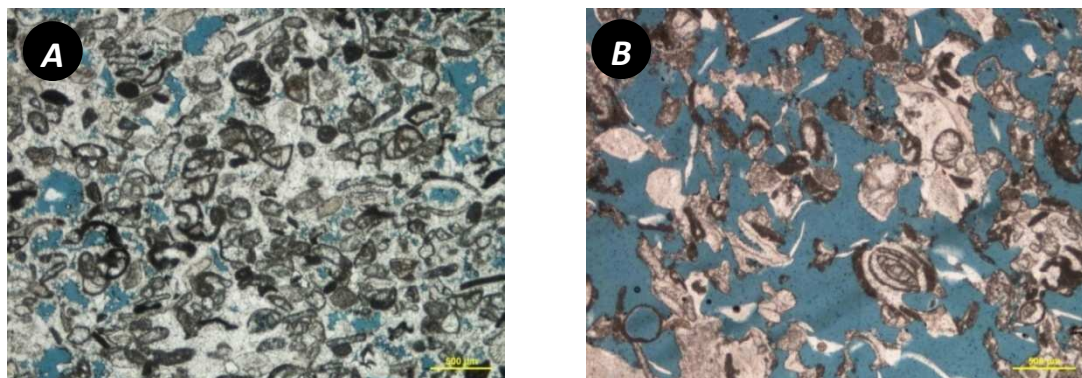


Fig17: Facies of the non-oxidized grainstone (white tint grainstone). A: The initial inter-granular porosity of this grainstone is highly reduced by a calcite cementation. B/C: Actually secondary leached (moldic and vugs) porosity coupled with this primary porosity is the predominant porosity in these rocks.

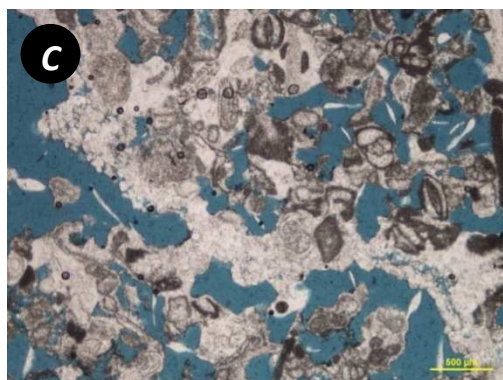


Fig17 continued: Facies of the non-oxidized grainstone (white tint grainstone).

B/C: This high leaching affecting these grainstone is illustrated on these thin sections characterized by a presence of vugs and dissolution channels. We notice that a late calcite cementation come slightly reduce the secondary dissolution porosity.

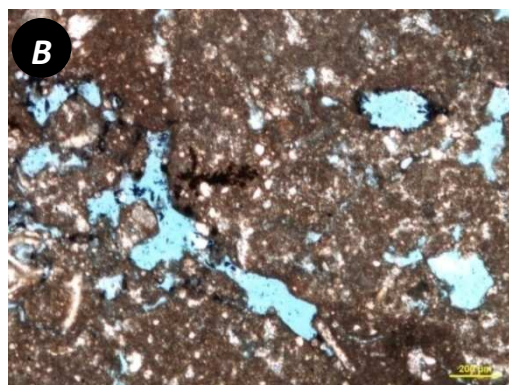
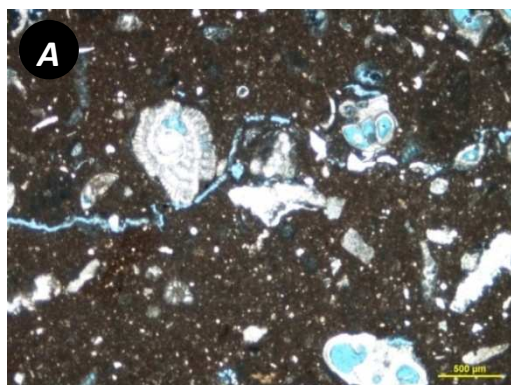


Fig18: Thin sections illustrating the facies of the brown shales. These shales (**A and B**) correspond to the skeletal wackstones denoting a good dissolution porosity arising as well to the leaching of the matrix (vugs and channel) as the dissolution of fossil shell (dissolution moldic). Fissure porosity is also represented in these facies.

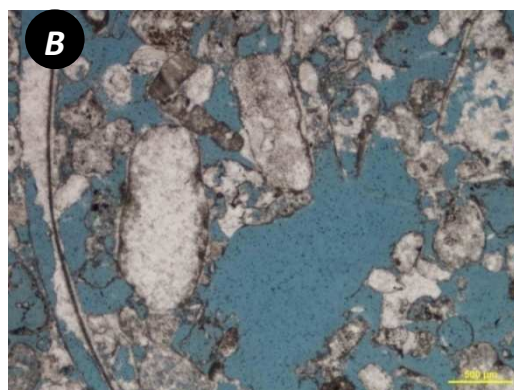
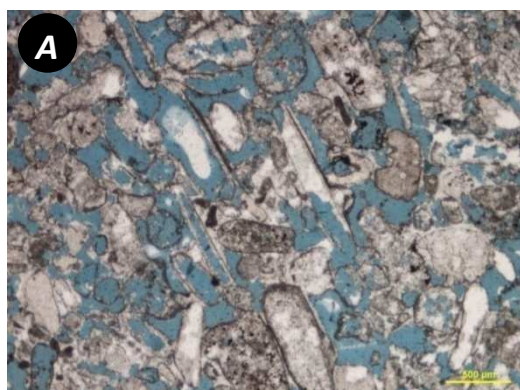


Fig19: Sections showing the facies of the grey grainstone (**A/B**). According to the large bivalves composing the rocks, the inter-granular porosity is very good and corresponds to large voids. On some layers these voids is slightly reduced by calcite cementation. In addition, secondary dissolution porosity is coupled with this good initial porosity. The secondary porosity of these facies arises well as from the leaching of bivalve's shells (dissolution moldic porosity) as from leaching of pre-existent cement (vugs). The slightly cementation of the initial porosity is probably due to a late re-precipitation in situ of dissolution sursaturated-fluid.

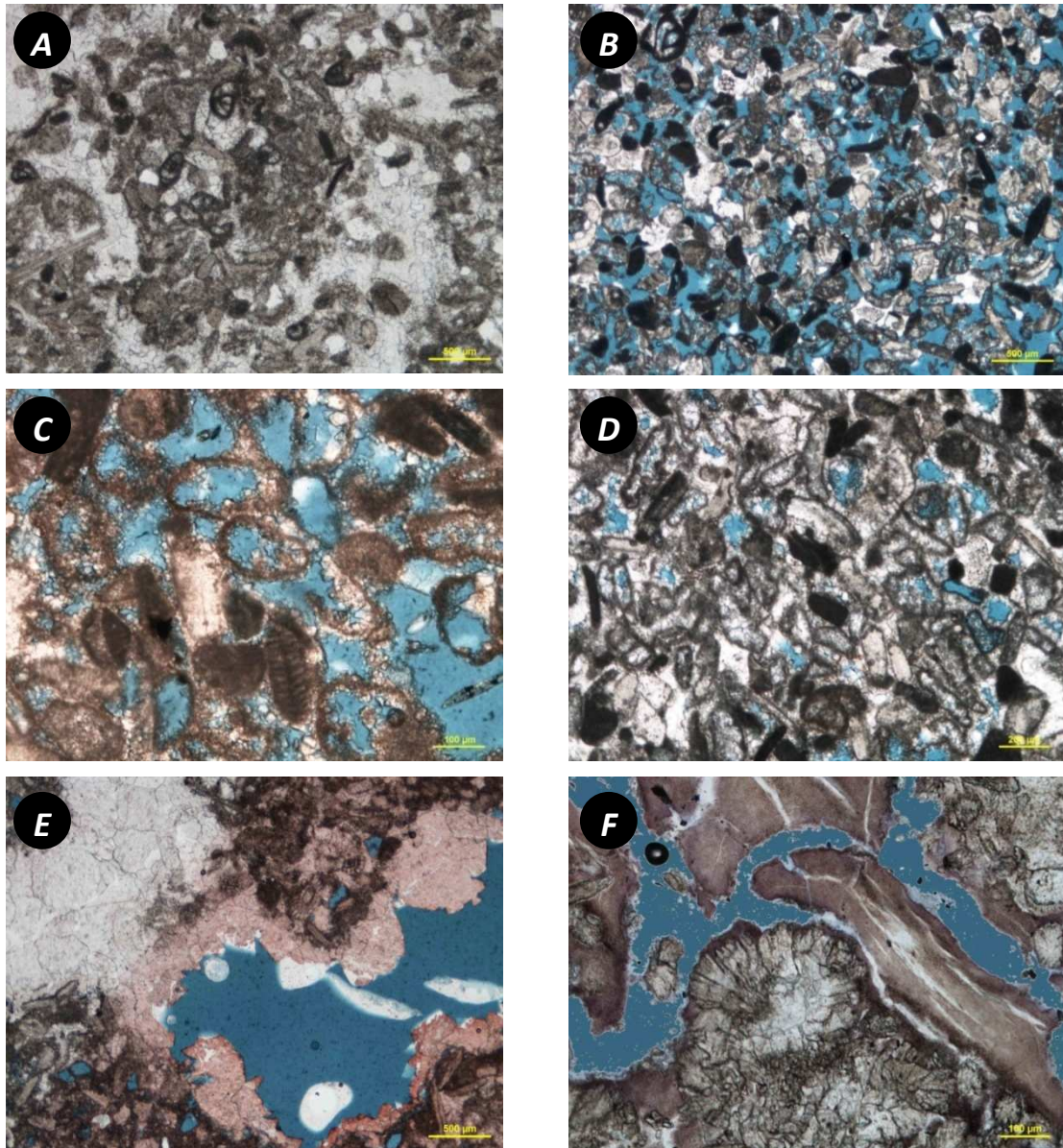


Fig20: Thin sections illustrating the facies of the chalky grainstone. **A:** The chalky grainstone correspond to high cemented facies. According to this cementation of the rocks, primary inter-granular porosity is generally totally occluded. The secondary leached porosity is affected too by this calcite cementation creating many fenestrae corresponding to paleo-dissolution channels totally occluded. **B/C:** The predominant porosity of these cemented rocks corresponds to a secondary leached porosity mainly arising from the dissolution of fossil shells. Nevertheless the secondary porosity is coupled with a fair initial inter-granular porosity corresponding to the primary inter-granular voids which is not cemented or slightly cemented. **D:** Thin section illustrating the good dissolution moldic porosity coupled with an inter-granular porosity which is slightly reduced by calcite cement. We notice that the moldic porosity is slightly reduced too. **E:** This dissolution moldic porosity is associated to vugs and dissolution caverns porosity. According the high potential of cementation existing in this zone, vugs and caverns are highly reduced by calcite cement. **F:** Currently in addition these dissolution structures are partly filled too by red clay.

Unit 2:

14.10 to 15.90m: Crystalline rock composed of coarse crystalline sparry calcite, and micro crystal of quartz (%). The rock shows a high percentage of karst which is estimated to 90%. According to this high karstification any thin sections are not taken on this core section. So for well know features of the rock (texture and porosity) we can referred to the description of well S26's unit 2 which is perfectly correlated to this unit (Fig10).

15.90 to 19.83 m: This interval corresponds to a void which is probably the result of karst action. So even though the facies of this unit are cemented, the large karst cavities affecting them can highly ameliorate the porosity.

Unit 3: (Fig 21)

19.83 to 28.15 m: Similar to well S26's unit 3, this sequence consists in polygenic breccias composed of carbonate pebble and grains of quartz. The rock is lithified by a white carbonate matrix. Contrary to well S26's unit3, lithoclasts constituted of bioclasts (miliolids and peneroplis) are common. The particles of the rocks are of micrometric to centi-metric size.

Similar to the rock of well S26's unit3, some layers of these breccias are highly dolomitized. The dolomite crystals present on are characterized by their clear rims.

The porosity is fair to poor, there is the intraclast porosity arising from the leaching of particle. Vuggy porosity due to the dissolution of matrix is coupled with this intra-particle porosity. Nevertheless the dolomitized layers show a very good porosity as inter-crystalline porosity, and crystal-moldic porosity which is generated by the leaching of the dolomite crystal's cores.

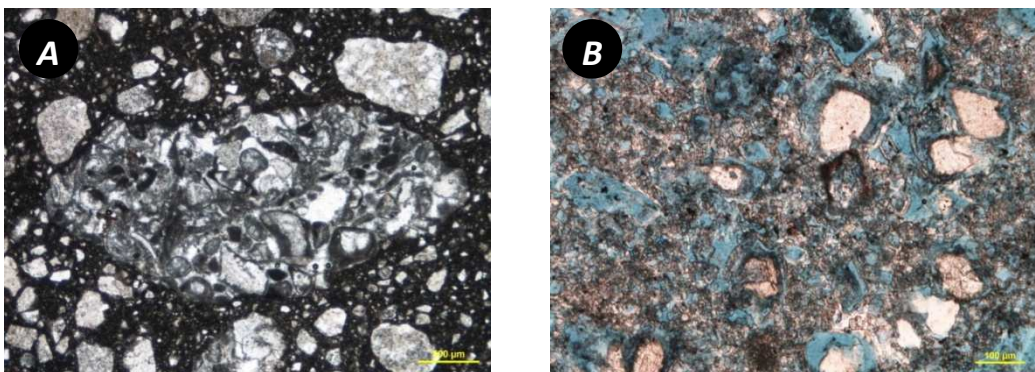


Fig21: Thin sections illustrating the texture of the unit3's rocks. **A:** These rocks correspond to polygenic breccias. The breccias are composed of carbonate pebbles and grains of quartz. We note the presence of lithoclast mainly constituted of bioclasts contrary to them of the well S26's breccias. Highly cemented, these breccias denote a very fair porosity. **B:** Dolomitized layers of these polygenic breccias. The porosity on these layers is very good. Inter-crystal dolomite porosity is coupled with a very good late porosity created by the selective leaching of the crystal dolomite's core.

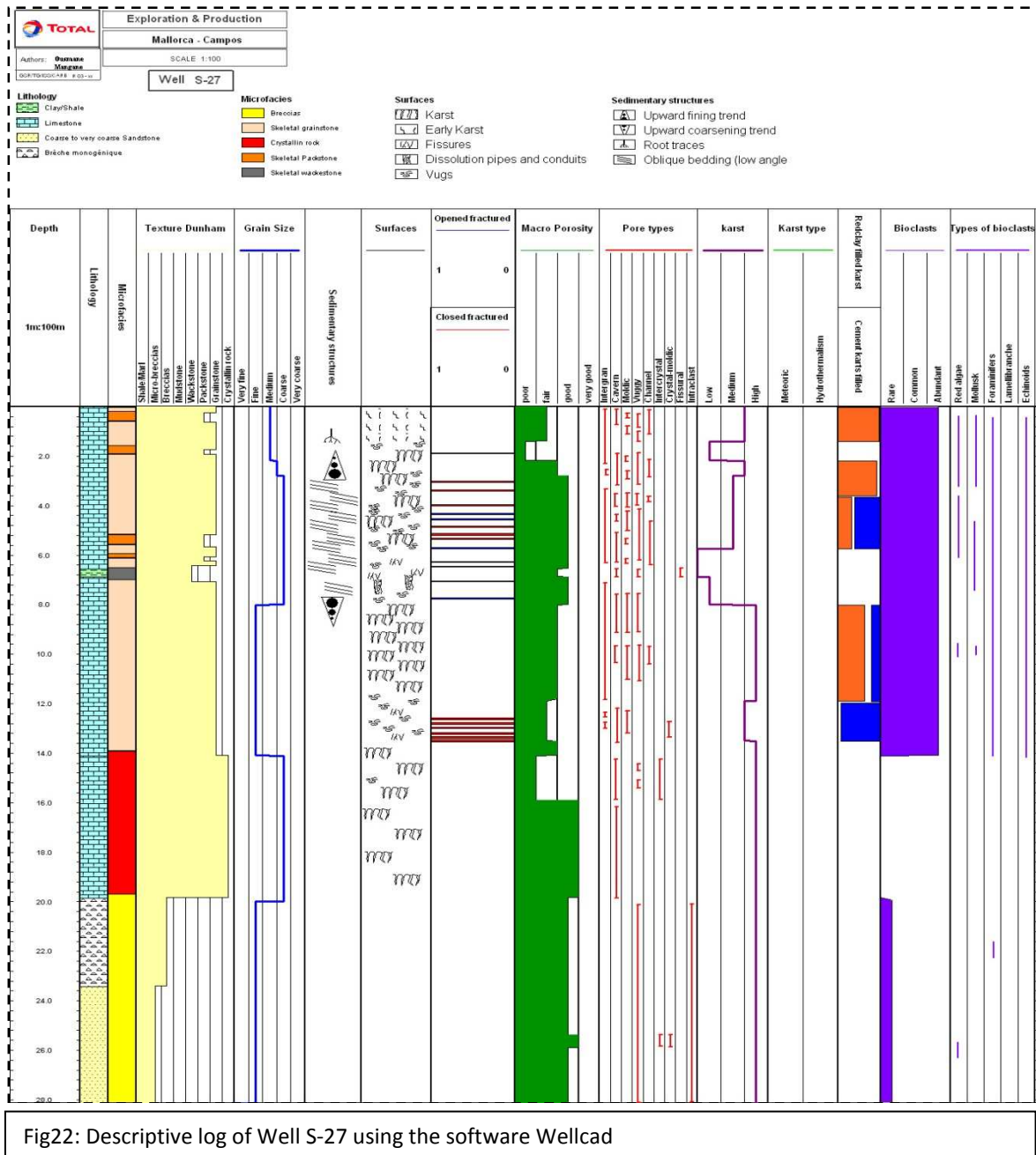


Fig22: Descriptive log of Well S-27 using the software Wellcad

b) Log data analysis: well (S27)

Similar to well S26, geophysic's data are available in this well S27 permitting, from their interpretations, to refine the characterization of well S27: Gamma ray log, Potassium/Thorium/Uranium log, Conductivity and Ph log, Electrical log (ILD), magnetic log (ILM).

Unit 1 (0.00 to 14.10 m): As unit 1 of well S26, the rocks of this sequence are characterized by a low electric's resistivity confirming their poorly compact feature. In fact, as previously observed, this zone is highly affected by karst thus creating a porous area, so a poorly compact rocks.

The superficial part of unit1 (from 0.00 to 6.10 m) where conductivity and pH data are not available corresponds to the exposure part of this basin (Fig23). Remember that pH and conductivity are only measured in aquatic context. This emerged zone can be interpreted as the vadose zone. Actually, according to the previously sedimentological description, this zone consists to oxidized rocks and karstified due to the directly fall of acid meteoric water onto these rocks.

Ph and conductivity data are available from depth 6.10 m corresponding to the entering depth of geophisic’s tools in the water zone. Thus the level, 6.10 m, can be interpreted as the water table corresponding to the transition vadose zone/phreatic zone.

From 6.10 to 13.85 m, conductivity log is stable and characterized by a low value (6.82 mS/cm) providing the presence of fresh water lens (Fig23). Ph log, constant too, shows an acid features (pH = 7.9) of this fresh water. This zone corresponds actually to the phreatic environment, which consists in a fresh and acid water lens created by the infiltration of acid meteoric water from surface toward the water table.

Unit 2 (14.10 to 19.83): Contrary to unit 1, rocks of unit 2 are characterized by a high electric’s resistivity (Fig23). This geophysics’ result provides and confirms the compact feature of theses facies, which correspond to poorly porous crystalline rocks (referred description).

In addition this unit is characterized by a slightly increasing of conductivity and in the same time by a slightly decreasing of pH (Fig23). These values of conductivity and pH result probably from mixing of fresh/acid water and salt/basic water.

Similar to unit 2 of well-S26, Gamma ray, Uranium, Potassium and Thorium logs show a substantial peak corresponding to the radioactive anomaly distinguished in Font Sant (Fig23). This high radioactivity will be subsequently interpreted from diagenesis studies.

Unit 3 (19.83 to 28.15): This third lithological unit shows a high electric’s resistivity too (Fig27). That can be explained by the compact feature of rocks composing unit3, which correspond to cemented breccias.

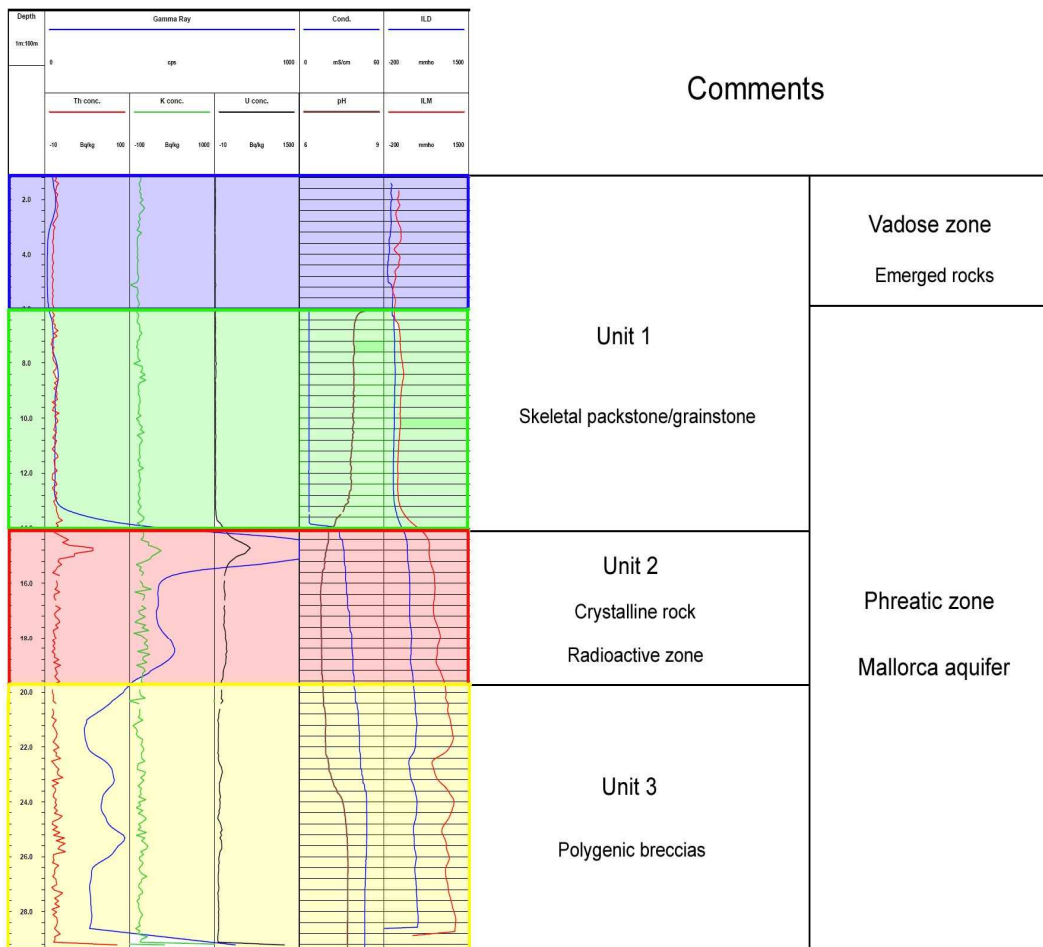


Fig23: GR, Thorium/Potassium/Uranium/, Conductivity/Ph, ILD (Electric’s log) and ILM (Magnetic’s log) in well S27, Font Sant, Mallorca.

IV) Diagenesis features

acies description previously established in this report corresponds to the macro-description of cores (S26 and S27) subsequently refined by a study of microscopic component (micro-facies, minerals, fossils and porosity). Actually the classic plugs are taken on these cores, in order to sample thin sections in the bottom of these plugs. These sections are mainly covered except them which subsequently used for the cathodoluminescence petrography.

A detailed petrographic study from these sections has also allowed to well-characterizing the major diagenetic fabrics affecting the different unit of Font Sant reservoir. According to the previous facies description the cementations (reduction of pore) and dissolution processes (amelioration of porosity) are recorded in these rocks. Thus during this microscopic investigation we mainly focus on the natures of cements (sparite/micro-sparite, micrite), their morphologies (meniscus cements, blocky) and on the features of the dissolution structures (type of structures, materials filling these structures).

On whole of the reservoir, three different fabrics of calcite are distinguished. These fabrics are classified in function of their crystal size: Micrite, micro-sparite, sparite. Generally the calcite fabrics, partly or completely filling the pores of Font Sant reservoir, correspond mainly to micro-sparite and micrite. Sparite cements are rare and are especially established surrounding large dissolution structures. Actually according to the high avoid space associated to these structures (large vugs and caverns), coarse crystals calcite growth into them. Currently sparite cement also form on echinoids fragments as syntaxial overgrowths calcite.

These fabrics show the characteristic morphologies, generally indicating the type of environment where they are originated.

1. Vadose fabrics

a) Cementation in undersaturated zone

Vadose zone fabrics are typically meniscus cements (Fig24). This fabric is characterized by a marked concentration of crystals at or near grain contacts. This localized distribution of cementation reflects the selective distribution of water in that environment. Actually near or at the grain contacts correspond to sites where capillary water films with curved meniscus boundaries would be concentrated. In other words the establishment of meniscus cements is influenced by the localized distribution of water by capillarity at grain contacts.

Reflecting the partial saturation of this environment, other cement morphologies termed microstalactitic cements are also represented in Font Sant Vadose zone (Fig24). These gravitational cements hang from the bottoms of grains which are the sites where water droplets would occupy. In addition to these localized cementations, abundant syntaxial overgrowths cement on echinoids fragments (Fig24). These overgrowths can form as well in the vadose zone as in the phreatic zone.

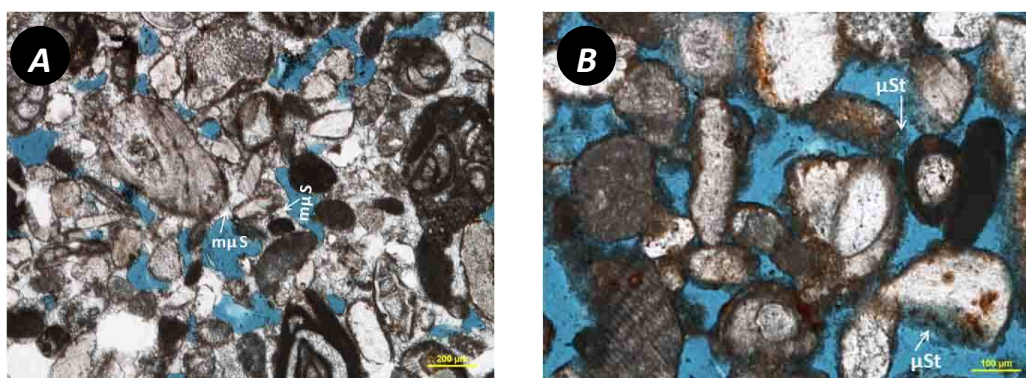


Fig24: Thin section illustrating the fabrics of vadose zone. **A:** Meniscus micro-spar cement (mμS) in grainstone. **B:** Facies showing micrite cements that hang from the bottom of grains (microstalactitic cement).

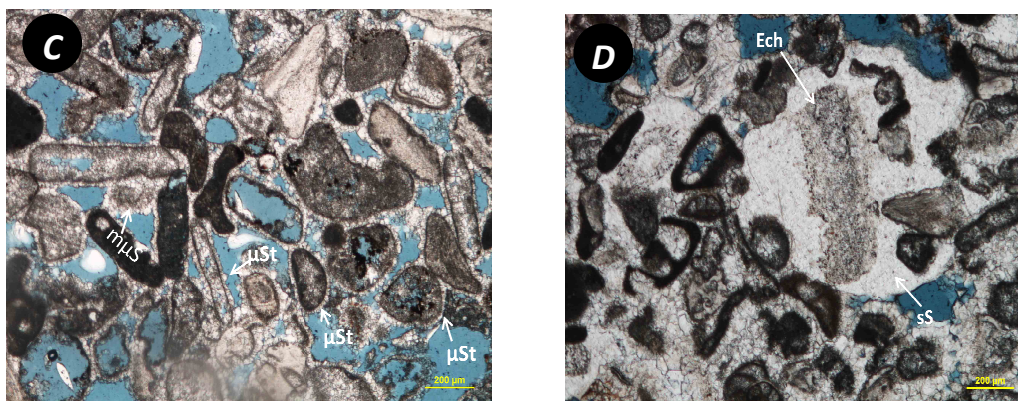


Fig24: Thin section illustrating the fabrics of vadose zone. **C:** Meniscus micro-spar cements ($m\mu S$) and Microstalactitic cement (μSt) in grainstone rich in large bivalves. **D:** Spar synthaxial (sS) overgrowth cement on echinoid fragment (Ech).

Although characterized by localized cementation, Font Sant vadose zone shows currently an extensive blocky cementation (complete pore fillings of equant calcite), so a more uniform distribution of water (Fig25). This uniform cementation is due to the re-precipitation of more stable carbonate from the oversaturated dissolution fluids. Actually during the extensive dissolution of unstable carbonate minerals in vadose zone (meteoric karst action); the acid meteoric waters have become over-saturated by continual incorporation of chemical elements (Ca^{2+} , Mg^{2+} , CO_3^{2-}). So the dissolution in vadose zone is followed by substantial re-precipitations of stable minerals generally far from the dissolution sites.

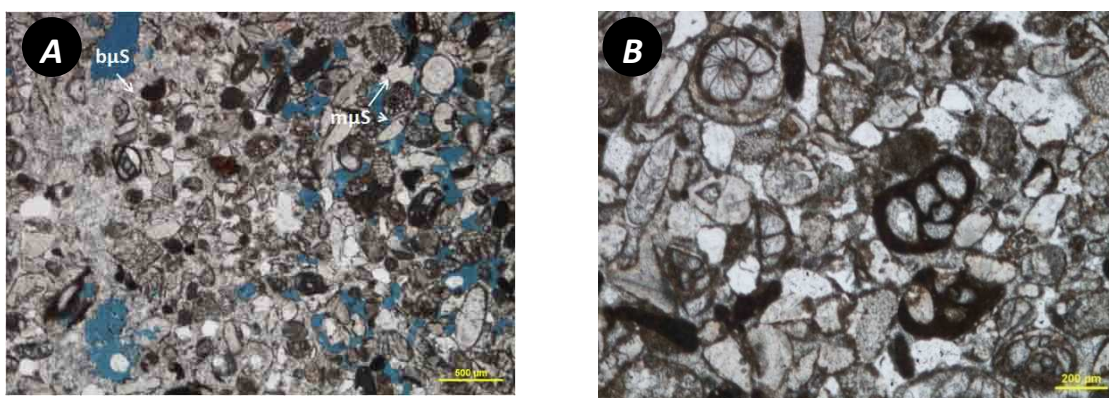


Fig25: Thin section illustrating the high potential of re-precipitation in vadose zone. **A:** Facies showing two distinct zones on the same thin section. One affected by vadose alteration: presence of microspar meniscus cements ($m\mu S$) and dissolution vugs. The second part shows a complete filling of pores by microspar blocky cement ($b\mu S$) resulting from re-precipitation of stable minerals in this vadose area. **B:** Grainstone rich in foraminifers showing an extensive cementation.

Near the water table, rocks of vadose zone commonly show phreatic fabrics (isopachous cement) and marine fabrics too (acicular cement also termed fibrous cement). Thus three diagenesis phases have been recorded on these facies: Vadose, phreatic and marine diagenesis (Fig 27/28). We must notice that the subdivision of Font Sant aquifer (Vadose/Phreatic zone), previously distinguished, corresponds to its actual configuration (Fig26). And throughout the time, configuration of this aquifer has currently changed. This variation is directly related to the fluctuations of limits vadose/phreatic (water table) and phreatic/marine. Rises and falls of these limits mainly result from the sea level fluctuations or from climatic conditions (recharge or discharge of ground water from

precipitations), and or from the agriculture use. Consequently in function of these fluctuations the rocks of Font Sant aquifer can be affected by different diagenesis processes of different environments.

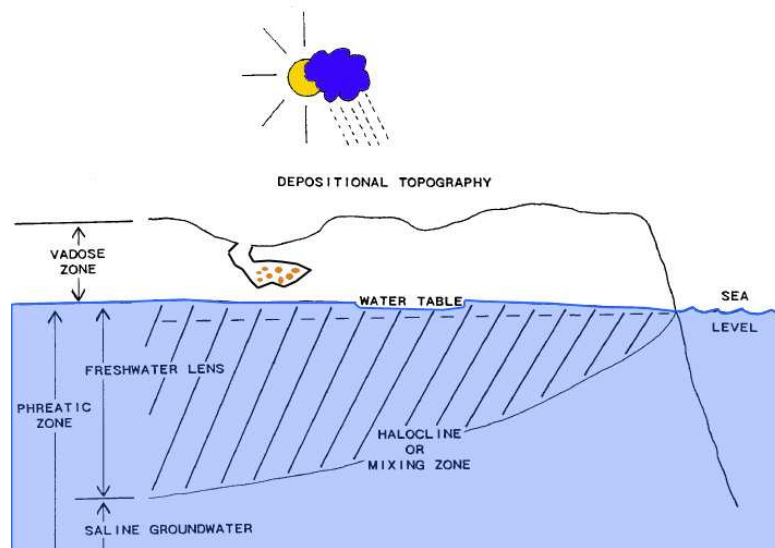


Fig26: Configuration of Santayi aquifer

Thin section at 5.36 m depth: Example of superposition of different diagenesis phase

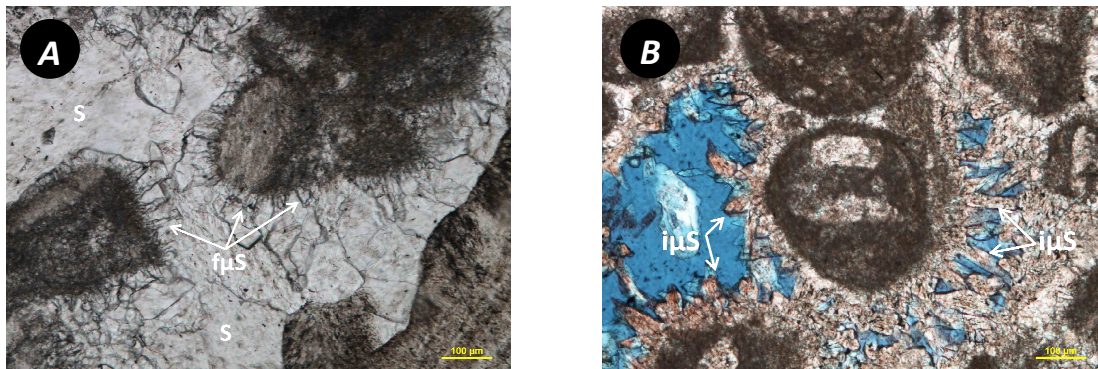


Fig27: Thin section at 5.36 m depth illustrating the superposition of three different diagenesis phases: Vadose, phreatic and marine. **A:** Currently fibrous microsparite ($f\mu S$) cements coat at the exterior surface of the grains. This marine cementation is coupled with a blocky sparite (S) cementation (phreatic cements). **B:** On this part of the thin section, that is isopachous microsparite ($i\mu S$ = phreatic cement) which grows at the surface of the grains partly filling the pores.

Hypothesis: On B only phreatic cements (isopachous not blocky) are represented. Therefore we can consider the acicular cement (fibrous cement) as original. And it is subsequently neomorphosed to bladed cement (phreatic cement). Probably, the present vadose zone corresponded initially to a marine environment which has subsequently become phreatic zone. This change of environment results probably from the tidal fluctuations, precisely from one fall of the sea level. On A the fibrous cement is not neomorphosed but it is coupled with late blocky cement (S) which is characteristic to phreatic environment.

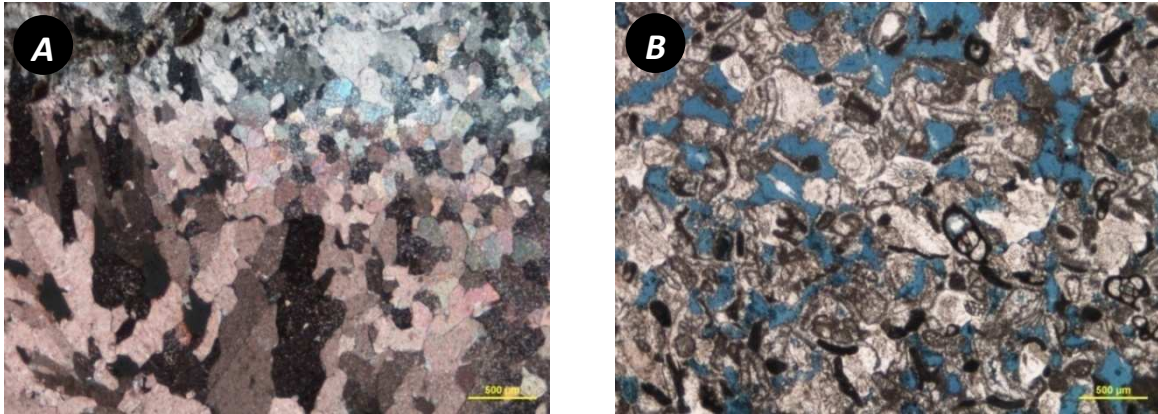


Fig28: **A:** Frequent dissolution structures (vugs, caverns, and channels) and meniscus cements are coupled with these marine and phreatic cements. Therefore the phreatic diagenesis was followed by vadose alteration.

Hypothesis: According to this vadose diagenesis, this zone was subsequently subaerial exposed. The passage in vadose zone is probably due to the drop of the water table.

B: We notice that some caverns resulting from the vadose diagenesis are partly or completely filled by equant calcite spar and bladed cement which are phreatic fabrics.

Hypothesis: Referring to these filling, the exposure phase was probably followed by a submersion episode in the fresh water lens. Consequently phreatic cements are created occluding partly or completely both the primary and the dissolutions pores.

The last and actual step corresponds to the re-exposure of this zone involving dissolution of the previous cements created in phreatic or marine zone.

a) Dissolution features

The vadose zone is also characterized by extensive dissolution due to the meteoric karst action: vugs, dissolution channels and moldic, and caverns (Fig29). Actually according to the subaerial exposure of this zone, the rocks are highly altered by the directly infiltration of the meteoric acid waters into them. As most of grains in that environment, the moldic pores are currently surrounded by micrite envelopes marking the location of leached grains. These envelopes play a substantial role in fabric preservation during the vadose alteration (Fig24C).

Generally the dissolution structures are partly filled by cements which hang downward or upward within these structures (gravitational cements). These fabrics precipitate from water droplets hanging from intra-and inter-granular surfaces. Sometimes these hanged cements (microstalactitic cements) show characteristic morphologies as dog tooth cement (Fig29).

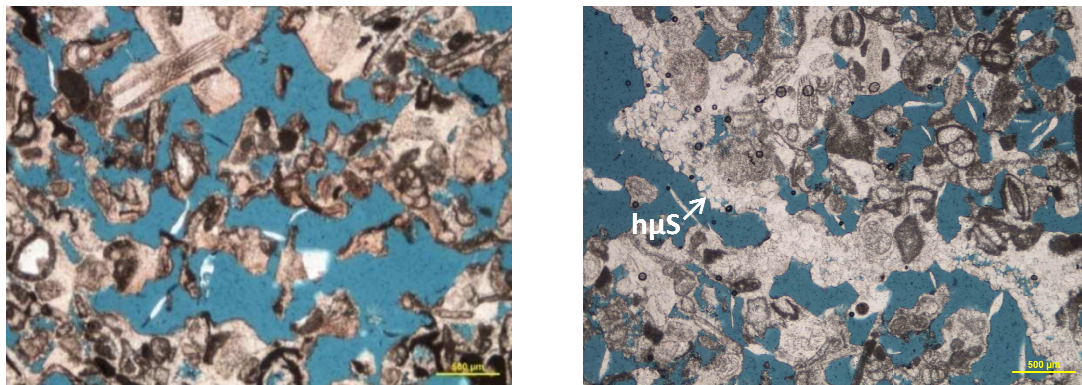


Fig29: Thin sections illustrating the extensive dissolution in vadose zone. **Left:** Large vugs and dissolution channels resulting from the leaching (karst action) in skeletal grainstone. **Right:** Partial filling of dissolution channel by microspar hanged cement ($h\mu S$) or gravitational cement in grainstone affected by vugs and dissolution channels.

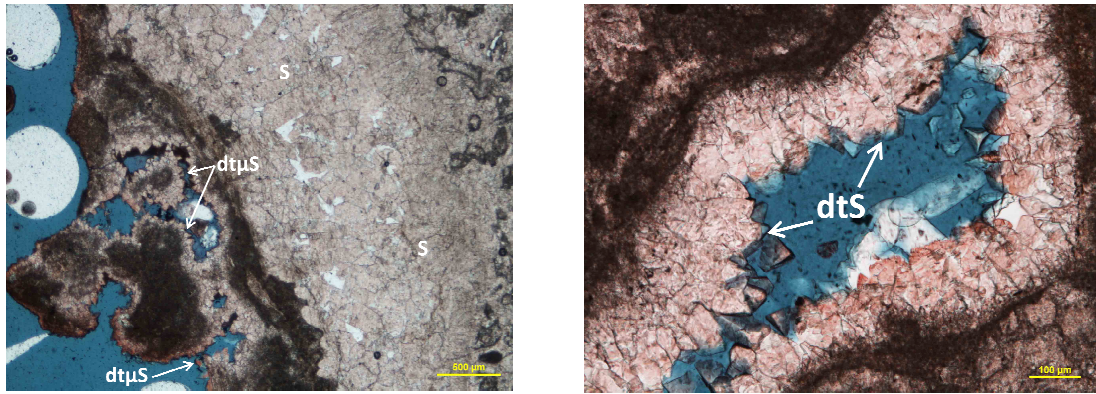


Fig29continue: Thin sections illustrating the extensive dissolution in vadose zone. **Left:** Karst cavity partly filled by dog tooth sparite cement (dts). **Right:** Cavity progressively occluded by sparite cement (S) and dog tooth microsparite cement (dtμS).

2) Phreatic fabrics

a) Cementation in saturated zone

Contrary to vadose zone, Phreatic area shows an extensive cementation (Fig30). The cements are more uniformly distributed, reflecting the complete saturation of pores with water in that environment. Actually the rocks of Font Sant phreatic zone show currently a complete filling of their primary porosity by equant calcite cement (blocky cement). In addition to this blocky fabric, calcite synthaxial overgrowth cement on the echinoid fragments.

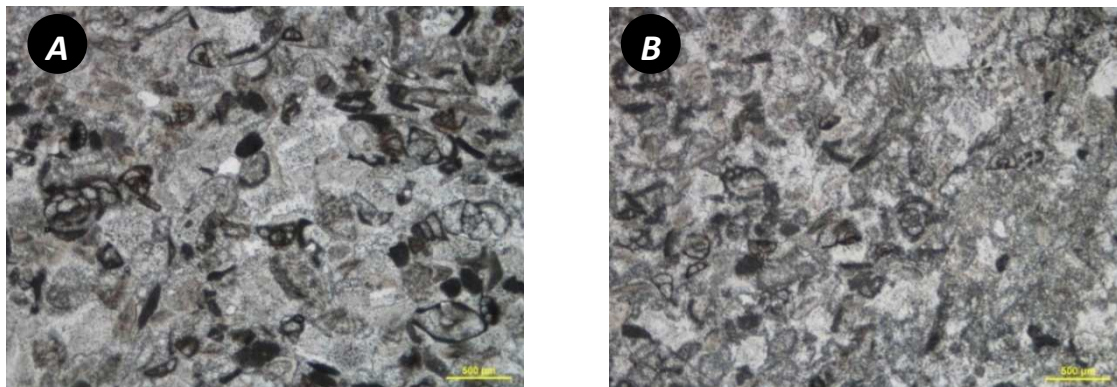


Fig30: **A/B:** Sections illustrating the extensive cementation in phreatic zone, reflecting the saturation of pores with water in that environment.

b) Fabrics in vadose-phreatic mixing zone

The upper part of this saturated zone is characterized by extensive dissolutions and fabrics of vadose cement as meniscus cement (Fig31). Localised below the water table, this zone corresponds to the vadose-phreatic mixing zone. The dissolution processes in that environment are principally related to the mixing of chemically-distinct waters.

This characteristic chemical dissolution is In addition coupled (Fig31) with vadose diagenesis (meniscus cement). This vadose alteration results probably from the regular exposure of this mixing zone due to the frequent fluctuations of the water table. Actually the water table surface rises after recharge of the fresh water lens, and is lowered as ground water is slowly discharged. When this transition is lowered, the paleo-mixing zone is exposed so affected by karst action and the establishment of vadose features (hanged cement, meniscus cement, and micrite envelope surrounding grains). Subsequently due to the rise of the water table, the paleo-mixing zone has

become submerged. So this area is again affected by chemical processes (extensive dissolution) and by phreatic cementation (blocky cement).

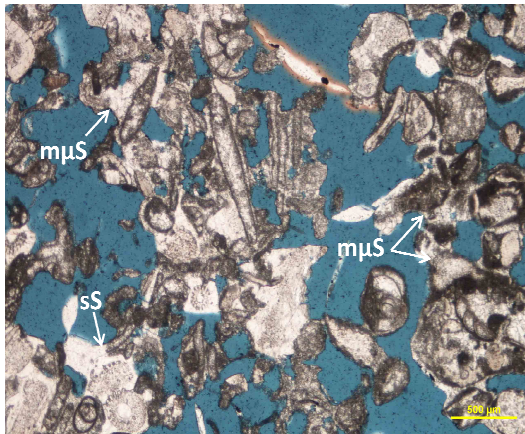


Fig31: Grainstone in vadose/phreatic mixing zone characterized by extensive dissolution. Microsparite meniscus cements ($m\mu S$) developing at grain contacts.

c) Dissolution features

In spite of the extensive cementation in phreatic environment, the rocks of Font Sant phreatic zone are affected by dissolution structures (vugs, moldic, dissolution channel and cavern). Nevertheless these leached pores are generally reduced by later growth of calcite. Currently some of them are partly filled by red clay (paleosoil materials). (Fig32)

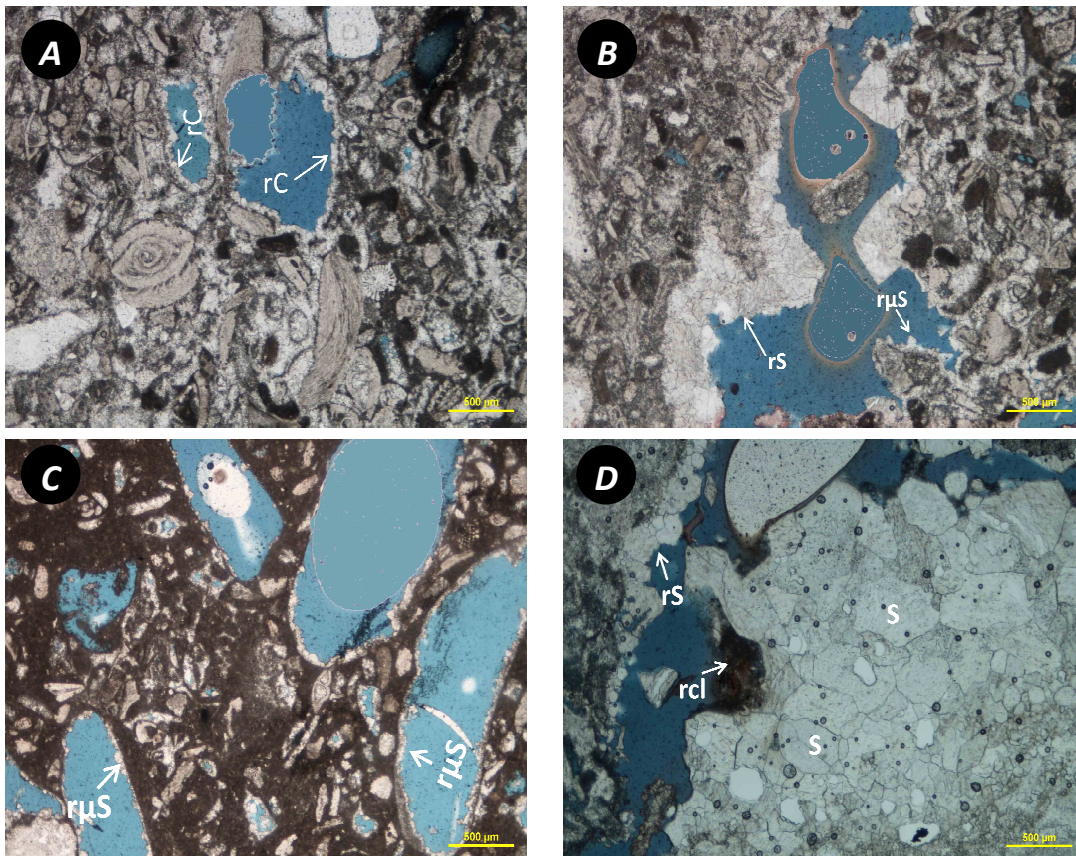


Fig32: Thin sections illustrating the dissolution structures in phreatic environment. **A:** Cemented grainstone affected by vugs which are lined by a growth of thin rim of calcite (rc). **B:** Cemented grainstone affected by dissolution channel which is partly filled by calcite cement. Growth of rim of sparite and microsparite cement (rs and $r\mu S$) line this channel. **C:** Large moldic pores partly filled by microsparite cement ($r\mu S$) in skeletal packstone. **D:** Cavity progressively occluded by sparite cement (S). The cavity is in addition partly filled by red clay (rcl).

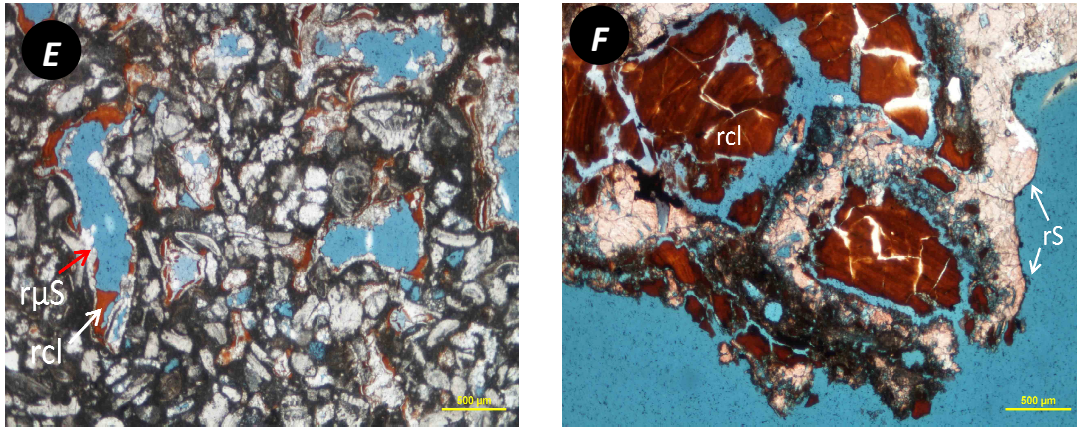


Fig32 continued: Thin sections illustrating the dissolution structures in phreatic environment. **E:** Large vugs and moldic pores partly filled by red clay (rcl) in skeletal packstone. Growth of thin rim of calcite ($r\mu S$ = rim of microsparite) lines these structures. **F:** Cavity partly filled by sparite cement (rs: rim off sparite cement) and red clay (rcl).

C.1. Origin of the phreatic's dissolution structures:

Referring to fig32, we notice that some cavities are lined by a growth of rim of calcite cement (rc, $r\mu S$, rS). That provides the dissolution processes in that environment are ante-cementation, and so correspond to early diagenesis processes.

Actually according to the presence of paleosol materials (rcl) into cavities, rocks of that environment were probably exposed soon after deposition. Consequently vugs, dissolution channel, moldic and cavern were generated, due to the meteoric karst action. Partial infilling of these dissolution structures by paleosol materials was synchronic to the meteoric karst action.

Subsequently the meteoric leaching was followed by the growth of rim of blocky calcite cement that lines the dissolution pores. These thin or large coating of calcite on the interior of the cavities are probably generated in phreatic environment, according to their blocky fabrics. Therefore the early exposure phase was followed by a submersion episode of the rocks in the phreatic area. Actually the present texture of the rocks shows an extensive cementation reflecting the complete saturation of pores (primary inter-granular pores) with over-saturated water as phreatic water. The changing of environment (vadose/phreatic) is related to the eventual recharges of the ground water.

3. Cathodoluminescence Microscopy

Generally cements occluding porosity of Santayi limestone are nonluminescent (Fig33). This nonluminescent response is typically assigned to oxidizing environment, as meteoric environment, in which the reduced forms of both Mn and Fe are unavailable for incorporation into the crystals of calcite precipitates. In addition oxidized forms of these elements present in these types of environment are not incorporated into calcite and, thus, there is nothing in the crystals to excite luminescence. That cathodoluminescence analyse certifies the meteoric nature of diagenesis affecting Santayi aquifer.

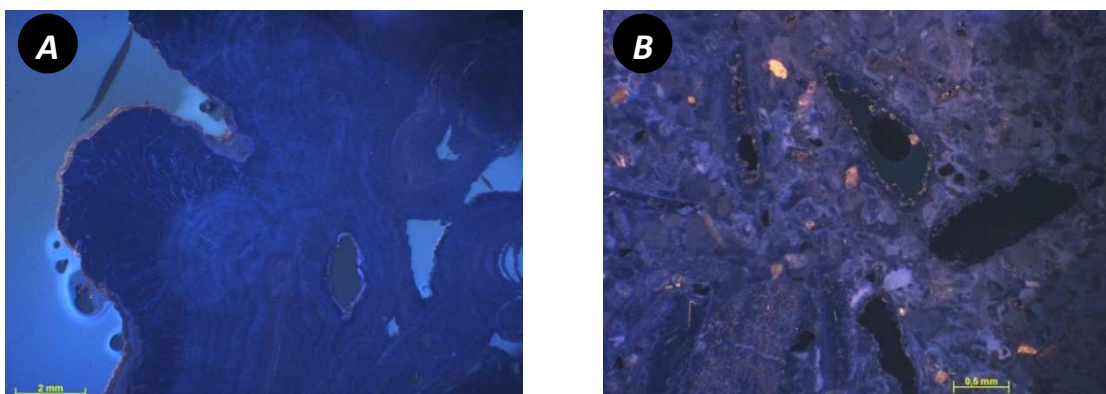


Fig33: Cathodoluminescence (CL) images of phreatic cements. **A:** CL image of karst cavity partially filled by gravitational cement (stalactite). Note the non luminescence of cements (blue colour). **B:** CL image illustrating the extensive cementation in phreatic environment.

4. Dolomitization of the breccias of unit3

Referring to sedimentology chapter, the Pleistocene breccias filling the paleokarst are partly dolomitized. The dolomite crystals consist of microcrystalline cement, and show planar fabrics (euhedral crystal). Although most of the microcrystals of dolomites are euhedral, they have considerable variation in crystal sizes: Polymodal dolomite cement.(Fig33)

These dolomites distinguished have cloudy cores and clear rims (Fig34/21/11). This textural feature is typically characteristic to replacement dolomites crystals. Conclusion the partial dolomitization of the breccias consists of a replacement dolomitization of the micrite matrix and the grains of calcite composing the breccias. The polymodal variability of the dolomite crystal size is a result of this replacement dolomitization of the hetero-metric breccias: coarse dolomite crystal corresponds to replacement of carbonates pebbles and the fine-size crystals correspond to the replacement of the micrite matrix.

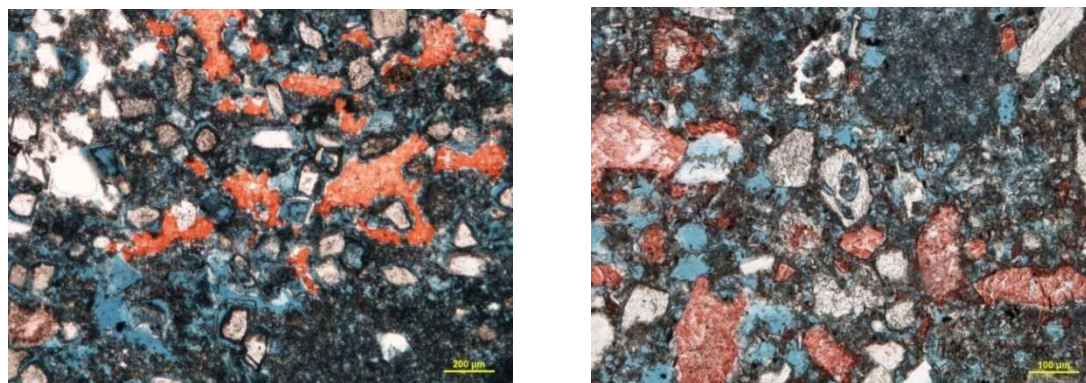


Fig34: Thin sections illustrating the replacement dolomitization of the breccias. Calcite here is stained in red and dolomite is unstained. Note the partial dolomitization of the breccias, according to the present of residual calcite. Note also the polymodal variability of the dolomite crystal.

Referring to diagraphies chapter, the unit 3 correspond to the most conductive area of the phreatic environment. This conductive area consists of the marine-meteoric mixing zone created by the intrusion of salt water in Mallorca aquifer. Many diagenesis processes as extensive dissolution and microcrystalline replacement occur in these chemical conditions.

According to the texture of the dolomite crystals, the partial replacement dolomitization of the breccias result probably from this marine-meteoric diagenesis process.

V) Origin of Font Sant anomaly (unit2/unit3)

The vertical sequence of lithofacies established in this investigation is not representative in regional scale. Actually according to the geological setting of Mallorca, lateral extension of unit 2 and unit 3 must be probably restricted to a very limited zone as Font Sant area. Therefore the facies of unit2 and unit3 are laterally lost. Nevertheless the thick sequence of lithofacies of unit1 shows a more pronounced lateral extension through the island: Santayi limestone.

According to their limited extension and their composition (polygenic breccias and coarse crystal of calcite), unit2 and unit3 can be interpreted as sequences of paleokarst-filling deposits. Actually these deposits are typically characteristic to them filling the large paleokarst affecting the Mallorca limestone.

Thus we consider that: **1-** Vertical sequence of lithofacies of Font Sant reservoir is only composed of Santayi limestone, which correspond to the skeletal grainstone /packstone of unit1. **2-** Locally in this reservoir, these limestone are affected by a large voids due to the karst action (meteoric? or hydrothermal?). **3-** And currently these paleokarst are totally filled, thus generating vertical sequences of lithofacies identical to them established in this investigation.

The overlaying of the breccias by the coarse crystal of calcite (unit2) provides that, the infilling of the paleokarst affecting the cored limestone is episodic (poly-phased infilling):

Firstly the cave is partly filled by polygenic fragments of rocks which are subsequently consolidated forming the breccias of unit 3. Finally the residual void of this paleokarst is filled by coarse crystal of calcite. The large size of these crystals reflects the important space available in this dissolution structure.

5. Origin of filled-paleokarst

Two hypotheses can be established to understand the process of formation of the filled-paleokarst distinguished in Font Sant.

a) Meteoric karst

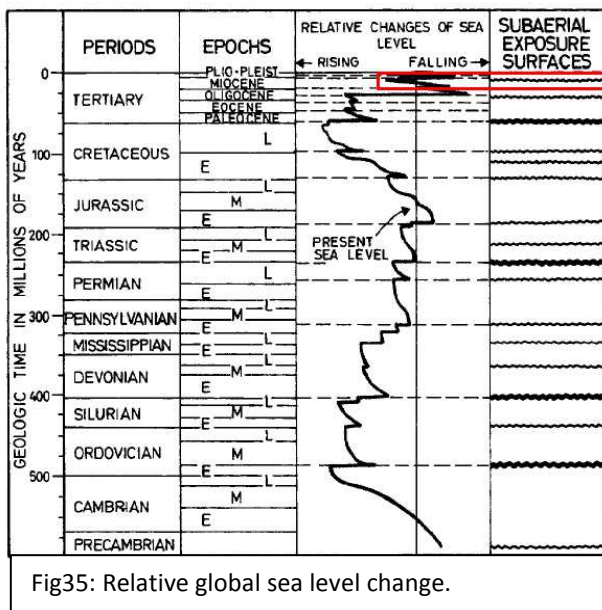


Fig35: Relative global sea level change.

Generally in Mallorca most of karst development is due to subaerial exposure of the limestone resulting to the high-frequency of sea level fluctuations during the Upper Miocene-Early Pliocene (Robledo and Pomar, 2000). Actually karst development occurs during the directly infiltration of acid meteoric water onto the limestone (Fig36). These cavities are typically in communication with the surface involving their progressive infilling by recent alluvial fan deposits overlaying the limestone (Fig36).

Referring to the chronostratigly of Mallorca (Fig35), the early-Pliocene consisted of a regressive episode (lowstand of sea level), which has involved a partly exposure of the Upper Miocene deposits, especially the Latest Messinian Santayi limestone (Fig38).

Consequently the Santayi limestone was probably affected by meteoric karsts (Fig36) similar to the filled-paleokarst distinguished in Font Sant. So chronologically this dissolution structure (unit2/unit3) is Early-Pliocene in age.

Referring to the facies description of unit2 and unit3, no facies deposits in Santayi platform (Skeletal grainstone/packstone) can be assimilated to the materials filling this cavity. That means the karst is not filled by fragments lifted to the country rock (unit1=Santayi limestone) by dissolution. In addition no deposits in Mallorca from Upper Miocene to Early Pliocene in age can be assimilated to the materials filling this cavity.

Therefore the infilling of the cavity is not synchronic to the karst action. And according to these observations, the breccias of unit3 come probably from the Pleistocene alluvial fan deposits (Palma siltstone) which overlay the Santayi limestone (Fig36). So the infilling of this karst is Pleistocene in age.

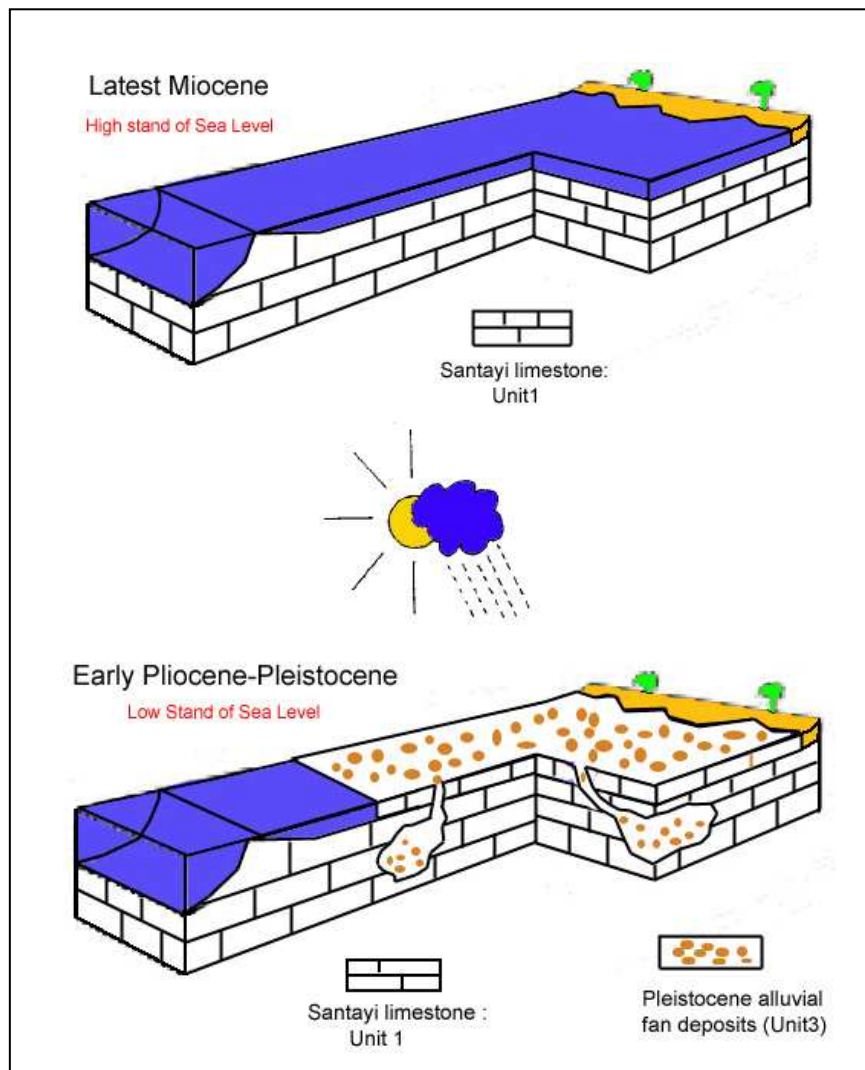


Fig36: Block diagrams illustrating the impact of sea level fluctuation, throughout the time, on configuration of Santayi platform. These blocks illustrate therefore the meteoric hypothesis: Santayi limestones corresponding to transgressive unit, Late Miocene in age, were subaerial exposed during the Early Pliocene Low stand. This exposure has involved meteoric karst development onto the limestone. At Pleistocene alluvial fan deposits (Palma siltstone) have overlaid Santayi limestone and partially filled paleokarst which have previously affected the platform.

During the Pliocene exposure phase, acid meteoric waters have infiltrated onto Santayi limestone, creating dissolution structures (karst, vugs) and have continually become oversaturated by incorporation of chemical elements (Ca^{2+} , Si) during their infiltration. Consequently Mallorca aquifer was recharged by these oversaturated waters (rise of the water table due to the precipitations), involving the continual submersion of exposed rocks (vadose zone) in phreatic environment. Therefore karst previously created in vadose zone, as Font Sant filled paleo-karst, can subsequently enter into this saturated area (Fig37). In consequent, according to the oversaturated waters saturating phreatic area and the important voids available in these karsts, coarse crystal of calcite and crystal of quartz can be re-precipitated into these large dissolution structures.

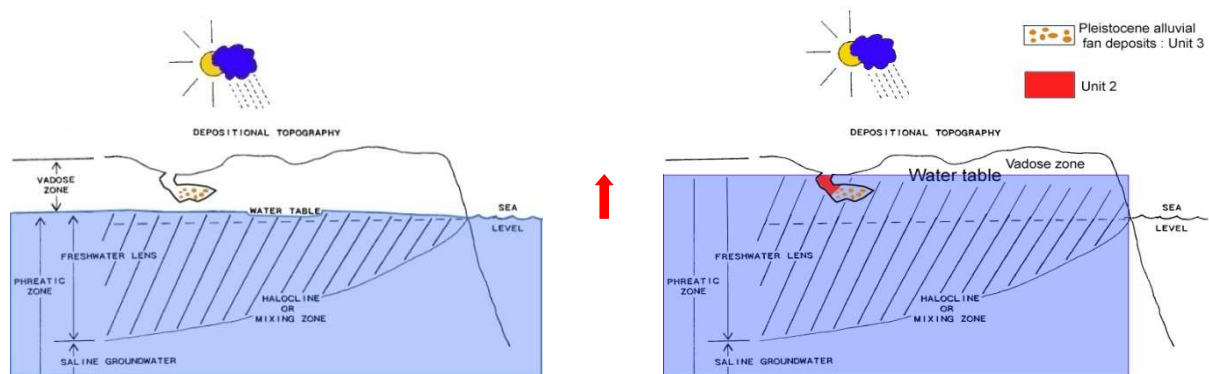


Fig37: Schemas illustrating variation of water table of Santayi aquifer. Meteoric charge of the aquifer involves a rise of water that submerges rock, previously exposed, in phreatic environment. According to the high potential of cementation in this environment, porosity of submerged rock as intergranular and dissolution structures (karst cavities) will be highly reduced by calcite cement.

Conclusion: According to the texture of rocks composing unit2 (coarse crystal of calcite and grains of quartz), the infilling of the residual void of Font Sant paleo-karst after the partial Pleistocene infilling (breccias), was probably due to re-precipitation processes from oversaturated water (phreatic water).

b) Geo/hydrothermal karst

A second hypothesis is based on the probably circulation of geo/hydrothermal fluid through one fault affecting the Santayi limestone in Font Sant (Fig38). Eventual corrosive or under-saturated fluid circulation controlled by fault can generate large dissolution structures (karst, large vugs) through the limestone. This phenomenon will be more pronounced if the fault is associated with fractures.

Actually in Font Sant, a possible post-alpine-fault crossing the geo/hydrothermal source of Font Sant can affect the Santayi limestone, and thus allowing a lateral thermal fluid circulation through the limestone. According to their corrosive feature, large karst can be generated due to percolations of geo/thermal fluid from the fault onto the Latest Messinian limestone (Fig38).

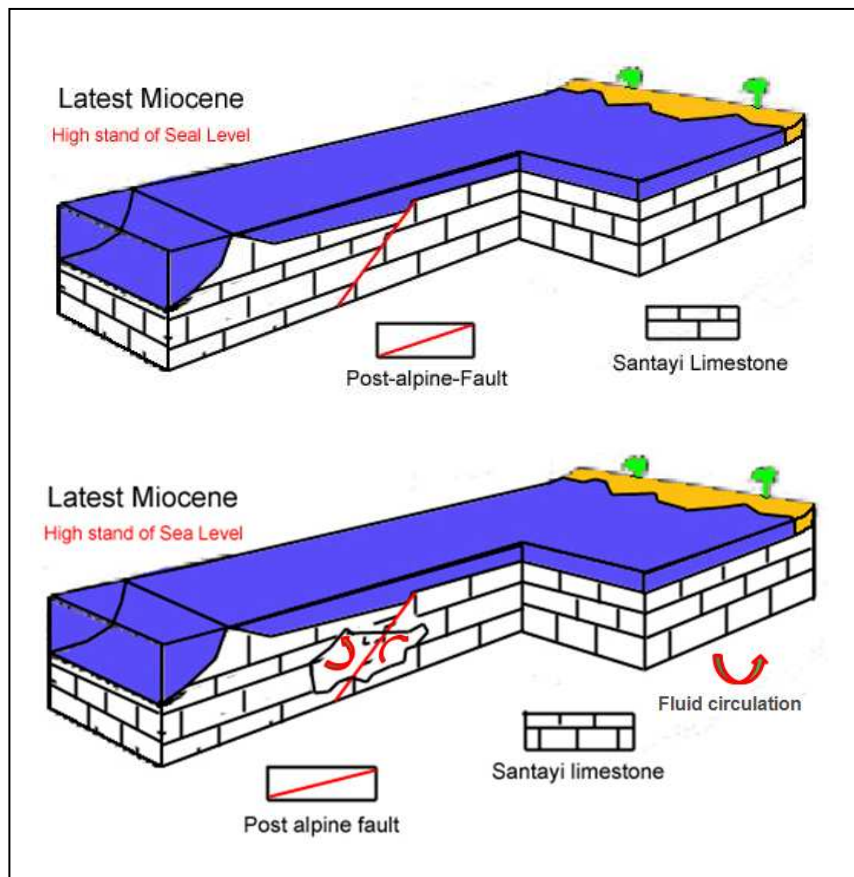
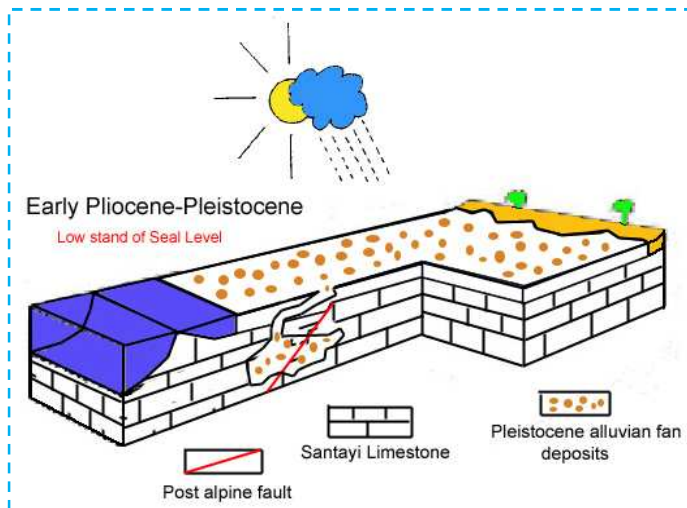


Fig38: Block diagrams illustrating hydrothermal karst development controlled by fault.

During the Pliocene exposure episode, this post-Latest-Messinian hydrothermal karst can be resumed by meteoric karst action, thus modifying the geometry of this structure: accentuation of dimensions of the karst (Fig42).



This meteoric karst development also allows to make in communication the paleokarst with the surface (Fig39), so involving its infilling by Pleistocene alluvial fan deposits.

For the filling of residual voids of the karst by coarse crystal of calcite (unit2), we can refer to the previous hypothesis: re-precipitation processes of crystal from oversaturated water (Phreatic water). (Fig 37)

Fig39: Schemas illustrating the resume of hydrothermal karst by late meteoric alteration, Early Pliocene in age (subaerial exposure episode).

Nevertheless in this case, the origin of the oversaturated water generating the coarse crystals can be meteoric or hydrothermal. Stable oxygen and carbon isotopic analyses from the cements composing

unit 2, are necessary for know the origin of these coarse crystals filling the residual void of the paleokarst.

c) Nature of unit2 cement

Firstly according to superposition of isotopic values (Fig40) of both cements (unit1 and unit2), cementation in unit1 (phreatic cement) and unit2 (coarse crystals of calcite) could be generated by the same diagenesis process.

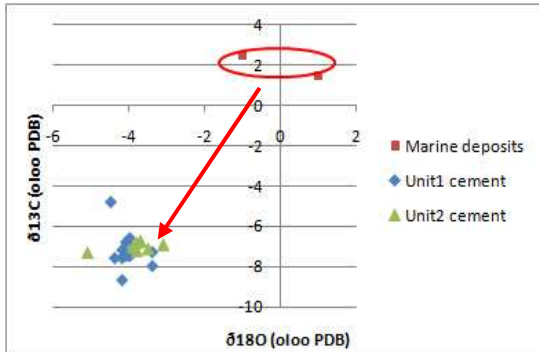
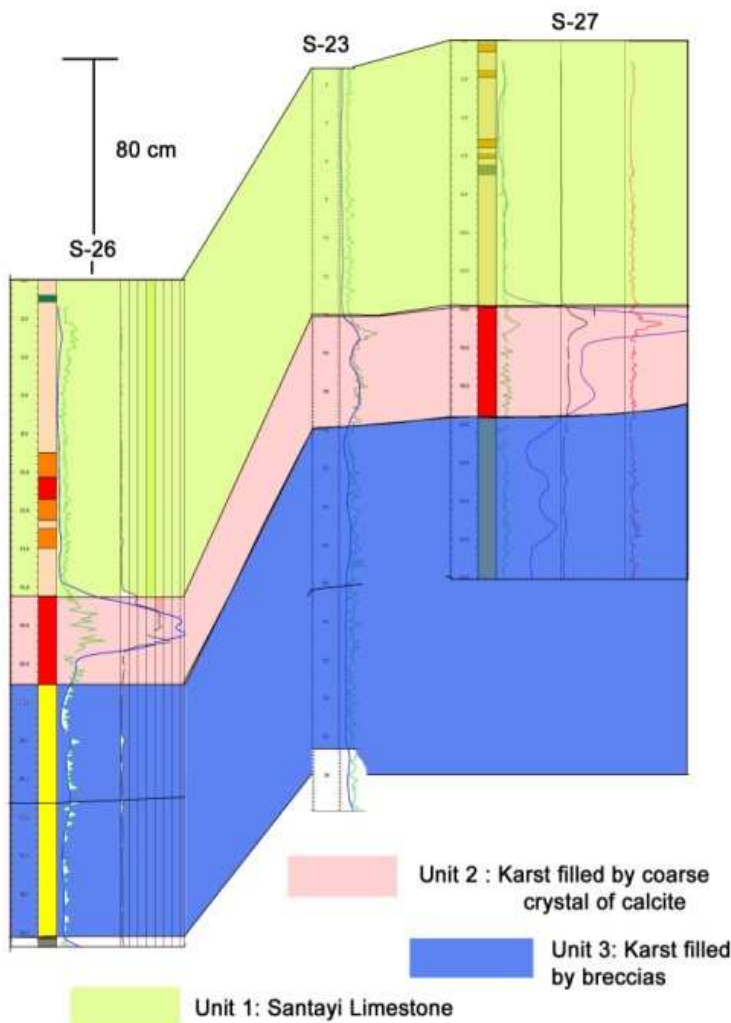


Fig40 : Cross plot $^{18}\text{O}/^{16}\text{O}$ vs $^{13}\text{C}/^{12}\text{C}$

Secondly the plot show a transversal shifting of Miocene marine deposits ($\sigma_0 = -1$; $1 - \sigma_C = 1.5$; 2.5) to slightly lighter $^{18}\text{O}/^{16}\text{O}$ (-3.1, -5.1) and substantially lighter $^{13}\text{C}/^{12}\text{C}$ (-6.7, -7.3).

This shifting is typically an effect of meteoric alteration (AAPG Memoir 77, P and D Scholle).

Thus, similar to cements of unit1 previously described, coarse crystals of calcite (unit2) filling the Font Sant paleokarst consist in meteoric product, not geo or hydrothermal product. The substantial lighter of $^{13}\text{C}/^{12}\text{C}$ result from incorporation of vegetal matter into meteoric karst cavity (referring to sedimentology of Unit2, Fig10D).



Conclusion: Unit 2 and Unit 3, distinguished on the vertical sequence of lithofacies in Font Sant, correspond to a filled-paleokarst, Pliocene in age (Fig41).

This paleokarst affects actually the Santayi Limestone (Unit1). So the country rock corresponds to bioclastic grainstone/packstone.

Its infilling has occurred at Pleistocene by breccias at its base and coarse crystals of meteoric calcite at its top.

Origin of this paleokarst can be meteoric or hydrothermal resumed by meteoric.

Fig41: Lateral and vertical sequence of lithofacies established between well S26/S27/S23 in Font Sant reservoir .

VI) Karst reservoir characterization

Referring to previous chapters Font Sant reservoir corresponds to a karst and fractured reservoir. Affected by these structures (karsts and fractures), these kinds of reservoir consist typically in heterogeneous reservoirs.

In resume, Karsts affecting Font Sant reservoir are mainly epigenetic, so arising from sub-surface karst action during the Pliocene subaerial exposure phase of Santayi platform. Later burial diagenesis processes can subsequently control the karst development during the submersion episodes of the shelf (hydrothermal karst/marine-meteoric mixing zone dissolution).

According to the extensive leaching due to the karst action, the predominant porosity in karst reservoir corresponds to dissolution porosity (vugs, dissolution channel, moldic and caverns). This substantial secondary porosity is coupled with matrix porosity (primary porosity) which is formed during the carbonate sedimentation that occurs when the platform is submerged. In addition in Font Sant reservoir the rocks are affected by opened-fractures which ameliorate the quality of the reservoir.

The location and type of porosity depend on the degree of platform exposure, the degree of acidification of infiltrated water, the lithology and the climate. Therefore the karst reservoir shows typically a high heterogeneous distribution of rock properties (porosity, permeability). This heterogeneous distribution is more pronounced if the karst reservoir is in addition fractured.

Actually Font Sant reservoir show a substantial lateral and vertical variations in amount and distribution of porosity and permeability. This high tridimensional heterogeneity is typically characteristic to the karst reservoirs.

For well characterize the porous system of Font Sant karst-fractured reservoir (pore types, distribution, geometry, connectivity and amount), petro-physical analyses are done from core X-Ray imagery. In addition visual description of pore types (karst, opened fractured) and estimation of porosity are previously realized from physical core, in order to analyze all the porous system of Font Sant reservoir from two distinct scales.

1. Petro-physical survey from X-ray image of cores

X-Ray tomography using CT scan on cores is a good approach to characterize the porous network in carbonate. Actually 2D -3D X-Ray image Analysis techniques constitute a helpful tools for qualitative (structure of pores systems) and quantitative (estimation of virtual porosity and permeability) characterization of carbonate reservoirs.

The pore system investigate by CT-Scan corresponds to the macro-porosity and partly meso-porosity. According to large and irregular pores characterizing karst reservoirs, this study of X-Ray image will be actually very decisive and interesting for our investigation. The micro-porosity won't be visualized in imagery but it is integrated to the X-Ray density measurement, then to the evaluation of virtual porosity.

a) Computed Tomography Scanning (CT Scan) presentation

The scan used for these analyses is similar to the medical X-Ray CT scanner: General Electric's LightSpeed 16. G.E.L 16 was used to acquire the CT (computed tomography) images.

The CT Scan measures the X-Ray density of materials (cores, plugs...) crossed by X-Rays. And the CT images obtained are reconstructed using the intensities of X-Ray collected around the cores. The transmitted X-Ray intensity is expressed as the CT number (Hounsfield, 1973), which characterize by the ratio of linear attenuation coefficient μ of the material (cores, plugs) to that of pure water μ_w .

$$\text{Hounsfield Units (H.U.)} = \frac{\mu - \mu_w}{\mu_w} \cdot 1000$$

From Amira software© the scan of cores allows to obtain two and three dimensional X-Ray images of them, especially consisting to visualize the porous network. Four image sections can be visualized: a virtual enrolled section, two perpendicular sections called Dip and Strike, and virtual tomography (Fig42).



S26

 Espagne
 S26
 CORE 1

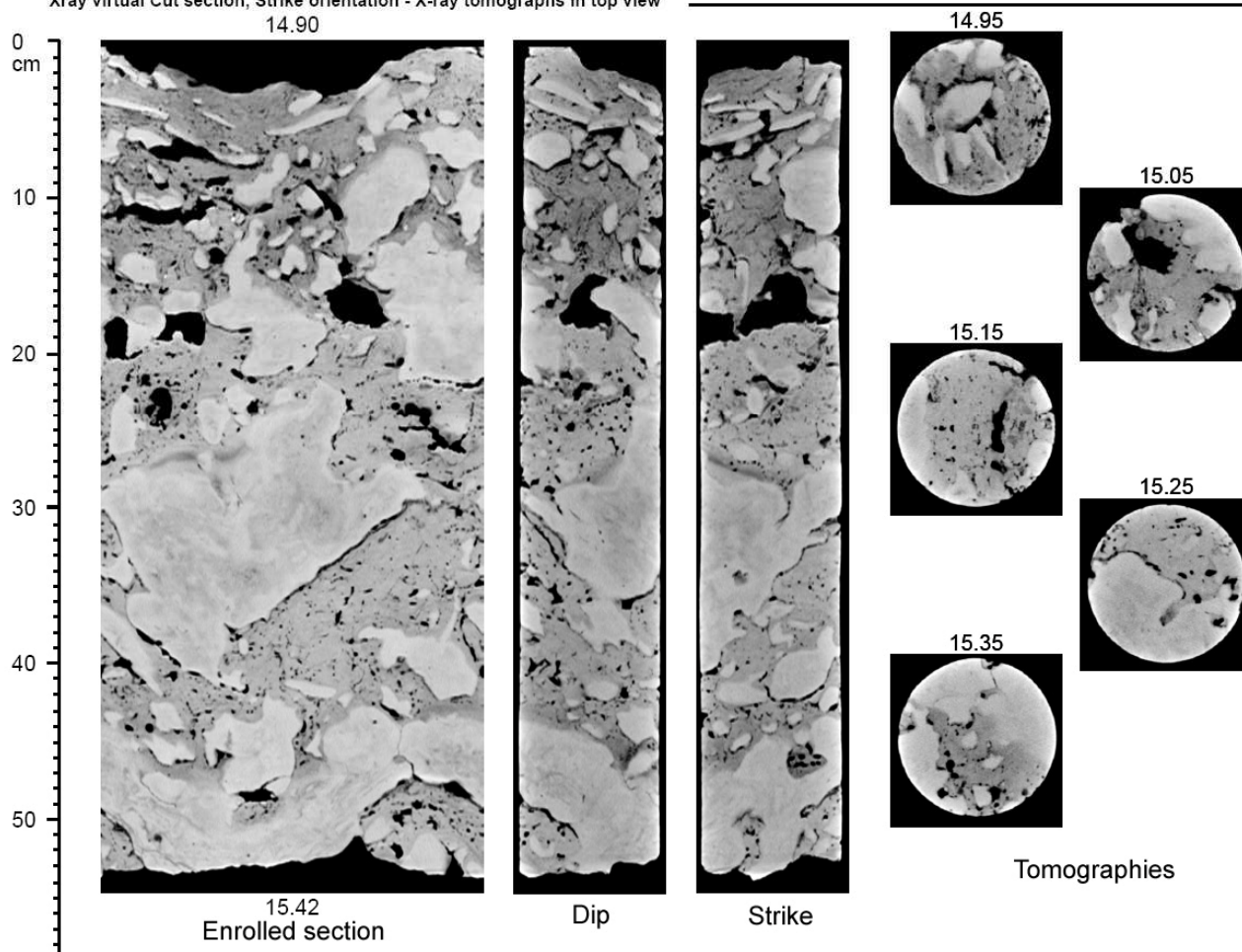
 Xray Cylindrical section Unrolled - Xray virtual Cut section, Dip orientation -
 Xray virtual Cut section, Strike orientation - X-ray tomographies in top view


Fig42: 2D X-Ray image from 14.90 to 15.42 m

2. X-Ray Image Interpretation

The study of the X-ray images permits to refine the previous classic description of core. In fact many structures as dissolution pore (vugs, cavern and channel), sedimentary structures (beds/laminas) and structures due to the circulation of fluids are not directly visible on the core.

Actually by studying the two dimensional X-ray images we have better visualized the porous system, especially the macro/meso-porosity, and distinguished the different pore types.

The X-Ray images obtained show characteristic grey tints (Fig43). Every tint corresponds to an X-Ray density value:

- The darker the core X-Ray image section is, the less dense and the more porous it is.
- The clearer the core X-Ray image section is, the denser and less porous it is.

In fact similarly to medical X-Ray radiography, the dark zones denote the presence of empty spaces corresponding to the porosity in geological case.

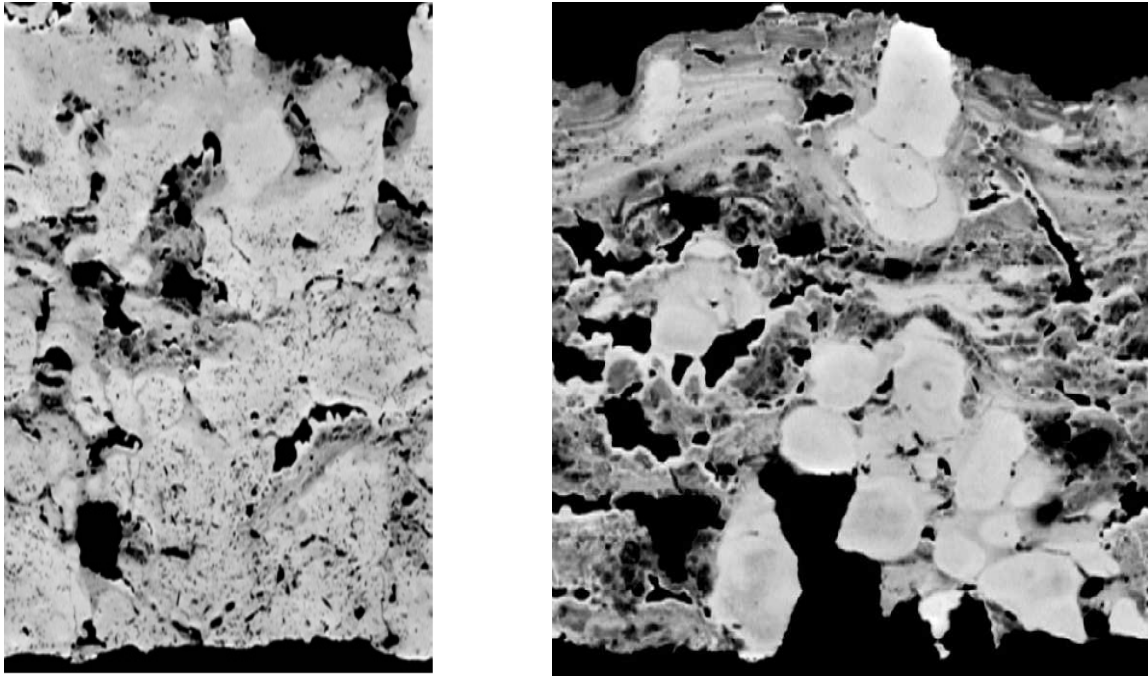


Fig43: Virtual sections of core S26 illustrating the empty dark spaces (not directly visible on the core) corresponding to the irregular vugs, cavern and dissolution channels created by the karst action. The clearer zones correspond to the matrix.

In addition the CT scan image can display internal sedimentary structures, tectonic structures, impacts of the fluids circulations (cementation, alteration, leaching) and textures of some facies as the breccias of unit3.

The rocks present in the vadose zone (superficial part of Unit 1) are highly altered due to the infiltration of meteoric acid waters (fig44). The vertical infiltration of these waters can be displayed by the CT scan images, which is characterized by vertical channels (fig44).

In Well S-27 fine laminas into the grainstone /packstone are displayed in this vadose (from 2.80 to 8.01 meters) zone by X-Ray images (fig44). Any sedimentary structures are not visible in well S-26 as well as directly on the core or from X-Ray images. This not available of sedimentary structures in well S-26 can be probably due to the infiltration of meteoric water into the rocks deleting all the preexisting structures.

Some opened or closed fractures slightly tilted (5°) affecting rocks of vadose zone are viewed. Areas surrounding some fractures in well S-27 show a very dark tint on the X-Ray images, so presents a good porosity. These porous zones are created by fluid circulations through these fractures, which have probably involved a high leaching of preexistent cements in the country rock around these fractures (fig45).

Facies of phreatic zone consist in very cemented and fractured rocks. The CT scan images of these cemented-rocks correspond to characteristic very bright X-ray images, so consist in very fairly porous rock (Fig45).

Corresponding to cemented rocks, lithofacies of unit2 show these same characteristic bright X-Ray images (fig45). Dissolution structures (vugs), which are not directly visible on the core, are displayed in this unit by the X-Ray images.

The texture of unit3's breccias is very well displayed by the X-Ray images. The matrix of this breccias present a slight dark tint, proving that matrix denote a very good micro-porosity which is not directly visible as well on core as on thin sections (fig45).

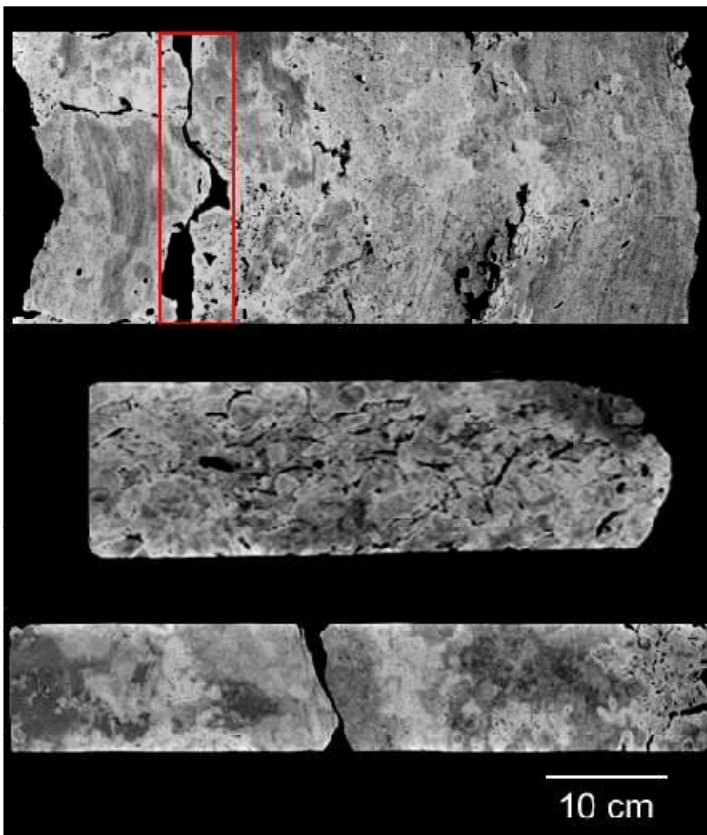


Fig44: Virtual core section illustrating the various impact of the infiltration of meteoric water, and showing some sedimentary and tectonic structures. **Left:** Rock of vadose zone highly altered by meteoric acid water. It is characterized by some irregular dark zones (more porous zone) which correspond to leached area due to the infiltration of meteoric water. Bright zones correspond to rocks affected by re-precipitation process in vadose, therefore they consist of cemented rocks. **Center:** Vadose core section affected by irregular sub-vertical channels created by the infiltration of meteoric water. **Right:** On this X-Ray core image low amplitude sinusoids corresponding to the fine laminas of the facies, are displayed. This laminated facies is affected by karst action (dark space = vugs/dissolution channel) and fractured (sinusoid is indicated in red).

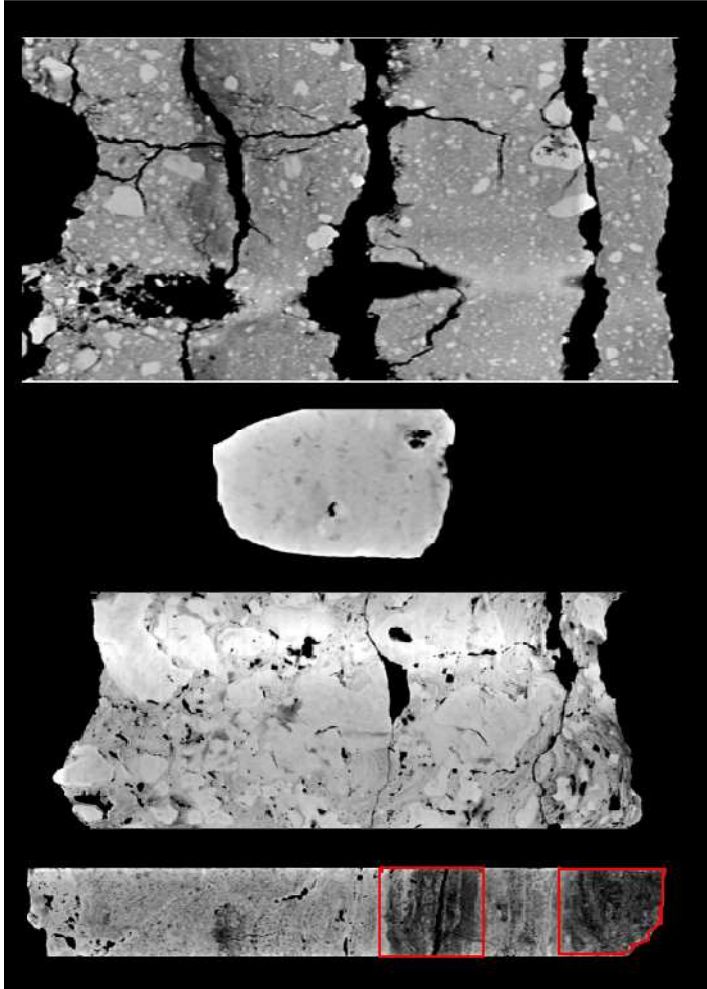


Fig45: Virtual sections showing tectonics structures (fractures), structures due to karst actions (vugs, cavern), and illustrating the impact of fluid circulation. From left to right: **First picture:** porous zones (dark zone indicated in red) surrounding fractures, probably created by leaching of preexistent cement due to the fluid-circulations through these fracture. **Second picture:** Very bright X-Ray section corresponding to cemented-rocks (Phreatic rocks). Dissolution structures (irregular dark zone) due to karst action affect the rocks (vugs, dissolution channel). Fractures (sinusoids) associating to karsts cavities (irregular dark zones), are displayed on this X-Ray image: These cavities are probably created by karst action controlled by fluid circulation through the fractures. **Third picture:** Very clearer X-Ray image corresponding to the cemented rocks of unit2. Some voids (irregular dark space) created by karst action affect these rocks. **Last picture:** Fractured Breccias of the unit 3. The carbonate pebbles are perfectly display on this X-Ray image. The matrix shows a dark tint reflecting its good micro-porosity.

Subsequently, using Amira software the X-Ray image treatments are done, in order to quantify and visualize the porous system.

3. Petro-physical treatment

a) Virtual Plugging and virtual porosity

To estimate petro-physical parameters in this investigation, we have preferred to take virtual plugs instead of Phi-K plugs. Take Phi-K plug in karst reservoirs for evaluate its petro-physical properties won't be representative. Actually according to the irregular large voids (macro-porosity) affecting the karst reservoirs, cylindrical phi-K plugs will be obligatory taken in avoiding the macro-porosity (cavern, vugs, fracture), so for principally evaluate the matrix porosity (fig46). So macro-porosity in karst reservoirs represents a characteristic part of the porous networks conferring to the types of reservoir a good capacity of stocking. Therefore the estimation of the petro-physical-properties of our karst reservoir (Font Sant) is realized from virtual plugging process consisting in continue plugging without avoid the karsts (fig46).

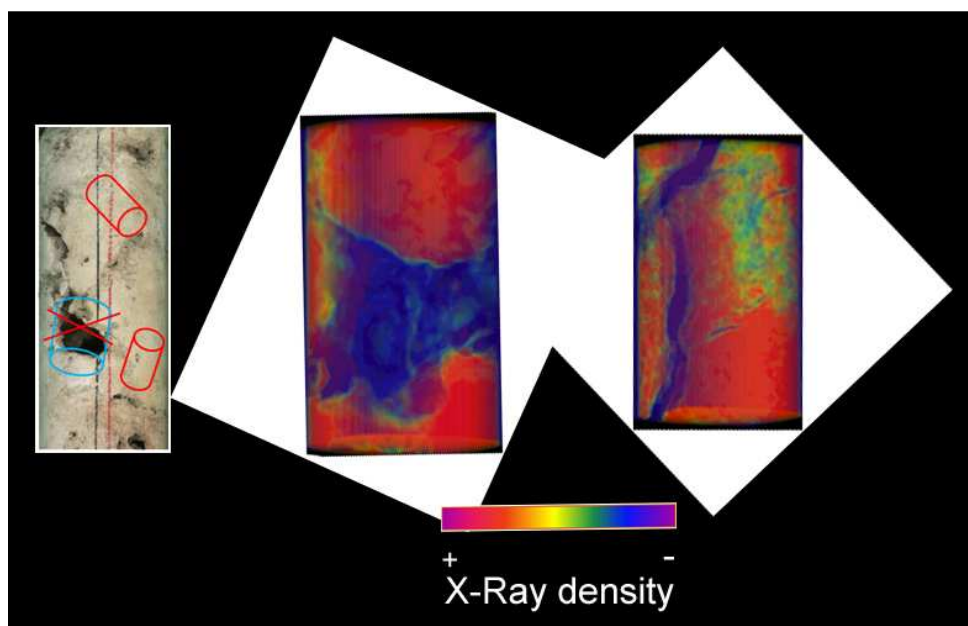


Fig46: Core section illustrating the method of an eventual Phi-K plugging in karstified rock and the example of virtual plugs. **Left:** The Phi-K plugs will be taken only in the not-karstified zone (cylinder in red) in avoiding the large voids (cylinder in blue). **Center:** Example of virtual plug taking into account a large pore (irregular structure colored in blue). This blue tint reflects the characteristic low X-Ray density of the voids (pores). "Actually the more porous the rock is, the less dense it is; the denser the rock is, the less porous it is". The red-colored part of the virtual plug corresponds to the fairly porous matrix. **Right:** Virtual plug taking into account a large opened fissure (vertical structure colored in blue).

From Amira Software©, the three dimensional X-Ray images can be used to sample virtual plugging. This survey consists in sampling, every 2 centimeters, virtual plugs of 30 millimeters in diameter and 50 millimeters in length all along the three dimensional core images. The assessment of X-Ray density, the virtual porosity and the percentage of heterogeneity are evaluated on every virtual plug taken (Fig47).

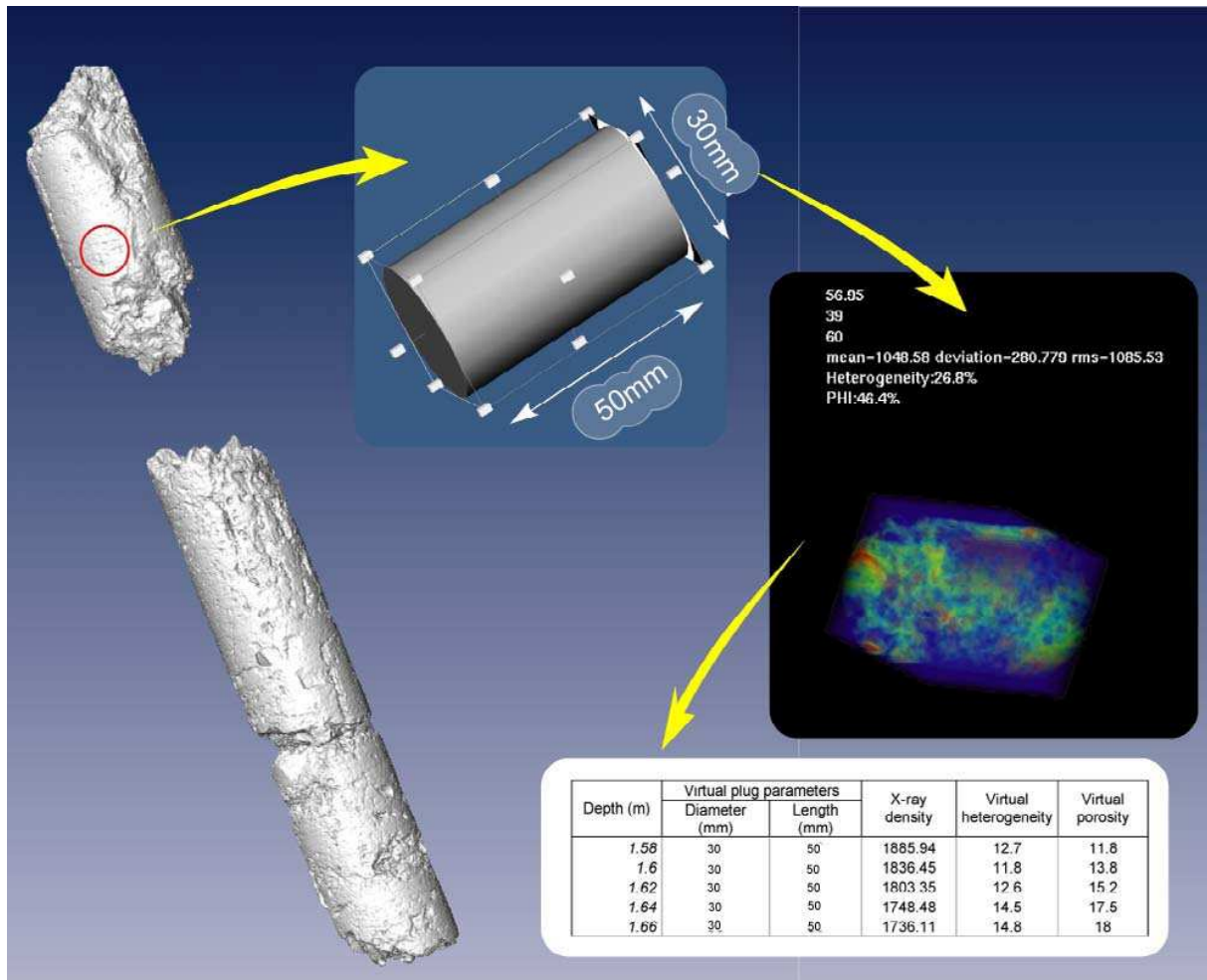


Fig47: Workflow of virtual plugging with Amira© software

On the other hand, before to sample these plugs for estimate their X-Ray density and virtual porosity, a calibration needs to be done considering the mineralogy all along the core as calcite. It consists in inputting in Amira software© command two calibration coefficients estimated from a linear relation established between the estimated porosity (non virtual) of some sections and their X-Ray density (Fig48). To establish this regression curve equation, three measures are realized:

- Volume of the sections in cm^3 evaluated by image analysis from Amira software©.
- X-Ray density of the sections evaluated by image analysis from Amira software©.
- Weight of the section in g.

Thus, the density (g/cm^3) of these sections is then deducted. If we consider the mineralogy on all along the core constant and corresponding to a calcite, their porosity can be estimated:

$$\Phi = \frac{2,71 - \left(\frac{\text{Weight}}{\text{Volume}}\right)}{2,71} \quad 2.71 \text{ g}/\text{cm}^3 = \text{Calcite density}$$

$$\frac{\text{Weight}}{\text{Volume}} = \text{Density (g}/\text{cm}^3) \text{ of the select core sections}$$

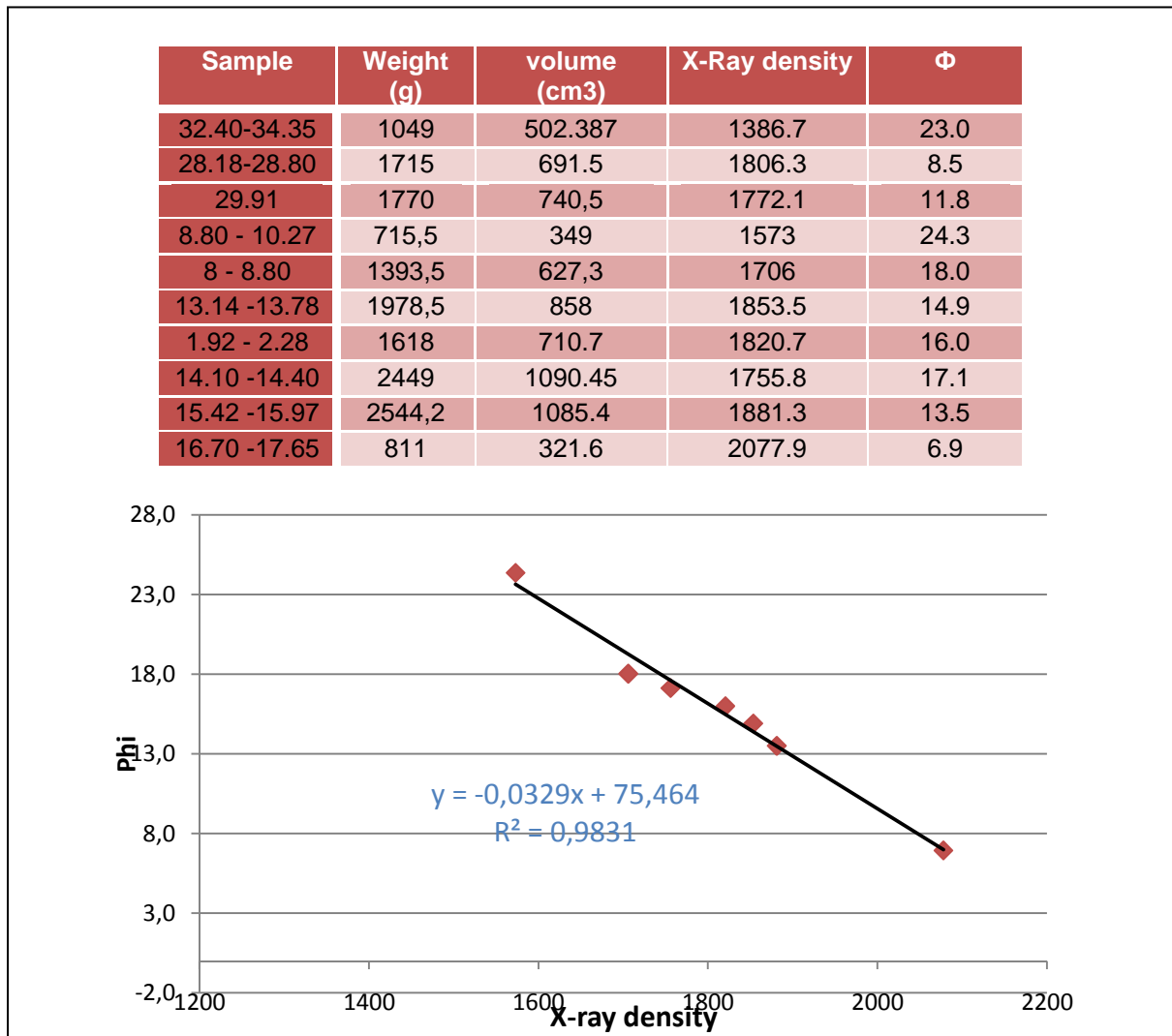


Fig48: Regressive curve established for the calibration of virtual plugging. Calibration realized with 10 samples from core S26. The same calibration is done for well S27.

Thus the regression curve can be established. Using equation of this curve $Y = a \cdot X + b$ the two calibration parameters are deduced:

$$1) -b/a$$

$$2) 100-b/a$$

The samples from breccias of unit3 used for realize this calibration was outside the regressive curve. Actually the mineralogical composition of these polygenic breccias is not constant and is not only represented by calcite. As previously described these breccias contain some dolomite and quartz. So the virtual petro-physical properties of the rocks of unit3 will be not calibrated and not integrated in this investigation. Nevertheless the samples of unit 1 and Unit 2 although they contain quartz, in addition of calcite, fit very well on the regressive curve. So theirs virtual petro-physical parameters will be calculated.

After inputting these parameters in Amira software©, the virtual plugs are taken every 2 centimeters on all along the core. Subsequently virtual porosity log and heterogeneity log are realized from Wellcad software© (Fig49).

b) Results: Case of Well S26

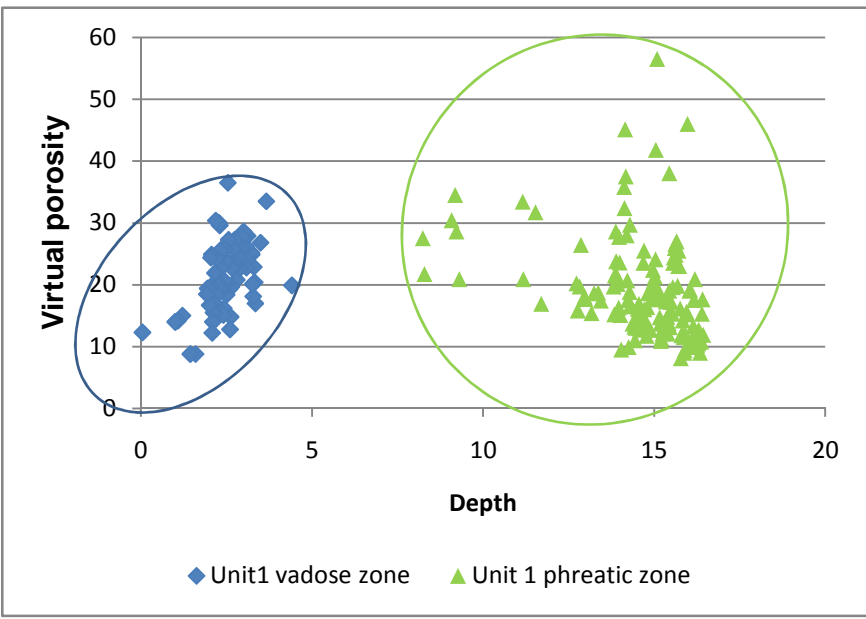
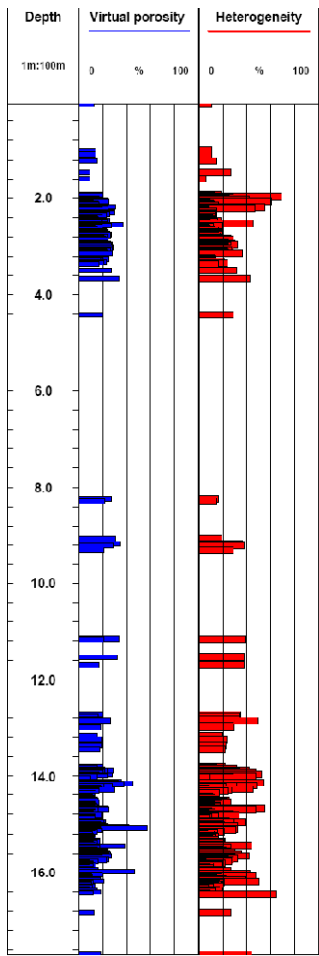


Fig49: Cross plot virtual porosity vs depth. **Vadose zone:** The rocks of vadose zone show fair to mean porosity. Values range is from 8.8% to peaks at 36.5%. **Phreatic zone:** The facies associated to this zone present a large range of porosity from fair to good (9.9% to 56.5%). **Unit2:** The porosity of these rocks is fair. The highest porosity reached in this zone is 18.2%. **Left:** Virtual porosity log vs percentage of heterogeneity log. Both are estimated by the virtual plugging process, in well S26.

c) Interpretation: The petro-physical results obtain from virtual plugging shows a relative variability of the porosity all along the core. Actually we can observe in fig 49 the heterogeneous variation in amount of porosity as well in the vadose zone as in the phreatic zone.

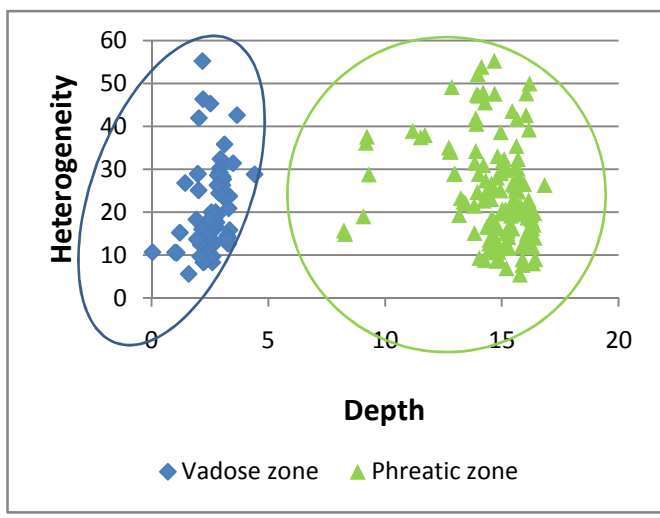


Fig50: Cross plot heterogeneity vs depth. Values of heterogeneity reflect the degree of alteration of rocks due to the karst action.

To interpret the large range of porosity, the curve of heterogeneity needs to be used. The heterogeneity of a rock depends on its percentage of alteration. When heterogeneity is high, it means that rock is highly affected by dissolution structures (vugs or caverns) which are created by the karst action. Therefore in karst reservoir, heterogeneity and porosity show often the same variations.

According to the cross plot (fig50), the degree of alteration is very variable all along the reservoir: every level in Font Sant reservoir is characterized by its own degree of alteration.

The large range of porosity and heterogeneity in **vadose zone** reflect some features as diagenesis and porous features previously characterized in this environment (refer to diagenesis chapter).

Generally in Font Sant vadose zone, heterogeneity is quite different to the porosity: heterogeneity is high reflecting the extensive dissolution in this environment; while the porosity is fair to mean (Tab1). This quite difference is the result of re-precipitation processes associated to the karst action in the vadose zone. Actually according to the high heterogeneity, the rocks of vadose zone are highly altered due to the karst action, but abundant re-precipitations of stable minerals occur in situ, reducing or totally filling the pores (primary and secondary dissolution porosity).

	Depth (m)	Heterogeneity (%)	Porosity (%)
Tab1	1.45	26.8	8.8
	2.02	25.1	16.7
	1.99	28.9	19.3

Contrary, at some depth heterogeneity in vadose zone is low while the porosity is mean to good (Tab2). According to the low heterogeneity, the rocks at these depths are fairly altered, so have fair dissolution porosity. Therefore this good porosity corresponds to an important primary porosity (inter-granular) which is coupled with fair dissolution porosity. Actually referring to sedimentology chapter, good matrix porosity is coupled with fair to mean secondary leached porosity at some depth in Font Sant vadose zone; depths which are not affected by re-precipitation processes (partial cementation in vadose zone).

This result proves that inter-granular porosity do not modified the heterogeneity of rock although it enhances total porosity.

	Depth (m)	Heterogeneity (%)	Porosity (%)
Tab2	2.63	9.7	14.8
	2.51	9.2	18.4
	2.61	8.3	12.8
	2.59	12.2	19.3
	2.81	19.3	20.08

Despite the abundant re-precipitation of stable minerals in the vadose, some peaks of higher porosity are present at some depth (Tab3). These important porosities are associated to peaks of higher heterogeneity. Therefore at some depth heterogeneity and porosity show the same variation. This is the consequence of karst action, and so the predominant porosity at these depths corresponds to dissolution porosity (vugs, cavern, moldic, and dissolution channel).

	Depth (m)	Heterogeneity	Porosity
Tab3	3.13	35.8	27.9
	3.67	42.6	33.5
	3.5	31.4	26.8
	2.19	55.2	30.04

Referring to cross plot (fig49), range of porosity in **phreatic zone** is globally ten percent lower than the porosity in vadose zone. This low in porosity reflects the extensive cementation in this environment: saturated area.

According to the cementation affecting the rocks of this environment, heterogeneity is generally quite different to porosity (cross plot heterogeneity and cross plot porosity):

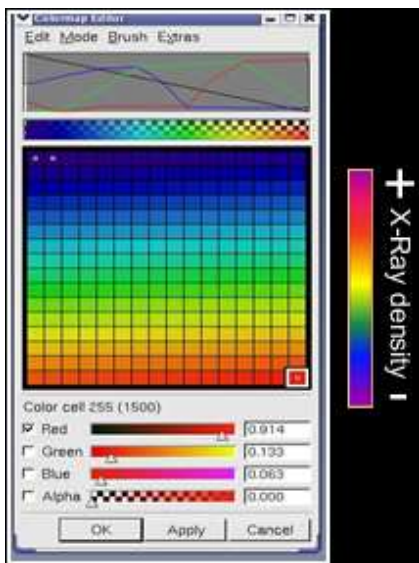
Some peaks of higher and meaner heterogeneity are regular present (Fig50/Tab4) in phreatic area. It proves that, actual rocks of the phreatic zone were probably soon exposed. At corresponding depths, the porosity is fair while the heterogeneity is mean to high. It means that, the important dissolution porosity created by karst action during the exposure episode is highly reduced by late cementation processes: vugs, moldic and dissolution channels partly occluded by a late growth of calcite (referring to diagenesis chapter).

	Depth	Heterogeneity	Porosity
Tab4	11.7	38	16.9
	14.81	33.1	18.6
	14.7	47.6	25.5
	16.16	39.3	17.5
	12.86	49.2	26.4

At some depth in this environment heterogeneity is low while the porosity is poor to fair (Tab5). It means that: the corresponding rocks are fairly affected by karst action (dissolution porosity of rocks is poor), and the primary inter-granular porosity which had to be the predominant porosity is highly reduced by phreatic cementation.

	Depth	heterogeneity	porosity
Tab5	15.78	5.5	8.1
	15.2	7	10.9
	15.29	11.7	13.8
	16.43	9.1	11.9

4. Visualization of porous network



The last X-Ray image treatment from Amira software© consists in making transparent the high X-Ray density level corresponding to the matrix, in order to visualize all the low X-Ray density area corresponding to the voids (vugs, cavities, karsts, channel). Thus the pore network and the high porous zones of our fractured-karst reservoir can be visualized in three dimensions.

This treatment allows characterizing the lateral and vertical connectivity of pore and distinguishing the different pore type all along the core.

Fig51: The color table in Amira software illustrating the range of X-ray density. Every color is assimilated to a value of X-ray density. For make transparent the high density zone, the “Alpha” value on color table of the reddest color corresponding to the highest density is put in zero.

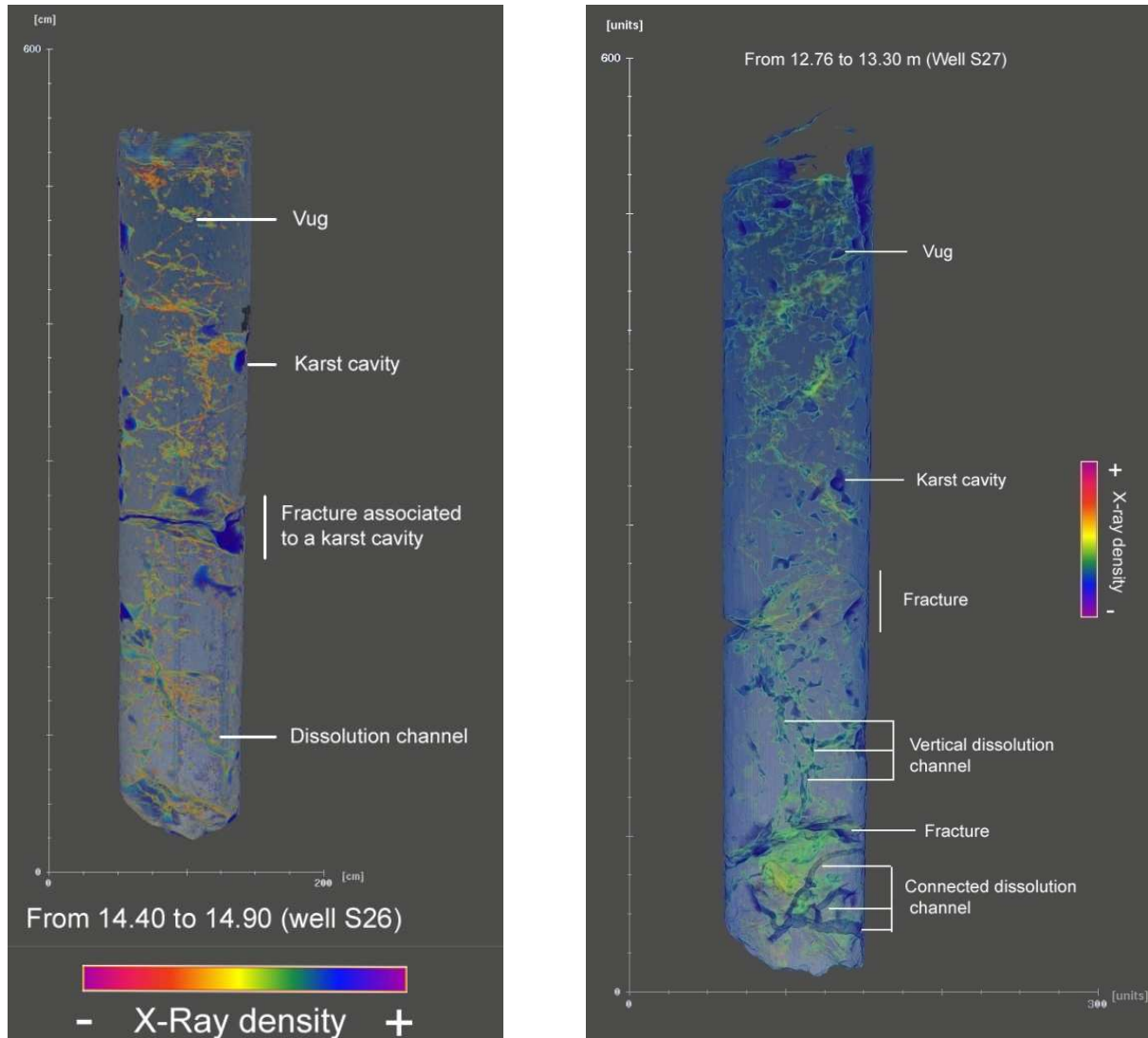


Fig52: Virtual core sections illustrating the porous network of Font Sant reservoir. The pores correspond to the irregular blue-colored structures (Blue colored = low X-Ray density). Left: The blue colored structures on this section are often associated to orange-colored shapes. This section of the phreatic zone is affected by different dissolution structures (vugs/dissolution moldic, caverns and dissolution channel) created by the karst action probably when this part of the phreatic zone was subaerial exposed. The porous network of this core section also denotes a fracture porosity which is currently associated to karst cavities. These karsts associated to the fractures correspond to a dissolution structures probably created by eventual under-saturated fluid circulations throughout the fractures, so these voids are not related to the infiltration of meteoric acid water. Although the density of dissolution structures is very high on this core (good porosity) we notice that their connectivity is fair, conferring to the rocks a low permeability.

Right: This section is also karstified (vugs, cavern, dissolution channels) and fractured. We note on this core section vertical dissolution channels connecting two sub-horizontal fractures. These structures are probably created by the vertical percolation from gravity effect into the rocks of fluid which circulated throughout the upper sub-horizontal fracture. These channels and karst associated to fractures (left picture) attest that dissolution processes in Font Sant reservoir are not only related to the directly infiltration of meteoric acid water onto the surface. Actually fluid circulation throughout opened fracture can create as well cavern, as vugs, as dissolution channel and as dissolution moldic ameliorating the capacity of stocking of Font Sant reservoir. In the top of this core the density of the dissolution structure is so high that the vertical and lateral connectivity between them is very good conferring a good porosity and good permeability at this section of our reservoir. The dissolution channels according to their high extension currently create a good connection between them, or between them and the other pores (vugs, caverns) cross by they: For example on the base of this section connected dissolution channels are showed.

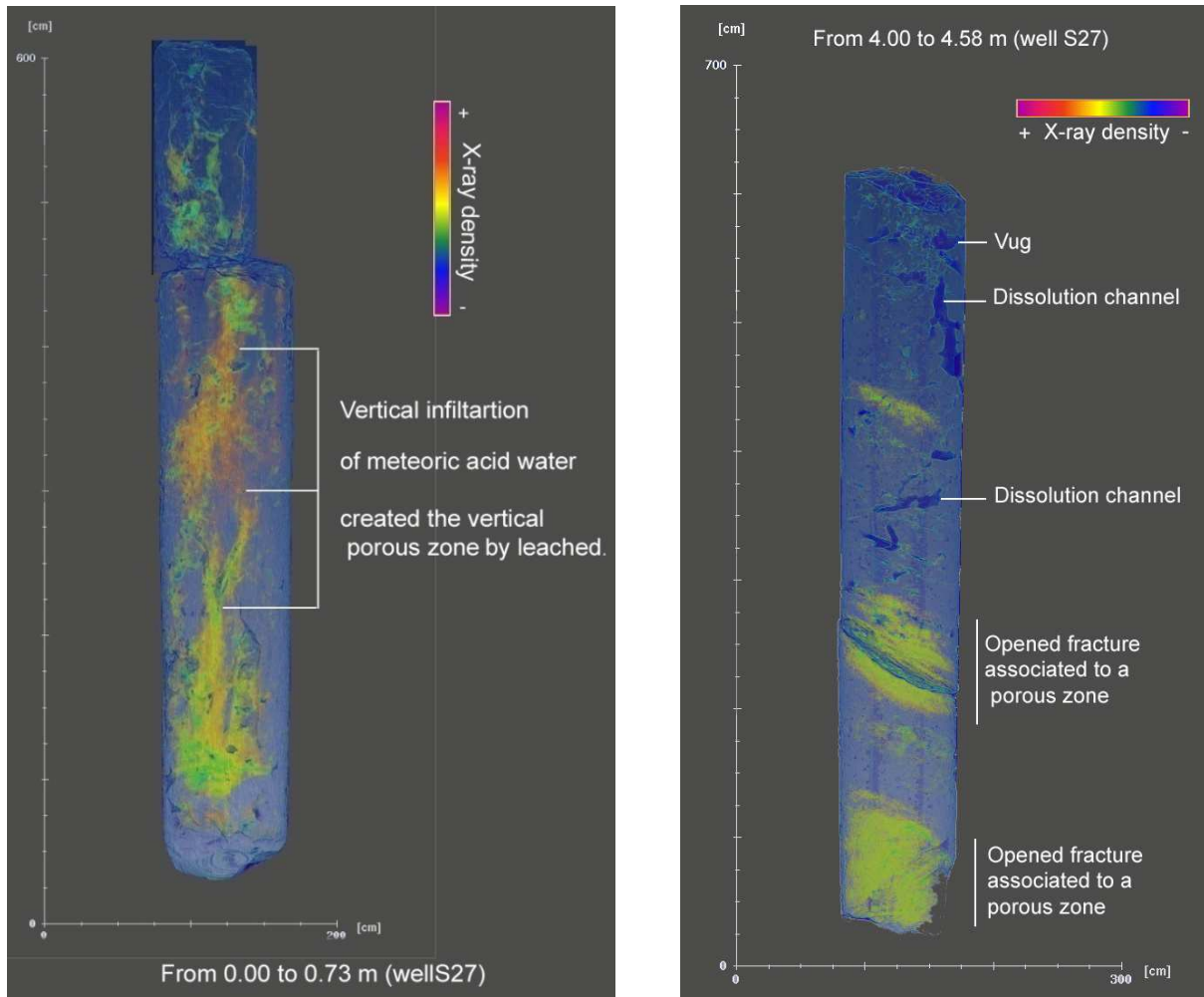


Fig53: Virtual core section illustrating the porous network of rocks constituting the vadose zone of Font Sant reservoir. The irregular blue-colored structures correspond to the low X-Ray density zone, so to the pores. Although the matrix of these rocks consisting in the high X-Ray density zone are made transparent for visualize the porous network, some levels of this matrix being very porous (low X-Ray density) can be display and correspond to the yellow/green colored level on these images.

Left: This virtual core section affected by leached porosity (vugs and channels) principally shows vertical porous zones into the rocks. According to their vertical geometry these porous zones are probably created by the directly vertical infiltration of the meteoric acid waters into the rocks. Actually dissolution processes occur during the percolation of these acid waters thus creating a high secondary leached porosity in the zones crossed by this infiltration. We note this porosity corresponding to matrix porosity (micro-porosity) is associated to a macro-porosity (vugs, channel) created by the same dissolution processes.

Right: The porous network of this core section is represented by vugs, channels and fracture porosity. In the zones where the density of dissolution structures is high (for example the top of this section) the connectivity between them is good conferring to the rock a good permeability. Surrounding fractures exist levels colored in yellow thus corresponding to low X-Ray density zone so to porous matrix zone. Previously study, this high matrix porosity around the fractures is the result of fluid circulation through these fractures. Actually leaching of preexistent cement affecting the country rock occurs during the eventual under-saturated fluid circulation throughout opened fractures. Once again this virtual petro-physical survey show the contribution of the fractures affected these rocks in the amelioration of the capacity of stocking of our reservoir.

VII) Discussion and Conclusion

Corresponding to the most productive oil reservoirs in the world, carbonates reservoirs show currently paleokarsts features (For example Sichuan reservoir, China; Rospo Mare, Italy). Karst processes affecting these reservoirs control substantially their petrophysical properties (porosity, permeability).

Sedimentological, diagenesis and virtual petrophysical survey realized on Santayi aquifer were really essential for the understanding of quality of reservoirs which are affected by karst alteration.

The analysis of two cores (S26 and S27) reveals the great impacts of Meteoric karst alteration on petrophysical properties of Santayi Limestone (First-thirteen meters). Extensive dissolution and cementation affect these limestone involving respectively increase and reduction of porosity and permeability.

The exposed rocks of carbonate reservoirs are affected by extensive dissolutions due to the meteoric karst action, giving place to good secondary leached porosity (caverns, vugs, moldic porosity and dissolution channels). This secondary porosity coupled with matrix porosity (primary porosity) ameliorates highly the capacity of the aquifer (quality of reservoir). Some subearial Santayi limestone reveals great values of virtual porosity, up 33.5%.

Nevertheless dissolution in vadose zone is associated with reprecipitation of stable carbonate. As consequence, primary porosity of subearial rock is commonly filled during meteoric diagenesis, and secondary porosity is created. Therefore karst alteration has not a strong effect on porosity of subearial rock. However permeability of rocks is highly reduced by this alteration through cementation of interconnected primary pores.

Referring to the diagenesis processes, secondary dissolution pores are often partly filled by growth of calcite related to reprecipitation processes in vadose zone. Thus karst process can reduce as well initial porosity as secondary porosity of rock: primary porosity totally occluded by reprecipitation process and secondary leached porosity partly filled.

Near the water table quality of carbonate reservoir can be highly ameliorated by extensive dissolution (karst features), that result essentially from the mixing of chemically-distinct waters (vadose-phreatic mixing zone). Values range of porosity near the water table in Santayi aquifer is from 27.5 to 34.5%.

Acid meteoric waters become oversaturated by incorporation of carbonate minerals (Ca^{2+} , CO_3^{2-}) during karst action in vadose zone, and subsequently recharge the aquifer of the karstified carbonate reservoir. So reflecting the complete saturation of pores with these oversaturated waters, quality of reservoir in phreatic environment is substantially reduced. This reduction of petrophysical parameters of karst reservoir results mainly from the extensive reprecipitation of stable carbonate in that environment. Referring to results of virtual petrophysical survey, porosity in phreatic area can be ten percent lower than porosity in vadose environment.

Related to climate condition and sea-level fluctuations, water table currently fluctuates changing the position of these environments. So throughout the time, reservoir quality of both environments (vadose/phreatic) is highly variable: Petrophysical parameters in phreatic environment can be frequently ameliorated by karst development, during eventual subearial exposures of that environment (fall of the water table).

Referring to stable isotopes analyses, origin of Font Sant anomaly (Unit2) is not hydrothermal, but is evidently meteoric. This unit and unit3 (Polygenic breccias) correspond in fact to deposits filling large paleokarst, which affects Santayi Limestone. According to the unavailable criteria proving existence of hydrothermal diagenesis, this large filled-paleokarst is probably created by meteoric alteration during Pliocene subearial exposure episode recorded in Mallorca. And In addition, no criteria prove the existence of possible fault in Font Sant.

Similar to Santayi aquifer, many carbonate reservoirs are affected by large dissolution structures, which can highly ameliorate their reservoir quality. Nevertheless these structures are often partly or completely filled by diagenesis cement (phreatic cement) or particles of deposits overlaying (breccias) the carbonate affected by them.

Use of CT scan in order to get petrophysical data (virtual porosity) and to visualize porous network of core in three dimensions, was relevant to characterize the impact of karst alteration on quality of carbonate reservoir. Results of virtual porosity confirm the importance of meteoric diagenesis (vadose/phreatic) on quality of Santayi limestone.

Visualisation of porous network in three dimensions shows a substantial variability of permeability (connectivity of pores) in karst reservoir. Potential of connectivity of dissolution structures (vugs, channel and cavern) depends on the type of pores (dissolution channels show good permeability and good connection) and on the degree of alteration of the reservoir (area with high density of dissolution structures shows good permeability).

According to reprecipitation process related to karst action, permeability of karst reservoir is commonly reduced. Fractures induced by uplift of carbonate reservoirs, similar to Santayi Limestone, can highly ameliorate permeability of karstic reservoir. Referring to results of virtual petrophysical analyses fractures affecting carbonate reservoir can control, in addition to meteoric alteration, the karst development. In addition to ameliorate permeability, fractures involve an increase of porosity due to fluid circulation throughout them.

In conclusion, analyse of two wells drilled in Santayi aquifer has procured important information about effect of karst action and fracture on carbonate reservoir. Results obtained in this investigation show karst-fractured reservoirs as heterogeneous reservoirs in term of porosity and permeability. Porosity and permeability are relatively variable all along the karst-fractured reservoir. This heterogeneity is mainly control by diagenesis process related to karst action (dissolution, reprecipitation, infilling of dissolution structures). Non-uniform distribution of fractures in the reservoir increases its heterogeneous feature.

Note that, the investigation is realized on the superficial part of karst reservoir (first thirteen meters); it is now interesting to drill more in depth for analysing and characterizing the nature of karst development (hydrothermal, salt water) and their impact on quality of reservoir in depth.

Even if no criteria are visible to prove existence of hydrothermal phase and fault affecting Font Sant rock, the filled-paleokarst distinguished in this area can nevertheless be interpreted as hydrothermal karst created by geo/hydrothermal fluid flow through a fault (Hypothesis 2 =Fig41). Therefore to choose one of both hypotheses (hypothesis1 = meteoric karst, hypothesis2 = hydrothermal karst associated to fault) we need in first to realise a detailed structural map of Font Sant area in order to know if our core zone is affected or not by a fault. In second, measure of temperature (temperature log) and chemic analyses must necessary be done in Font Sant aquifer, in order to confirm or invalidate the hydrothermal hypothesis.

BIBLIOGRAPHY

Acosta, J., Muñoz, A., Herranz, P., Palomo, C., Ballesteros, M., Vaquero, M., Uchupi, E., 2001. Geodynamics of the Emile Baudot Escarpment and the Balearic Promontory, western Mediterranean. *Marine and Petroleum Geology*, vol. 18, 3, pp. 349-369.

Acosta, J., E. Ancochea, M. canals, M.J. huertas, E. Uchupi., 2004. Early Pleistocene volcanism in the Emile Baudot Seamount, Balearic Promontory (western Mediterranean Sea). *Marine geology* 207, 247-257.

Bonnier B., 2005. Etude sédimentologique et géochimique des récifs Miocènes de Majorque (Baléares, Espagne). Influence des caractéristiques diagénétiques sur les propriétés physiques des roches carbonatées. Ms Thesis, 31p. (unpublished), Université Paul Cézanne, CEREGE, Aix-en Provence.

Dan W.J. BOSENCE, Luis Pomar, D. A. Waltham, and Thomas H.G. Lankester, 1994. Computer Modeling a Miocene Carbonate Platform, Mallorca, Spain. AAPG Bulletin, V. 78, No. 2, P. 247-266

Duboin, F-A., 2008. Sedimentological description and 3D image analysis of MC10 cores from Mallorca, Spain. Report of DSTG (unpublished), diplôme de technicien Supérieur en Géologie.

Esteban. M., Colin. F. Klappa., 1983. Subeareal exposure environment. The American Association of petroleum Geologists.

Esteban M., 1979. Significance of the Upper Miocene reefs of the Western Mediterranean. Palaeogeogr. Palaeoclimatol. Palaeoecol., vol. 29, pp.169-188.

Hounsfield GN., 1973. Computerised transverse axial scanning (tomography) I. Description of system. Br J Radiol, vol. 46, pp.1016-1022.

Knap, F., 2008. Sedimentologic, diagenetic and petrophysical study of the Upper Miocene Paleokarsts from Mallorca (Spain). Report of DSER (unpublished), Université de Bourgogne, Centre des Sciences de la Terre, Dijon, 65p.

Mylroie, J.E., Carew J.L., 2003. Karst development on carbonate islands. *Speleogenesis and Evolution of Karst Aquifers* 1, pp. 1-21

Pomar L., Ward W.C., 1999. Reservoir-Scale Heterogeneity in Depositional Packages and Diagenetic Patterns on a Reef-Rimmed Platform, Upper Miocene, Mallorca, Spain. AAPG Bulletin, 83, pp. 1759-1773.

Pomar L., 1991. Reef geometries, erosion surfaces and high-frequency sea-level changes, Upper Miocene Reef Complex. Mallorca. Spain. *Sedimentology*, vol. 38, pp. 243-269.

Pomar L., Brandano, M. and Westphal, H. Environment factors influencing skeletal grain sediment associations : a critical review of Miocene examples from the Western Mediterranean. *Sedimentology*, 51 (3), 627-651. June.

Pomar L., M. Marzo, A. Baron., 1983. EL TERCARIO DE MALLORCA. En : El Terciario de las Baleares. GUia de las Excursiones del X Congreso Nacional de Sedimentología. Menorca, 26-30.

Pomar L., Ward W C.; 2006. Reservoir-scale heterogeneities in Upper Miocene carbonate platforms of the balearic Islands, Spain. Field Seminar.

Pomar L.; 2006. Reservoir-scale heterogeneities in Upper Miocene carbonate platforms of the balearic Islands, Spain. Field visits – Guide book.

Rebledo, P.A., 2005, Los Paleocolapsos kársticos en las plataformas carbonatadas del Miocene superior de Mallorca: análisis geográfico, genético, geológico y evolutivo, PhD thesis, Universidad de las Islas Naleares. Palma de Mallorca.

Rebledo, P.A., J.J. Duran., and L. Pomar., 2004, Paleocollapse structures as geological record for reconstruction of past karst processes during the Upper Miocene of Mallorca Island. *Int. J. Speleol.*, 33 (1/4), 2004: 81-95.

P.A Scholle., and D.S Ulmer-Scholle., 2003, A color guide to the petrography of carbonate rocks: grains, textures, porosity, diagenesis. AAPG Memoir 77

J.D Waele., M. Mucedda., L. Montanaro., 2009, Morphology and origin of coastal karst landforms in Miocene and quaternary carbonate rocks along the central-western coast of Sardinia (Italy). *Geomorphology* 106, 26-34.